AD-754 410

ADVANCED RESEARCH PROJECTS AGENCY-NAVAL RESEARCH LABORATORY LASER PROGRAM

Naval Research Laboratory

Prepared for:

Advanced Research Projects Agency

November 1972

DISTRIBUTED BY:

NTIS

National Technical Information Service
U. S. DEPARTMENT OF COMMERCE
5285 Port Royal Road, Springfield Va. 22151

BEST
AVAILABLE COPY

AD754410

NRL Memorandum Report 2529

ARPA-NRL Laser Program

Semiannual Technical Report
to
Advanced Research Projects Agency
January 1, 1972 - July 31, 1972

ARPA Order No. 2062

Laser Physics Branch
Optical Sciences Division

November 1972

Reproduced by
NATIONAL TECHNICAL
INFORMATION SERVICE
U S Department of Commerce
Springfield VA 22151

D D C
RECEIVED
JAN 29 1973
B

Details of illustrations in
this document may be better
studied on microfiche

NAVAL RESEARCH LABORATORY
Washington, D.C.

Approved for public release; distribution unlimited.

UNCLASSIFIED
Security Classification

DOCUMENT CONTROL DATA - R & D

(Security classification of title, body of abstract and indexing annotation must be entered when the overall report is classified)

1. ORIGINATING ACTIVITY (Corporate author)
Naval Research Laboratory
Washington, D.C. 20390

2a. REPORT SECURITY CLASSIFICATION
UNCLASSIFIED

2b. GROUP
---

3. REPORT TITLE
ARPA-NRL LASER PROGRAM - Semiannual Technical Report to Advanced Research Projects Agency 1 January 1972 - 31 July 1972

4. DESCRIPTIVE NOTES (Type of report and inclusive dates)
Semmiannual Technical Report - 1 January 1972 - 31 July 1972

5. AUTHOR(S) (First name, middle initial, last name)
Laser Physics Branch
Optical Sciences Division

6. REPORT DATE
November 1972

7a. TOTAL NO. OF PAGES
~~162~~ 159

7b. NO. OF REFS
40

8a. CONTRACT OR GRANT NO.
NRL Problems K03-08A, N01-21
b. PROJECT NO R08-45, K03-53
c. ARPA Order 2062
Program Code 2E20
d. Program Element Code 62301D

9a. ORIGINATOR'S REPORT NUMBER(S)
NRL Memorandum Report 2529

9b. OTHER REPORT NO(S) (Any other numbers that may be assigned this report)
N/A

10. DISTRIBUTION STATEMENT
Approved for public release; distribution unlimited.

11. SUPPLEMENTARY NOTES
N/A

Details of illustrations in this document may be better studied on microfiche

12. SPONSORING MILITARY ACTIVITY
Advanced Research Projects Agency
Washington, D.C. 20350

13. ABSTRACT

The ARPA-NRL high energy laser program is concerned with the development of laser technology in four program areas; Chemical Lasers, Electric Discharge Lasers; High Power Glass Lasers and New Laser Techniques. This report summarizes the progress made in those areas during the last half of FY 72.

DD FORM 1 NOV 65 1473 (PAGE 1)
S/N 0101-807-6801

UNCLASSIFIED
Security Classification

14. KEY WORDS	LINK A ROLE	LINK A WT	LINK B ROLE	LINK B WT	LINK C ROLE	LINK C WT
Lasers						
Glass Lasers						
Chemical Lasers						
Electrical Lasers						

iB

TABLE OF CONTENTS

FOREWORD iii

ABSTRACT iii

PROBLEM STATUS iii

AUTHORIZATION iii

CHEMICAL LASER PROGRAM 1

DF-CO_2 Supersonic Transfer Chemical Laser (TCL) 1

CO Laser Research 1

Flame Lasers 1

CO Transition Probabilities 3

SHORT PULSE CO_2 MOLECULAR LASERS 4

Short Pulse Oscillator 4

Double Raman Conversion 4

TEA Pre-Amplifiers 4

10 Liter e^- beam Amplifier 5

Saturable Absorbers 5

NEW LASER TECHNIQUES 6

HIGH POWER GLASS LASER PROGRAM 8

Introduction 8

French Laser Modifications 8

Disc Laser Test Results 10

1-2 kJ Disc Amplifier Design 11

Short Pulse Bandwidth Limited Oscillators 14

APPENDIX A - A Method for Measuring Relative Transition Probabilities of Cascading Molecular Bands: Application to CO Fundamental Bands A-1

APPENDIX B - Cold Cathode Electron Beam Controlled CO_2 Laser Amplifier..... B-1

APPENDIX C - Damage Measurements with Subnanosecond Pulses.... C-1

APPENDIX D - Reflectivities of Owens Illinois Laser Glasses with Different Surface Preparations..... D-1

APPENDIX E - Disc Laser Test Results..... E-1

APPENDIX F - Fluorescence Amplification and Parasitic Oscillation..... F-1

APPENDIX G - Faraday Rotation of EY-1 Glass..... G-1

APPENDIX H - Mode Locking of CaLaSoap:Nd..... H-1

PUBLICATIONS AND PRESENTATIONS FOR FY-72..... 1-1

FOREWORD

The Laser Physics Branch of the Optical Sciences Division, Naval Research Laboratory, Washington, D.C., prepared this Semiannual Report on work sponsored by the Advanced Research Projects Agency, ARPA Order 2062. Co-authors of the report were J.R. Airey, O.C. Barr, N. Djeu, J.L. Emmett, J. Holzrichter, T. Kan, J.P. Letellier, J. Marzolf, J.M. McMahon, S. Searles, J. Stregack, J. Trenholme, W.S. Watt, W. Whitney.

ABSTRACT

The ARPA-NRL high energy laser program is concerned with the development of laser technology in four program areas; Chemical Lasers, Electric Discharge Lasers; High Power Glass Lasers and New Laser Techniques. This report summarizes the progress made in those areas during the last half of FY 72.

PROBLEM STATUS

This is a semiannual technical report; work is continuing.

AUTHORIZATION

NRL Problems K03-08A, N01-21, R08-45, K03-53

SEMI-ANNUAL TECHNICAL REPORT

Reporting Period
1 January 1972 - 31 July 1972

1.	ARPA Order	2062
2.	Program Code Number	2E20
3.	Name of Contractor	Naval Research Laboratory
4.	Effective Date of Contract	1 July 1971
5.	Contract Expiration Date	30 June 1972
6.	Amount of Contract	$1,012,500
7.	Contract Number	63201D
8.	Principal Investigator	John L. Emmett
9.	Telephone Number	(202) 767-2074
10.	Project Scientist	John M. McMahon
11.	Telephone Number	(202) 767-2730
12.	Title of Work	High Power Lasers

Sponsored by

ADVANCED RESEARCH PROJECTS AGENCY

ARPA Order No. 2062

CHEMICAL LASER PROGRAM

1. DF-CO_2 Supersonic Transfer Chemical Laser (TCL)

The concept of a supersonic DF-CO_2 chemical laser capable of cw operation without a vacuum pump has been discussed in the preceeding semiannual technical report.

During the past six months complete installation and modification of the AVCO Mark III GDL has been accomplished to permit DF-CO_2 chemical laser operation. Figure 1 shows the completed device fully assembled in our new chemical laser facility. Not visible in the photograph are the bottled gas tank blocks and exhaust gas scrubber installation located outside the building.

At this writing the cold flow tests and burner testing have been completed. We are now making measurements of exhaust gas composition to establish the correct flow conditions in preparation for the introduction of fluorine and deuterium gases. When these preliminary steps are completed we will begin a series of laser power measurements with a multimode mirror configuration. A multiple hole output mirror and calorimeter configuration will be employed in this series of tests. It appears reasonable to expect laser power tests to begin about October 1, 1972. Dr. Cool is returning to Cornell University at the end of August, but will continue his association with this project as a consultant to NRL.

While the laser installation has occupied most of our time during the past six months, attention has also been given to potential problems associated with the formation of carbonyl fluoride (COF_2) in the present device. Our measurements of the rate of deactivation of CO_2(00°1) by COF_2 and the measurement of absorption of CO_2 laser radiation by COF_2 performed at the Air Force Rocket Propulsion Laboratory have permitted our estimate of the expected effects of COF_2 on laser performance. We expect no serious handicap from COF_2 formation provided the partial pressure of COF_2 does not exceed about 2 torr which would appear to be an unreasonably large amount of COF_2 in the present device.

2. CO Laser Research

Flame Lasers

We have experimentally investigated the C_2H_2-O_2 flame for possible optical gain in the product CO molecules. Acetylene was chosen because it is known to produce vibrationally highly excited CO molecules in reaction with O atoms. It has the advantage over CS_2 of being a gas at room temperature, so that one can more readily go to higher pressures with the C_2H_2-O_2 flame.

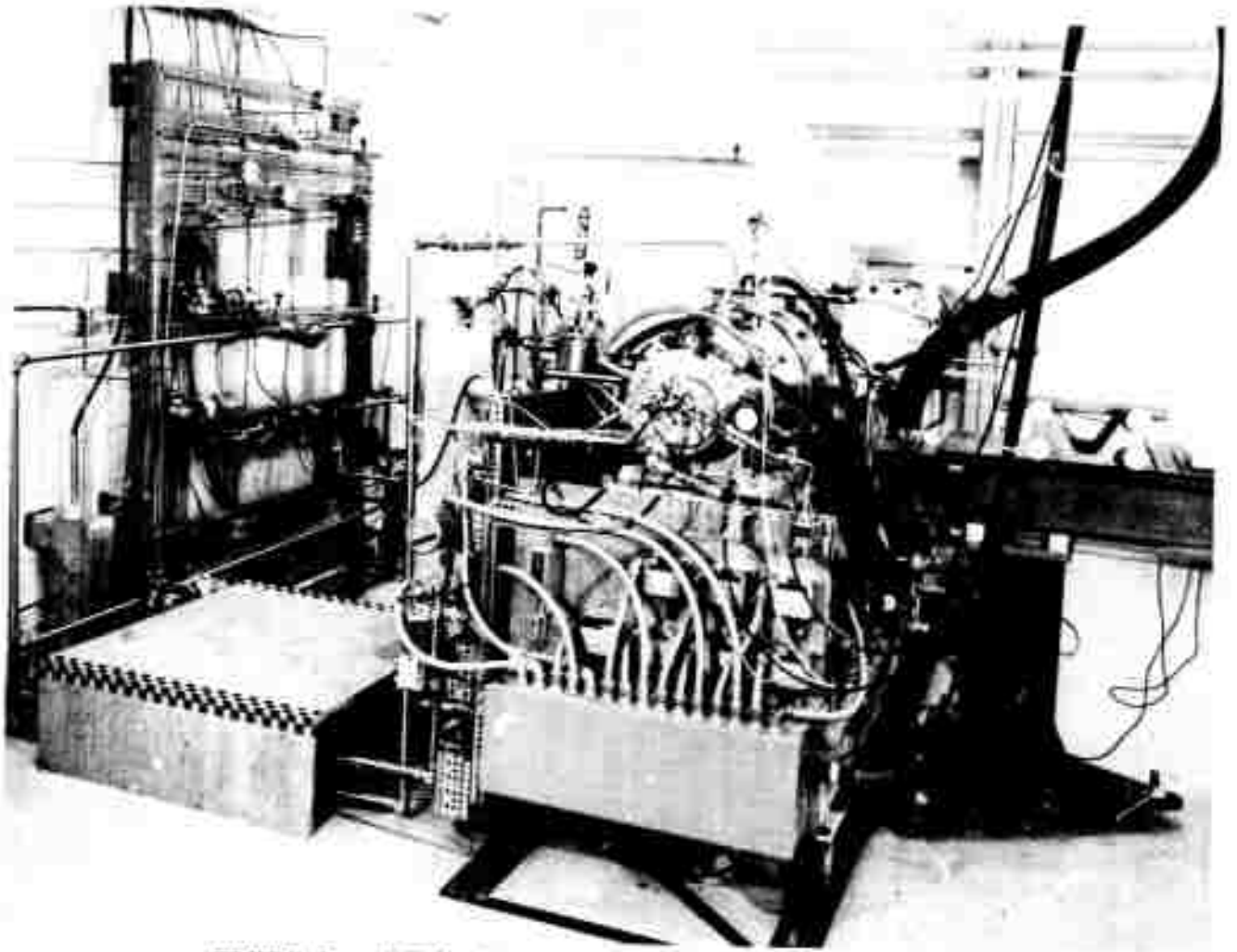

FIGURE 1. DF-CO_2 Supersonic Transfer Laser Apparatus

The laser oscillation range technique was used to probe the C_2H_2-O_2 flame. This is the very sensitive method for measuring gain developed by us that led to the successful operation of the first flame laser. Quantitative measurements of the optical gain for the $P_{9-8}(12)$ transition were made across the profile of the C_2H_2-O_2 flame at several pressures around 10 torr. The highest gain measured was 0.05% cm^{-1}. The results of the work lead us to conclude that a CO laser based on that system is feasible. However, because of the relatively low gain attainable in the flame, such a laser would probably have a low chemical efficiency.

CO Transition Probabilities

Although a knowledge of the transition probability is central to the understanding of any laser system, these quantities have never been measured for the CO laser transitions because of experimental difficulties. We have succeeded in obtaining the CO vibrational transition probabilities indirectly by measuring the ratios of transition probabilities for adjacent bands and fitting them to a theoretical form.

The ratios were obtained by correlating the rotational gain distributions of adjacent bands using the fact that the distribution for each band is characterized by the corresponding inversion ratio and the temperature of the medium. The experimental results show that the square of the electric dipole matrix element varies linearly with the upper state vibrational quantum number to within a few percent for the CO molecule through V = 12.

The particular method that we have developed for this experiment is applicable to the determination of relative transition probabilities for cascading bands in any molecules. A paper describing the techniques and the results obtained for CO has been submitted to the Journal of Chemical Physics and is given as Appendix A to this section.

SHORT PULSE CO_2 MOLECULAR LASER

1. Short Pulse Oscillator

Mode locking and pulse shuttering have been used to generate a nanosecond pulse from an atmospheric pressure TEA laser. The mode locker utilizes the acousto-optic effect in germanium to modulate the internal loss of the laser at the cavity mode separation. Problems of AR coating damage to the modular element due to the high fluxes in the cavity have been eliminated by the use of a Brewster-angle Ge modulator. Alternative techniques to achieve mode-locking of the laser utilizing saturable absorbers and a liquid CS_2 acousto-optic cell have not been satisfactory to date. The saturable absorbers investigated have either too low or too high a saturation flux and the CS_2 acousto-optic cell exhibits very high attenuation to acoustic-drive frequencies in the region of interest below 100 MHz. The pulse shutter consists of a 50 mm long GaAs Pockels cell driven by a transmission line triggered from a laser triggered spark gap. The nanosecond pulse of $>$ 1 mJ is limited at the present time by the low gain of the 1½ meter spiral TEA laser oscillator. This oscillator will be replaced by a 1 meter long distributed discharge oscillator in the near future. This conversion will produce nanosecond pulses whose energy will then be limited only by damage to coatings on the output coupling optics. We are confident 5-10 mJ in a nanosecond pulse can be generated.

2. Double Raman Conversion

Preliminary Raman scattering experiments in H_2 to shift the Nd^{3+}:YAG line into the 9.4 μ band of CO_2 have been undertaken. These experiments were hampered by the necessity to share the use of the YAG short-pulse oscillator driver for the glass laser system. These experiments will be continued when a second separate short pulse oscillator system now being assembled is finished. Although 5% conversion of 1.06 μ to 1.9 μ has been achieved, the second conversion step has not been observed. Since the Raman gain for the second scattering process is lower than the first step, competing scattering processes could be depleting the 1.9 micron pump. These questions will be investigated more fully.

3. TEA Pre-Amplifiers

Two types of volume TEA discharges were investigated as short pulse preamplifier elements. One utilizes two solid Rogowski electrodes with surface preionization created by UV emission from an auxiliary discharge while the other utilizes a segmented cathode with surface preionization created by corona discharges between metal blades and glass rods. The solid electrode UV initiated devices achieved higher peak gains, better pulse to pulse reliability and were more durable than the devices containing dielectrics. The one meter long 2 cm x 2 cm aperture TEA amplifier has displayed a short pulse gain of $\sim$ 20

indicating a gain coefficient of 3.2% cm^{-1}. Slightly higher gains can be achieved with additional energy storage. A second identical amplifier unit is now being prepared to be followed shortly by a third 3 cm x 3 cm amplifier. The final 6 cm x 6 cm preamplifier will be a set of Lumonix 9 cm x 9 cm 0.5 meter TEA lasers now under procurement and due to arrive at NRL in November. The preamplifier chain will then be an all metal system without fault-prone dielectrics and will be a reliable and very rugged system.

4. <u>10 Liter e^-beam Amplifier</u>

Intensive efforts were undertaken in this last reporting period to investigate the suitability of the cold cathode high current density electron gun as the pre-ionizer for the 10 liter e^-beam amplifier. A joint series of experiments were conducted with Maxwell Laboratories and the Institute of Fluid Mechanics in Marseille to study the laser properties of a 10 liter discharge stabilized by a 10 cm x 100 cm cold cathode gun device. The experiments were successful and demonstrated that high current density beams can pump CO_2 in a short-pulse energy-storage mode. A peak gain of 4.9% cm^{-1} was achieved in a 3:½:1 mixture of $He:N_2:CO_2$ for a energy deposition of 226 J/ℓ. This figure represents an instantaneous energy storage of 5-6 joules of optical, 10.6 μ energy which can be extracted in a short pulse. A paper describing this experiment is included in the latter part of this report. A complete 10 cm x 100 cm cold cathode e^-beam system is now in the final stages of procurement. It is slated to be delivered to NRL in mid-December.

5. <u>Saturable Absorbers</u>

While a suitable gaseous or gaseous-mixture absorber which suppresses the entire CO_2 gain bands has not yet been discovered, these experiments are being continued. Present studies are now being concentrated on pressure broadened N_2F_4 and mixtures containing this gas because it displays an extremely wide absorption band. Since a suitable gas mixture which can cover the entire CO_2 spectrum will be difficult to find, experiments are also underway to investigate a combination of a dispersive element like a diffraction grating and a passive absorber. The diffraction grating would select out a single CO_2 transition by angular dispersion along the optical train while the saturable absorber would be needed to control the gain in the single transition of interest.

NEW LASER TECHNIQUES

During this reporting period several experiments have been planned and their construction initiated.

Prior investigations of the properties of potential vapor dye laser molecules were conducted using a laser fluorescence technique. A N_2 laser was borrowed for this task but had to be returned. Consequently the purchase of a N_2 laser has been negotiated and it will be delivered to NRL in October 1972. The laser will be used to help evaluate lifetimes of potential visible laser molecules.

Several optical components have been purchased to aid in the evaluation of solid state materials for high energy storage. These include etalons and frequency doubling crystals for YAG systems. This topic has a direct bearing on the solid state, ARPA supported, program.

Most of the current effort has been directed towards the production of visible laser systems, either chemically or electrically excited. It is unlikely that in general exothermic chemical reactions will selectively produce electronic state inversions in product molecules. Available data is sparse but suggests that reactions of the type $M + X_2 \rightarrow MX + X$ hold some promise. (M - rare earth; X - halogen). Fluorescence spectroscopy of Zare and coworkers on the reaction $Ba + F_2 \rightarrow BaF + F$ has shown that the A and B states of BaF are not produced but that the higher C state is. This is perhaps the only example of a simple metathetical reaction where an electronic inversion is created. In order to capitalize on this fact a reaction system has to be built so that the reagents can be mixed at a sufficiently high density to produce a useful gain on say the $C \rightarrow A$, or $C \rightarrow X$, transitions. An R-F induction heater has been built which will be used to vaporize Ba (or Ca etc.) in an oven which will act as a high pressure source of the metal atoms. The oven is also presently under construction. These will form a part of a high pressure, fast flow, fast mixing system in which the alkaline earth-halogen reactions will be investigated.

It is felt that electrical excitation of electronic states holds more promise in the future than chemically excited systems. The electron energy in a system can be tailored to match specific excitation cross-sections and the range of energies available is wider than those available in purely chemical driven schemes. The concept of double-pulse electrical excitation is being pursued. For example, all attempts to initiate copper vapor laser action using a simple pulse technique using a copper compound as the starting material rather than atomic copper have so far failed. The discharge conditions in a single pulse are most probably not suitable for both dissociation and subsequent excitation. A double-pulse technique where each pulse may be engineered to perform the individual tasks should hold more promise. Similarly, if laser action is to be attempted using chemically metastable radicals as the medium, it would be useful to have a pulse to form the radicals

(which takes a finite time governed by the reaction kinetics) followed by the excitation pulse. A combined R-F, TEA double discharge pulse apparatus is being designed to use as indicated above.

HIGH POWER GLASS LASER PROGRAM

1. Introduction

At the close of the last reporting period there were clearly a number of problem areas which required resolution if the NRL laser system was to operate at or near specification:

(a) the original configuration of the French VD 640 laser appeared drastically inappropriate for short pulse amplification. An intensive research effort was launched to optimize the system for subnanosecond pulses;

(b) a parasitic oscillation problem was discovered in the disc amplifier caused by self oscillation of individual discs at stored energy levels of about 0.4 J/cm^3. An experimental program was begun in which we evaluated a series of oscillation suppressing edge coatings developed by Owens Illinois Glass Co.

A parallel but closely coupled design effort to design a 1-2 kJ disc laser amplifier has been launched and a preliminary design is in hand.

We have also developed a mode-locked Nd:LaCaSoAp oscillator which produces time-bandwidth-limited operation for pulses as short as 5 psec. This represents a substantial extension of the state of the art from mode locked Nd:glass oscillators.

2. French Laser Modifications

During operation of the VD 640 with subnanosecond pulses in the previous reporting period, self-focusing damage was noted at levels well below that expected from reports of short pulse operation at other laboratories (Hindsight reveals that in the cases of Sandia and Rochester a large fraction of the energy was not contained in the short pulse but in the background.) Consideration of the self-focusing problem revealed several generally true prescriptions for operation when self-focusing is the limiting damage mechanism:

- use a minimum path length of glass (i.e. maximum gain per unit length),
- propagate a divergent spherical wave through the system as this will have a much higher self-focusing threshold,
- propagate a TEM_{oo} spatial mode.

Experiments on self-focusing in the various laser glasses were performed and it was found that ED-2, LG-56 and MG-915 had essentially the same nonlinear index of refraction and additionally the nonlinear index of refraction was a constant for pulses from 20 psec to 250 psec. This implies that the self-focusing can follow any

temporal modulation on the pulse and give a much lower threshold for self-focusing. Thus, a further prescription for optimum operation is

- use a time-bandwidth limited oscillator.

These experiments are reported in more detail in Appendix 1.

These dicta were implemented in the following fashion to optimize the VD 640.

- modification of the oscillator to incorporate a bandwidth selecting etalon as the front mirror of the oscillator. In this mode of operation, if a pulse is generated it has no fine grain modulation (if the etalon is misaligned no pulse is generated). Zero degree sapphire was chosen since the etalon reflectivity (25%) is very near the optimum coupling reflectivity,

- Owens-Illinois ED-2 rods were obtained for the system (on another contract). The higher gain/joule stored of this glass allowed us to reduce the path length of glass in the system by 85 cm and also to stage for a 4 x energy gain/stage,

- very careful alignment procedures were worked out to ensure that the mode propagated would in fact remain very close to a TEM_{oo} spatial mode.

Figure 1 shows the present system configuration as used for experiments (through the 45 mm stage) and for disc laser testing with the full system. The improved alignment has worked quite well to a point, in that through the 45 mm amplifier 25 joule, 250 psec and 40 joule, 900 psec pulses have been obtained with an essentially diffraction limited beam quality for several hundred shots. Figure 2 shows a shear plate interferogram of the pulse at 25 J in 250 psec (10^{11} watts) before recollimation. It can be seen that the maximum deviation from fringe linearity is $\sim 1/3$ fringe.

Unfortunately, this happy state of affairs does not prevail through the 64 mm rod at full power when there is pre-existing internal (or surface) rod damage. Up to $\simeq$ 40-50 joules in 250 psec the beam is well behaved and the shear pattern shown in Figure 3a is obtained. Above that level a rather dramatic change takes place. The beam essentially blows up in the sense that the divergence becomes abnormally high ($\sim$ 20-30 mr) and the beam becomes essentially depolarized and incoherent. Figure 3b shows a shear pattern taken when this effect is occurring. Experiments were run to elucidate the functional dependence of this phenomena at 250 psec and 900 psec. These experiments substantiated several features:

- when the effect occurs the output becomes essentially incoherent in that when it intercepts a straight edge, no diffraction pattern downstream is created,

- the effect seems to scale with power density in that the onset is proportionally higher at longer pulsewidths and near threshold only the beam center will show this behavior,

- geometrical effects (thermal lensing in the laser rods) are not of primary importance,

- the effect is not gross self-focusing of the entire beam in that the output wave does not originate from a point, but rather corresponds to severe wavefront distortion on a point-by-point basis,

- the effect is related to the past history of the laser rod in that a rod with no damage will operate without showing this effect up to quite high levels (> 100 J in 250 psec). Realistically it is a limitation to routine operation, since damage will occur sooner or later.

The most likely candidate effect is wavefront distortion around any damaged regions in the rod which at high intensity is strong enough to stabilize the Fresnel diffraction pattern downstream from the point of inception and give very severe localized wavefront distortion and subsequent beam steering. This mechanism has the requisite features to explain the experimental observations and the level at which it occurs ($\sim 10^{10}$ watts/cm^2) is reasonable.

3. Disc Laser Test Results

Since the close of the last reporting period, the parasitic oscillation problem in the present disc laser has been solved and a sufficient theoretical understanding has been developed to define the requirements for edge coatings for larger disc lasers.

To achieve the first objective, a black coating was designed by Owens-Illinois and applied to the NRL laser discs. The coating had an index of refraction of $\simeq 1.8$ at 1.06 μ and was sufficient to suppress parasitic oscillation at energy storages up to the design level of 0.6 J/cm^3 (see Appendix B for coating test). A series of experiments on the small signal gain coefficient of the disc laser with coated and uncoated discs were performed (Appendix C) and the performance with the coated discs was found to agree closely with the computer calculations.

The present generation coating is not unambiguously a success in that the laser-glass coating interface must be shielded from direct lamp irradiation to prevent shear damage in the laser glass caused by differential heating. Shields have been designed and installed which prevent this.

Table I lists the results of the latest sequence of active tests of the disc laser. It was not possible to achieve operation in the 400-500 joule regime because of the effects noted in the previous section but an output of 320 joules in a 900psec pulse was obtained.

The chief hinderance here was some depolarization of the input beam leading to a loss coefficient of ≃ 2% cm, rather than the much lower value of .5 - .75%/cm obtained with a well polarized input. The table lists the pump energy, input energy, actual output, computed output (with the actual loss) and computed output with the lower loss.

TABLE I

E_P(kJ)	E_{IN}(J)	E_{OUT}(J)	E_{CALC}(2%)	E_{CALC}(.75%)
118	60	220	220	250
113	70	280	275	320
150	110	320	325	395

The disc edge shields occluded ≃ 20% of the disc area so that a smaller beam diameter than that originally envisioned had to be used (50 cm^2 rather than 60 cm^2) which lowered the output level by ≃ 10%.

The output beam appeared to be well behaved and not subject to the beam breakup phenomena noted with the final rod amplifier although the energy density was 50% higher. This is reasonable since the path length through a disc is very short compared to an equivalent rod amplifier.

In summary, the disc amplifier seems to functionally behave as designed and we feel that the physics questions as to the viability of this concept have been answered. We are still limited at the present time in preparing a suitable input pulse to run the system to energies in excess of 400 joules but at least have a good understanding of system behavior at energy densities equivalent to operation at 400 joules.

4. 1-2 kJ Disc Amplifier Design

During the reporting period several design alternatives for a 1-2 kJ disc amplifier were generated and tradeoffs done on each one. The design constraints were:

- output energy of at least 1 kJ with a 300 joule input pulse; output of at least 2 kJ with a 500 joule input pulse,
- output energy density no higher than in the present device at the 500 joule level,
- aperture size no larger than practical to fabricate from a glass manufacturing standpoint at the present time,
- gain across the aperture no larger than practical from a parasitic oscillation standpoint (see Appendix D),

TABLE II

$\langle\epsilon\rangle$ J/cm^2 (at 2000 J	System No.	N(J/cm^3) (αD=2.5)[1]		ϵ_o (on all inputs a beam expander with 85% trans. was assumed)[2]			No. of 2 cm thick discs
				300 J Input (255 real input)	400 J Input (340 real input)	500 J Input (425 real input)	
4	20 x 40 cm discs 500 cm^2 aperture	0.4	exp 2.5	1500 J	1840 J	1920 J	17
			exp 3.0	1920 J	2100 J	2250 J	21
			exp 3.5	2250 J	2500 J	2600 J	24
6	17 x 34 cm discs 330 cm^2 aperture	0.5	exp 2.5	1280 J	1520 J	1870 J	15
			exp 3.0	1500 J	1870 J	2100 J	17
			exp 3.5	2000 J	2100 J	2300 J	20
8	14 x 28 cm discs 250 cm^2	0.6	exp 3.0	1490 J	1670 J	2000 J	15
			exp 3.5	1750 J	1970 J	2190 J	17
			exp 4.0	2010 J	2190 J	2360 J	19

1 This is parasitic oscillation limit estimated

2 A loss of 1%/cm was assumed in all cases

3 Assumes useful aperture is 6/7 of disc area (ratio for present device)

- coupling efficiency assumed to follow ZAP scaling as lamp packing densities are changed,

- loss coefficient assumed to be ~ 1%/cm.

Three design alternatives were chosen and the major features of each are specified in Table II. The first entry is a direct scaleup of the present system to twice the aperture size and the last represents the largest disc Owens-Illinois feels it is practical to fabricate with good optical quality at this time. The intermediate case represents a system with an output intensity at 2 kJ equivalent to what we have run in the present disc. In all cases the energy storage was varied to give a gain no higher than exp. (2.5) across the disc.

Present indications are that either the first or the second (and probably the second) is the best choice from the standpoint of efficiency. One further design constraint has been added from a systems standpoint:

- the aperture size shall be small enough to permit a Faraday rotator isolator to be added on the output to isolate the laser from the target.

The tradeoff here is not as clear in detail but certain features are obvious. For a given uniformity (i.e. extinction ratio) the energy in the rotator magnetic field will increase as the cube of the diameter. The difficulties of obtaining high Verdet constant, high damage threshold glass in this size cannot be exactly evaluated yet but they are appreciable. Table III illustrates this dilemma for a coil designed for 10^3 extinction ratio with Owens-Illinois EY-1 and Schott SF-6

TABLE III

DESIGN	$E_{(EY-1)}$ kJ	$E_{(SF-6)}$ kJ
1	60	360
2	130	780
3	200	1200

Owens-Illinois EY-1 is a variant of the basic ED-4 glass with 40% Terbium oxide by weight. If the glass technology proves out this glass will be the choice for large aperture Faraday rotators. The numbers given in Table III are based on the measurements done at NRL (Appendix E).

5. Short Pulse Bandwidth Limited Oscillators

During this reporting period, we have investigated extending the methodology used to develop the mode locked Nd:YAℓG lasers to other hosts with the objective of generating shorter pulses while maintaining time-bandwidth limited operation.

The selection criteria for materials for this usage were:

- broader fluorescence linewidth than neodymium:YAG

- crystalline host so that the nonlinear index of refraction would be small compared to Nd:glass.

The first candidate material tried has been evaluated and found to perform with fairly spectacular results. This material is Nd doped into a Lanthanum Calcium Sodium Apatite structure (SOAP) which has been developed by Westinghouse. Our results to date indicate: (see Appendix F)

- time bandwidth limited operation ~ 5-6 psec pulses

- pulse trains with > 10% of the energy in the strongest pulse

- an emission wavelength 10611.4A which overlaps the second strongest transition in Nd:YAℓG preamps which can be used to amplify the oscillator pulses. A formal publication is in preparation at this time. Figure 4A shows a typical pulsetrain and Figure 4B shows the output spectrum of the pulses.

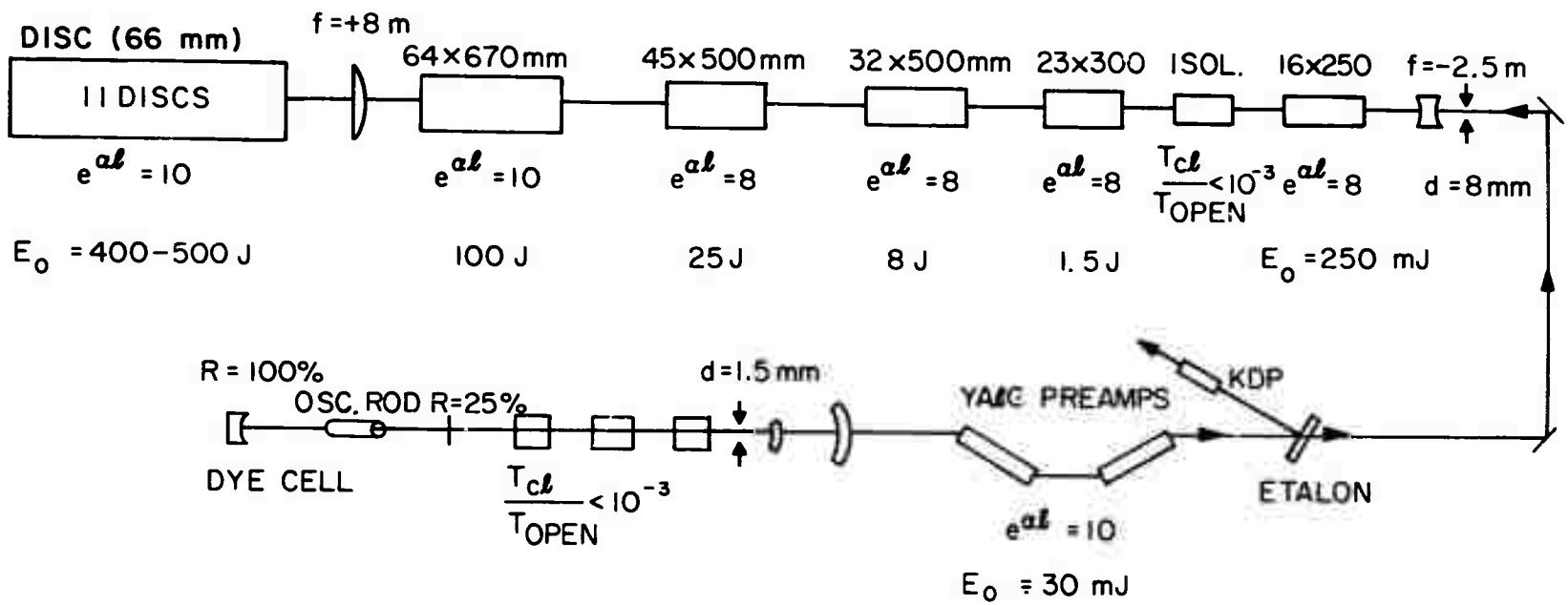

FIGURE 1. Present NRL Laser Configuration

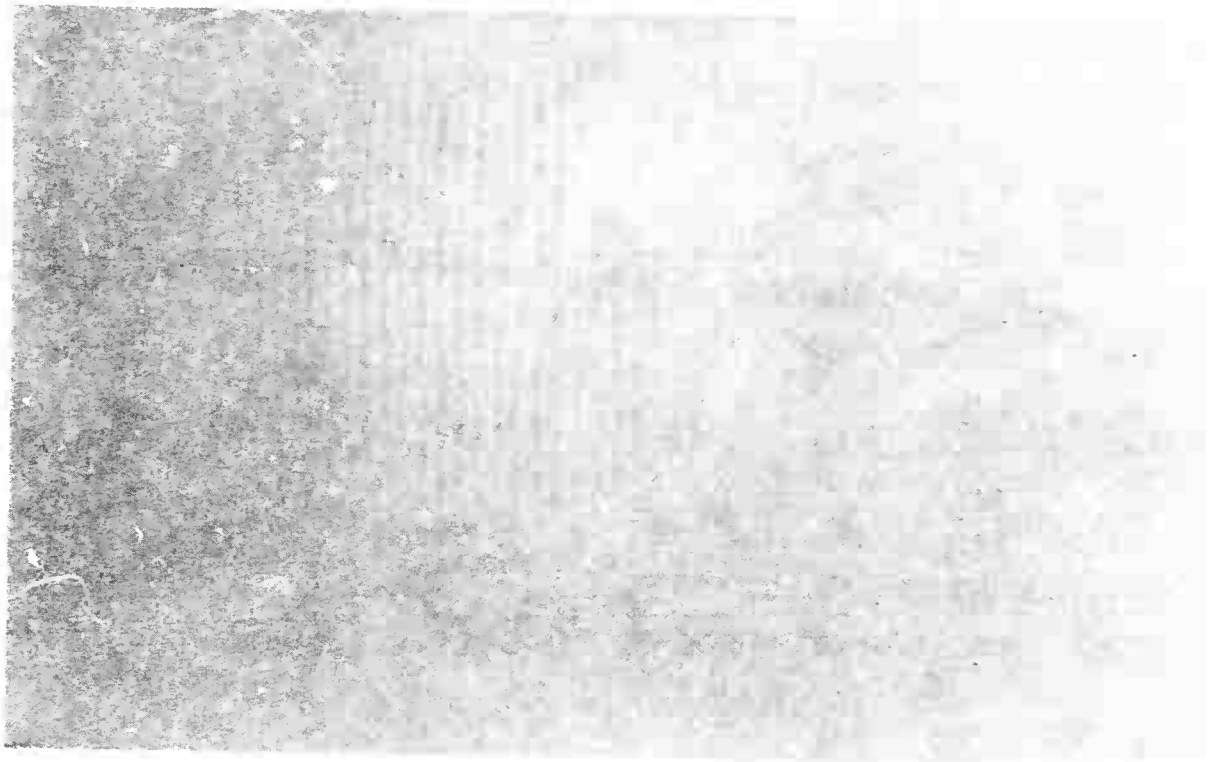

FIGURE 2. Shearing Plate Interferogram of 10^{11} W pulse

Reproduced from best available copy.

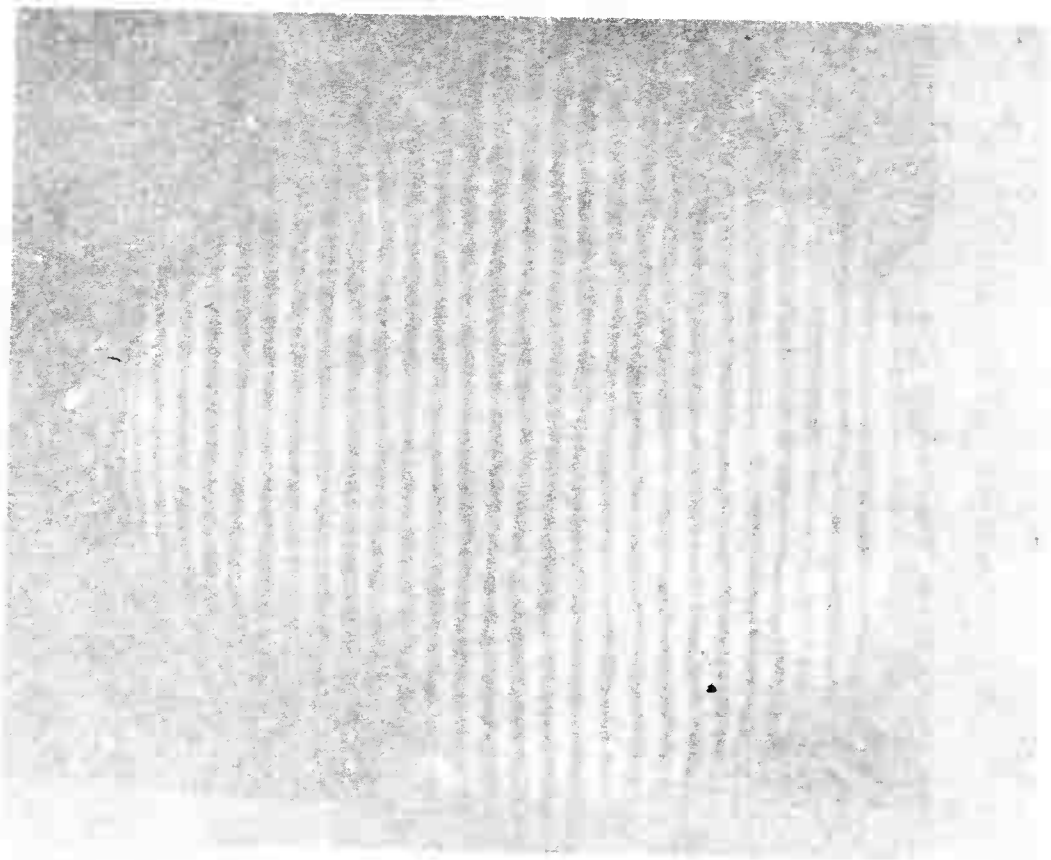

FIGURE 3a. Shearing Plate Interferogram of 50 J 250 psec pulse

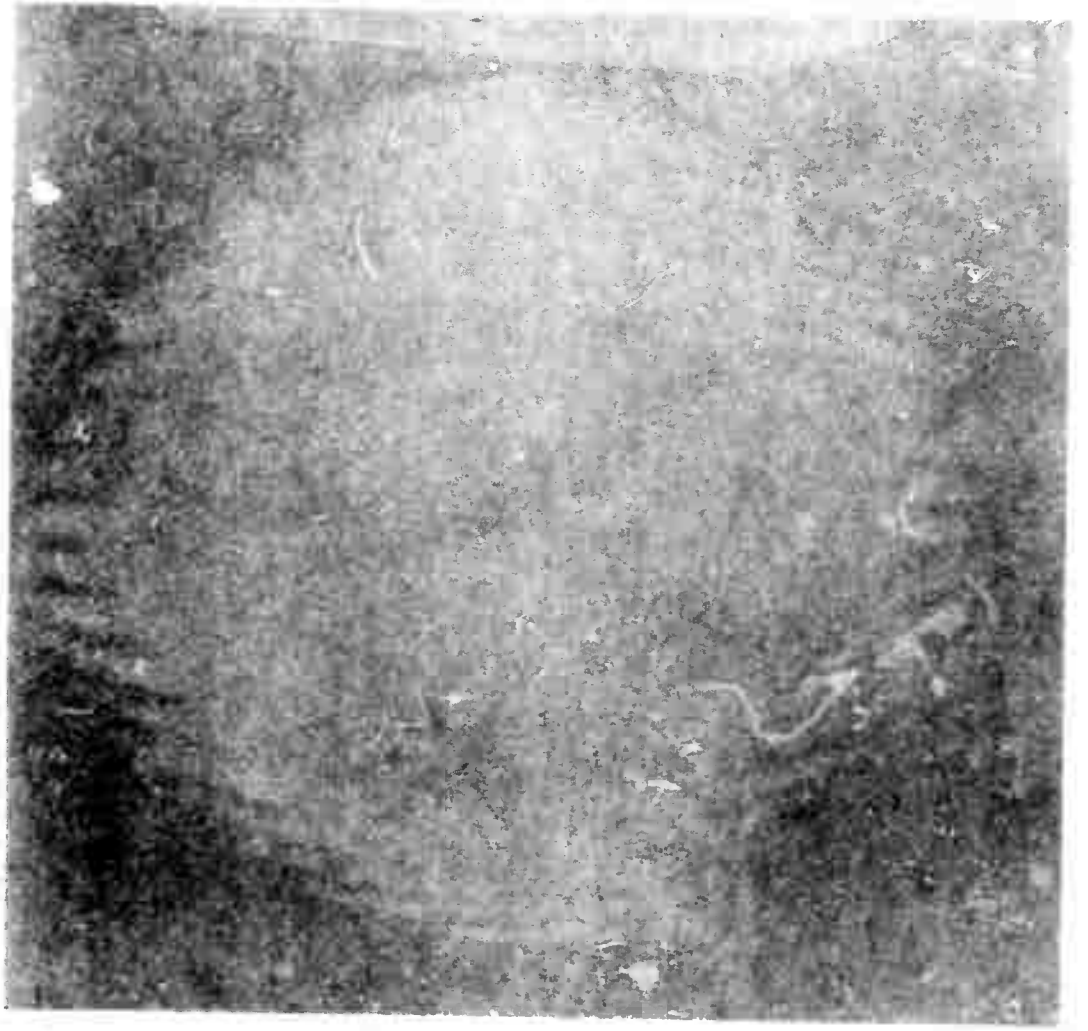

FIGURE 3b. Shearing Plate Interferogram of 60 J 250 psec pulse

APPENDIX A

A METHOD FOR MEASURING RELATIVE TRANSITION PROBABILITIES OF CASCADING MOLECULAR BANDS: APPLICATION TO CO FUNDAMENTAL BANDS*

N. Djeu
S.K. Searles

Laser Physics Branch
Optical Sciences Division

Naval Research Laboratory
Washington, D.C. 20390

ABSTRACT

A general method is presented to determine the relative transition probabilities for two molecular bands which have one vibrational level in common. It is based on optical gain (or loss) measurements on a number of vibration-rotation transitions in each of the two bands. The method has been applied to CO fundamental bands in the ground electronic state to yield $|R_v^{v+1}|^2/|R_{v-1}^v|^2$ for v = 6 through v = 11, where R_{v-1}^v is the rotationless matrix element of the dipole moment connecting the v-1th and vth vibrational levels. The results were fitted by using the wave function approximation for R_{v-1}^v, and the ratio $R_0^4/R_0^1 = 0.0002_1$ was obtained.

I. INTRODUCTION

Experimental radiative transition probabilities are directly available only for the lowest few vibrational bands in molecules, since they are determined from absorption or emission intensity measurements which require appreciable known populations in the absorbing or emitting states. Relative transition probabilities can be found for bands which share the same upper or lower vibrational level, inasmuch as no knowledge of the population density of the common level is required. But conventional intensity measurements do not yield information on the relative strengths of cascading bands. In this paper we report a general method which gives the transition probability for one band relative to that of a second which originates from the vibrational level that the first band terminates in. This opens up the possibility of determining the absolute transition probabilities for highly excited bands from known low lying band intensities through

* This work was supported under ARPA Order 2062 by the Advanced Research Projects Agency.

successive ratios.

In the case of CO, the $v = 1 \rightarrow v = 0$ in the ground electronic state is the only fundamental band for which the transition probability has been measured[1]. Though various calculations yield values for the squares of the electric dipole matrix elements $|R^v_{v-1}|^2$ which agree with each other to within a few percent up through $v \simeq 10$, there has never been any direct experimental evidence to support those calculations. In measuring directly the ratios $|R^{v+1}_v|^2/|R^v_{v-1}|^2$, the present experiment corroborates the results of those calculations. The ratios $|R^{v+1}_v|^2/|R^v_{v-1}|^2$ are first obtained from gain measurements on the P branch transitions of the $v = 6 \rightarrow v = 5$ through $v = 12 \rightarrow v = 11$ bands in a cw CO laser. They are then fitted to the theoretical model using the wave function approximation for the matrix elements. Each R^v_{v-1} is expanded in terms of $R_0{}^1$, with the expansion truncated after the first four terms. Using known values of $R_0{}^2/R_0{}^1$ and $R_0{}^3/R_0{}^1$, we determine $R_0{}^4/R_0{}^1$ from the experimental data. These numbers are then used to calculate $|R^v_{v-1}|^2$ in terms of $|R_0{}^1|^2$.

Because of the relatively low gain present in the CO laser, we had to resort to a rather unconventional method for gain measurements in order to obtain highly accurate data. A single mode, frequency scanned laser is used for that purpose. The laser oscillation range technique for measuring relative optical gains is described in some detail in Section III. Additional considerations about this technique can be found in a forthcoming paper[3].

II. BASIS FOR EXPERIMENT

Consider a molecular system with its vibrational levels greatly overpopulated with respect to the translation-rotation temperature. These conditions are commonly found in electrical discharges, exothermic chemical reactions, gasdynamic expansions, etc. The optical gain (or loss) distribution of the rotational fine structure of a vibrational band in such a system is characterized by the rotational temperature and the ratio of the population densities of the two connected vibrational levels. The distribution is a very sensitive function of the latter if the two vibrational levels have comparable population densities. This fact allows one to determine the relative densities of the two vibrational levels from the rotational gain-loss distribution of the band.[4] If measurements are made on two cascading bands in a molecule, the ratio of the two corresponding transition probabilities can be found. In what follows we restrict our attention to diatomic molecules, but the principle can clearly be extended to polyatomic molecules.

The small signal optical gain coefficient for the P branch vibration-rotation transition $(v, J-1) \rightarrow (v-1, J)$ with mixed Doppler and pressure broadening can be written as follows:[5,6]

$$\alpha^{v,v-1}_{P(J)}(\nu) = \frac{8\pi^3}{3kT}\sqrt{\frac{Mc^2}{2\pi kT}}\ |R^v_{v-1}|^2\ J\ f(v,P(J))$$

$$X\left[N_v B_v \exp\left(-F_v(J-1)h\ c/kT\right) - N_{v-1}B_{v-1}\exp\left(-F_{v-1}(J)h\ c/kT\right)\right]$$

$$X\ \mathrm{Re}\ w\left(\frac{2(\nu-\nu(v,P(J))}{\Delta\nu_D(\nu)}\sqrt{\ln 2} + i\ \frac{\Delta\nu_p(v,P(J))}{\Delta\nu_D(\nu)}\sqrt{\ln 2}\right) \qquad (1)$$

Here k is the Boltzmann constant, T is the temperature of the medium (assumed to be the same for translation and rotation), M is the molecular mass, c is the velocity of light, and N_v and B_v are the population density and the rotational constant for the vth vibrational level. Also $|R^v_{v-1}|^2$ and $f(v, P(J))$ are the rotationless matrix element and the vibration-rotation interaction factor for the transition, and $\nu(v, P(J))$ and $\Delta\nu_p(v, P(J))$ are the line center frequency and the pressure broadened width (including natural broadening) of the transition. The rotational energy function $F_v(J-1)$ and the Doppler broadened width $\Delta\nu_p(\nu)$ are given by

$$F_v(J-1) \simeq B_b(J-1)\ J$$

and

$$\Delta\nu_D(\nu) = \frac{2\nu}{c}\sqrt{\frac{2kT}{M}}\ \ln 2.$$

Finally, Re w (x + iy) is the real part of the complex error function.[7]

This somewhat involved expression can be understood in two parts. The part preceeding Re w gives the gain at linecenter of the vibration-rotation transitions,[5] while the function Re w itself is simply the lineshape function for mixed pressure and Doppler broadening.[8] Note that the linecenter gain distribution is not appreciably altered by pressure broadening so long as the J dependence of the pressure broadened width is slight.

In general, all the spectroscopic constants in Eq. (1) are known so that the only parameters to be determined are T, $\Delta\nu_p$, $|R^v_{v-1}|^2$ N_v and N_{v-1}. However the last three quantities only appear in the form of the products $|R^v_{v-1}|^2\ N_v$ and $|R^v_{v-1}|^2\ N_{v-1}$. This means that there are in effect only four unknowns in Eq. (1). It also means that neither the matrix element $|R^v_{v-1}|^2$ nor the population densities N_v and N_{v-1} can be

determined uniquely from fitting Eq. (1) to experimental data on rotational gain distributions. However, if gain distributions are known for two successive bands $v + 1 \rightarrow v$ and $v \rightarrow v - 1$, it is clear that the ratio $|R_v^{v+1}|^2/|R_{v-1}^v|^2$ can be obtained from $|R_v^{v+1}|^2 N_v$ and $|R_{v-1}^v|^2 N_v$. Furthermore, only relative gains for the two bands are needed, since the population density of the common vibrational levels cancels itself when the ratio is taken.

For some applications, the quantity of real physical significance is the Einstein A coefficient. For the P(J) transition it is related to the rotationless matrix element $|R_{v-1}^v|^2$ by the equation

$$A(v, J-1) = \frac{64\pi^4}{3h\lambda^3} \frac{|R_{v-1}^v|^2 \, J \, f(v, P(J))}{2 \, J-1} . \tag{2}$$

So long as the vibration-rotation interaction is small (i.e. $f(v, P(J)) \simeq 1$), we have

$$\frac{A(v+1, J-1)}{A(v, J-1)} = \left(\frac{\lambda_{P(J)}^v}{\lambda_{P(J)}^{v+1}}\right)^3 \frac{|R_v^{v+1}|^2}{|R_{v-1}^v|^2} \tag{3}$$

where $\lambda_{P(J)}^v$ is the wavelength of the P(J) transition in the $v \rightarrow v - 1$ band. It should be pointed out that the ratio in (3) is taken between A coefficients for transitions connecting the same rotational levels. This condition is implicitly assumed whenever we mention ratio of Einstein A coefficients in this paper.

III. TECHNIQUE

The ratios $|R_v^{v+1}|^2/|R_{v-1}^v|^2$ are expected to vary only slightly with v after the first few vibrational levels. It is therefore essential that highly accurate relative gain distributions be obtained, so that the v dependence of the matrix element ratios is not obscured by the scatter of the experimental results. Conventionally gain measurements are made by sending the output from a laser oscillator through a second gain tube (the amplifier) and noting the increase in the transmitted signal when the amplifier is turned on.[4] But with that method it is very difficult to measure small gains with good accuracy. Typically the relative error for a measurement giving a 10% optical gain would be roughly 10%. To circumvent this difficulty, we have developed a new technique which has the additional advantage of requiring only one gain tube, the oscillator itself. The remainder of this section will be devoted to a detailed description of this new technique.

We begin with a discussion on the operation of a single mode frequency tuned laser. Consider first the single mode oscillation condition in a laser illustrated in Fig. 1. The gain profile of the laser medium as a function of frequency is given by the factor Re w in Eq. (1). The cavity loss, on the other hand, is generally frequency independent. It is represented by the horizontal dashed line. The laser cavity as a whole has net gain only in the frequency range $\Delta\nu$. But the condition that there is net gain over part of the gain curve does not by itself mean that there will be laser oscillation. Whatever medium is inside a laser cavity of length £, there can be oscillation only at the discrete set of frequencies given by n c/2£, where n is an integer.[9] The cavity is said to have modes separated by c/2£ shown as short vertical lines on the frequency axis. Whenever one of these cavity modes falls at a frequency for which laser gain exceeds cavity loss, there will be oscillation at that frequency. For the case illustrated in Fig. 1, there would be oscillation at the frequency of the middle mode. Furthermore, the middle mode is the only mode that falls within $\Delta\nu$, creating a situation known as single mode operation.

When the cavity length is changed, each cavity mode will move along the frequency axis. In that process, the frequency of laser oscillation changes accordingly, resulting in a frequency scanned (or tuned) laser output. For a cavity length change equal to one half the wavelength of the laser transition, one cavity mode is moved to the position previously occupied by its adjacent mode. In practice, the change in cavity length can be accomplished by, for example, the use of a piezoelectric transducer which converts an applied ramp voltage into a linear translation. So long as $\Delta\nu < c/2£$ there can be at most one mode oscillating at any time. The output of such a laser is then called a single mode frequency tuning curve. Since $\Delta\nu$ is the frequency range over which there is oscillation as the cavity length is swept, it is known as the laser oscillation range. A schematic of a single mode tuning curve is illustrated in Fig. 3 near the detector. The frequency range covered by each mode is c/2£ centered at the line center of the transition.

Consider now a distribution of gain profiles for a number of P branch transitions in a vibration-rotation band as illustrated in Fig. 2. The actual spacing between lines is typically 10^3 times the linewidth at a pressure of a few torr. The precise distribution of these lines, including the frequency dependence of each, is given by Eq. (1). In the particular example shown in Fig. 2 three of the transitions have sufficient gain to overcome threshold. Therefore, each of these can be made to produce a single mode frequency tuning curve in a wavelength selective cavity, provided that the oscillation range for the P(J) transition $\Delta\nu_{P(J)} < c/2£$ for each J. The dispersive element used for wavelength selection is typically a prism or a diffraction grating. If the wavelength dependence of its optical loss is slight in the region of interest, one can assume that the cavity loss is the same for all transitions. It is clear then that there is a

definite relationship between the cavity loss and the oscillation ranges $\Delta\nu_{P(J)}$ on the one hand and the parameters in Eq. (1) on the other hand. Given a sufficient number of $\Delta\nu_{P(U)}$ for a fixed cavity loss, one should be able to determine the products $|R^{v}_{v-1}|^2 N_v$ and $|R^{v}_{v-1}|^2 N_{v-1}$ (relative to the cavity loss), the pressure broadened width $\Delta\nu_p$, as well as the temperature of the medium T. Suppose one introduces a frequency independent variable loss ℓ, e.g., variable diameter iris, into the laser cavity in addition to the fixed loss L. Then the experiment can be done for a number of $L + \ell$, and statistical averages can be taken.

IV. EXPERIMENT AND RESULTS

The experimental arrangement used for making the relative gain measurements is shown schematically in Fig. 3. The CO gain tube contained a flowing mixture of 0.3 torr CO, 0.2 torr air, and 2.5 torr He. It was excited by a 3 mA D.C. glow discharge with less than 1% ripple. The discharge was 0.5 m long, and approximately 85% of its length was cooled by liquid nitrogen. The 2.55 m cavity was formed by a 3 m radius of curvature silver mirror and a 300 lines/mm grating blazed for 4 μm. The mirror-grating assembly was mounted on an air-bags suspended steel beam which was physically isolated from the discharge tube. The mirror was attached to a piezoelectric transducer modulated by a ramp voltage repeated at $\sim$ 1 sec intervals. A variable-diameter iris was placed directly in front of the mirror both to insure fundamental mode operation and to act as a variable loss device. To minimize water vapor interference, the regions between the NaCl Brewster's angle windows and the mirror (grating) were flushed with N_2 except for about 10 cm near the grating. The frequency scanned laser output was coupled off the grating and sent into a gold doped germanium detector. One sweep of the piezoelectric transducer would generally cover two modes. Photographs were taken of the frequency scanned signal displayed on an oscilloscope. Since the separation between adjacent modes, $c/2\mathcal{L}$, is known, the oscillation ranges were readily calculated.

The experiment was done in two steps. The first was a determination of the lineshape function Re w, for which $\Delta\nu_p$ and T were needed. The oscillation ranges of four or more P branch transitions in one band were measured for a given setting of the iris. For a chosen set of $\Delta\nu_p$ and T the line center gain $\alpha^{exp}_{P(J)}$ relative to total cavity loss $L + \ell$ was calculated for each transition according to

$$\frac{L + \ell}{\alpha^{exp}_{P(J)}} = \frac{\mathrm{Re}\ w\left(\frac{\Delta\nu_{P(J)}}{\Delta\nu_D}\sqrt{\ln 2} + i\ \frac{\Delta\nu_p}{\Delta\nu_D}\sqrt{\ln 2}\right)}{\mathrm{Re}\ w\ \ i\left(\frac{\Delta\nu_p}{\Delta\nu_D}\sqrt{\ln 2}\right)} \qquad (4)$$

where the J dependence of $\Delta\nu_p$ has been dropped. Then a linear least square fit by varying $|R^v_{v-1}|^2 N_v$ and $|R^v_{v-1}|^2 N_{v-1}$ was performed to minimize

$$\chi^2 = \sum_J \left| \frac{\alpha^{exp}_{P(J)} - \alpha_{P(J)}}{\alpha^{exp}_{P(J)}} \right|^2 \qquad (5)$$

where $\alpha_{P(J)}$ is the line center gain calculated from Eq. (1) using the assumed T, $|R^v_{v-1}|^2 N_v$, and $|R^v_{v-1}|^2 N_{v-1}$. The value of χ^2_{min} minimized by the parameters $|R^v_{v-1}|^2 N_v$ and $|R^v_{v-1}|^2 N_{v-1}$, as a function of $\Delta\nu_p$ and T showed a local minimum at T = 90°K and $\Delta\nu_p/\Delta\nu_D = 0.27$.[3] These numbers are very reasonable in view of the following considerations. The value of the optical collision frequency of 6.2×10^7 sec^{-1} implied by the measured $\Delta\nu_p$ is to be compared with the hard sphere collision frequency of 6×10^7 sec^{-1} for ground state CO at the partial pressures of He, CO, and air used and a temperature of 90°K.[11] On the other hand, assuming that all the electrical energy into the discharge is dissipated into heat which is distributed uniformly across the laser tube, we estimate a temperature of 94°K at the center of the tube.

Once the lineshape function was determined, a second experiment was performed to get more accurate values for the parameters $|R^v_{v-1}|^2 N_v$ and $|R^v_{v-1}|^2 N_{v-1}$. Oscillation ranges for all the lasing transitions within each band were measured at a large number of cavity losses. Relative line center gains at each $L + \ell$ were calculated using Eq. (4) with the previously determined values of $\Delta\nu_p$ and T. Relative gains obtained at different cavity losses were all normalized to one arbitrary scale so that averages could be taken. Two runs, each covering four consecutive bands, were made under slightly different gain medium conditions. The respective averaged results are summarized in two columns in Table 1. The numbers given for each run are on the same arbitrary scale, but the results for the two different runs should not be compared directly.

The linecenter gains given in Table 1 were least square fitted by Eq. (1) without the lineshape factor to yield $|R^v_{v-1}|^2 N_v$ and $|R^v_{v-1}|^2 N_{v-1}$. The least square error χ^2_{min} was calculated according to Eq. (5) with the temperature T varied 1°K at a time. The minimum in χ^2_{min} occurred at the same temperature for all bands to within a few degrees. The T giving the smallest χ^2_{min} regardless of band was chosen as the true temperature for each run. They were T = 91°K and 93°K for the first and second runs respectively. The experimentally measured gain distribution and the best theoretical fit for the $v = 7 \rightarrow v = 6$ band are shown as the points and the solid curve in Fig. 4. The largest deviation of an

experimental point from theory is about 1%. Finally, ratios of the best $|R_v^{v+1}|^2 N_v$ and $|R_{v-1}^{v}|^2 N_v$ at the true temperature were taken, and we obtained the ratios of the matrix elements shown as open circles in Fig. 5. Each circle in this figure actually represents a grand average inasmuch as it is derived from a statistical fit of the relative rotational gain distributions of two consecutive bands which are averages of data obtained at different cavity losses.

V. ANALYSIS

The matrix elements in Eq. (1) are defined by

$$R_v^{v+1} = \int \Psi_v M(r)\ \Psi_{v+1}\ dr \tag{6}$$

where Ψ_v and Ψ_{v+1} are the vibrational wave functions, and the dipole moment function $M(r)$ is usually expressed in a Taylor series expansion about the equilibrium nuclear separation r_e as

$$M(r) = \sum_{i=0}^{\infty} M_i\ (r - r_e)^i \quad . \tag{7}$$

For the CO molecule, the coefficients M_i have been determined through $i = 3$ from absorption intensity data on the fundamental and the first two overtone bands.[1,12] However, the matrix elements $|R_v^{v+1}|^2$ calculated by Young and Eachus using their derived dipole moment coefficients are noticeably smaller than those implied by our results. The discrepancy is perhaps to be expected in view of the large uncertainties in the M_i. Moreover, probably the quartic term in Eq. (7) should be included in the evaluation of $|R_v^{v+1}|^2$ for the high v levels needed in the present work.

An alternative way of expressing the dipole moment function is to expand it in terms of all the matrix elements connecting the ground vibrational level as follows:[2,13]

$$M(r) = \sum_{i=0}^{\infty} R_0^i\ \Psi_i/\Psi_0. \tag{8}$$

The matrix elements for the fundamental bands can then be written as

$$R_v^{v+1} = \sum_{i=1}^{\infty} R_0^i \int \left(\Psi_{v+1}\Psi_v/\Psi_0\right) \Psi_i\ dr. \tag{9}$$

Because of the rapid decrease of R_0^i with i, only the first few terms are needed in the actual calculation. After Trischka and Salwen,[2] we shall refer to this approach as the wave function approximation. The integrals $C_v^{v+1}(i) = \int\left(\Psi_{v+1}\Psi_v/\Psi_0\right)\Psi_i dr$ appearing in Eq. (9) have been evaluated by Herman and Rubin[14] for the case of the Morse oscillator. They obtained the formula

$$C_{v-1}^{v}(i) = \sqrt{\frac{(S-2i-1)_{2i}\,(S-2v+2)_{v-1}\,(S-2v)_v}{i!\,(v-1)!\,v!\,(S-2i)_i\,(S-2v-i)_{i+1}(S-2v-i)_{i-1}}}$$

$$\times \sum_{\ell=0}^{v-1}\sum_{m=0}^{v} \frac{(-v+1)_\ell}{\ell!}\,\frac{(-v)_m}{m!}\,\frac{(S-2v-i)_{\ell+m}}{(S-2v+2)_\ell\,(S-2v)_m}\,(2v-i-\ell-m)_i \qquad (10)$$

where

$$(a)_n = \begin{cases} a(a+1)\cdots(a+n-1); & n \geq 1 \\ 1; & n = 0 \end{cases}$$

and

$$S = 4\,D_e/\omega_e,$$

where D_e is the dissociation energy referred to the minimum of the potential curve and ω_e is the vibrational frequency for infinitesimal amplitude.

We chose to fit our results with the wave function approximation instead of the Taylor series expansion for two reasons. First, the matrix elements R_0^i (i = 1, 2, 3) are known with higher accuracy than the coefficients M_i (i = 1, 2, 3). Hence, the chances of improving the expansion in the former case seemed better. Also, the task of evaluating the coefficients $C_v^{v+1}(i)$ is simpler than doing the necessary integrals for the Taylor series expansion.

Since only the first three R_0^i in Eq. (9) are known, an approximation for R_v^{v+1} of the following form was used:

$$R_v^{v+1} = \sum_{i=1}^{3} R_0^i\,C_v^{v+1}(i) + R_0^{4*}\,C_v^{v+1}(4). \qquad (11)$$

The notation R_0^{4*} is used here to signify that the effect of the

truncation is absorbed by the last term.

Toth et al[1] have compiled in their paper a list of the various measured intensities of the CO 1-0, 2-0, and 3-0 bands. Taking the mean value for each band, we calculated the ratios $R_0^2/R_0^1 = 0.061$ and $R_0^3/R_0^1 = 0.0042$. The signs of all three matrix elements have been shown to be the same in Cashion's convention[13] by Young and Eachus.[12] These ratios were used in the data analysis.

The coefficients $C_v^{v+1}(i)$ were evaluated with $S = 4D_e/\omega_e = 167$[15] by use of a computer. All the necessary $C_v^{v+1}(i)$ could be calculated with sufficient accuracy when double precision arithmetic retaining 25 significant figures was employed. The ratios $|R_v^{v+1}|^2/|R_{v-1}^v|^2$ were then numerically least square fitted to the experimental data with the assumption that all experimental points have equal uncertainties. The smallest mean square error occurred for $R_0^{4*}/R_0^1 = 0.00014$ in the sign convention of Cashion. The ratios of matrix elements calculated from Eq. (11) using the R_0^2/R_0^1 and R_0^3/R_0^1 quoted in the preceding paragraph and the best R_0^{4*}/R_0^1 determined from the present experiment are shown as dots in Fig. 5. The dependence of the $C_v^{v+1}(i)$ on v and i is such that the contribution of higher R_0^i to R_v^{v+1} is greater for larger v. Consequently, the value of R_0^{4*} was determined mainly by the experimental points with higher v. This explains the relative closeness between the best calculated results and experiment to the right of the figure.

For $v \simeq 10$ each term in Eq. (11) is roughly one half of its preceding one in magnitude and has the opposite sign. If this trend continues for a few more terms, as one may reasonably expect, then the true R_0^4 should be approximately $1.5\ R_0^{4*}$. We thus estimate that $R_0^4/R_0^1 = 0.0002$. This, to our knowledge, is the first quantitative determination of R_0^4 for the CO molecule.

From the opening statement of the last paragraph, one sees immediately that a 10% change in R_0^{4*}/R_0^1 will be caused by a 2% change in R_0^2/R_0^1 or a 5% change in R_0^3/R_0^1. On the other hand, a 1% change in each of the experimental ratios in the same direction would result in a 40% change in R_0^{4*}/R_0^1. It thus appears that the principal uncertainty in R_0^{4*} may come from experimental errors in the present work. Figure 5 shows that the largest deviation of an experimental point from the best fit is about 2%. The laser tube used in the present experiment has only 85% of its discharge length cooled by a tube wall at 77°K. It is therefore expected that there would be slight axial variations in the vibrational level population densities as well as in the temperature. A laser tube with a more uniform active medium should yield improved results.

Once R_0^{4*}/R_0^1 is known, the matrix elements $|R_{v-1}^v|^2$ can be calculated with high accuracy from Eq. (11). The results when normalized to $|R_0^1|^2$ are displayed in Table 2. The variation of

$|R^v_{v-1}|^2$ with v is seen to be almost exactly linear, indicating that the effects of mechanical and electrical anharmonicities almost exactly cancel each other. Also shown in the table are the normalized Einstein A coefficients. Due to the frequency factor, they increase much less rapidly with v.

VI. CONCLUSION

In summary, we have presented a new method for measuring the relative transition probabilities of two consecutive molecular bands. The principal requirement for good accuracy of the technique is that all three vibrational levels involved be nearly equally populated. An application of this method to the fundamental bands in the CO ground electronic state has yielded for the first time the ratios $|R^{v+1}_v|^2/|R^v_{v-1}|^2$ for seven consecutive bands. The experimental ratios substantiate earlier calculations of $|R^v_{v-1}|^2$ for the same transitions. They imply an almost exactly linear dependence of $|R^v_{v-1}|^2$ on v.

It is of interest to compare the results from the present work with the theoretical calculations of Cashion.[13] By equating $R_1{}^v$ from the harmonic oscillator model to $R_1{}^v$ from the Morse oscillator model, he obtained an expression for $R_0{}^v/R_0{}^{v-1}$. He showed that all the $R_0{}^v$ should have the same sign for sufficiently low v. This has been demonstrated to be the case for CO, as we mentioned earlier, for the first three v by Young and Eachus.[12] The present experiment extends Cashion's contention to v = 4. The magnitude of $R_0{}^4$ obtained by us is only about 2/3 of the theoretical value calculated by Cashion. However as we have indicated in the last section, our value for $R_0{}^4$ could be in error by a fairly large fraction.

The method of measuring relative transition probabilities described inin this paper can be applied most immediately to the other existing molecular laser bands. In cases where the single pass optical gain is large, it may be more convenient to use the direct probe method for measuring gain rather than the laser oscillation range method which involves a fair amount of work in data reduction.

It is worthwhile to point out that an elaborate experimental procedure was adopted in the present work only because we desired an accuracy close to one percent for the ratios of the matrix elements. For many applications considerably lower accuracies would probably suffice.

The approach presented in Section II can also be used to deduce relative matrix elements for parallel bands which share the same upper or lower level. We emphasize that the method is equally applicable to molecular bands which are mostly absorbing. Thus, relative transition probabilities in molecular systems with optical loss can also be measured. This is an important point for the widespread use of the method, since only a limited number of molecular bands have been

observed to exhibit optical gain. Experiments on non-lasing bands should be practicable with the use of a tunable IR laser. Investigations of this type should prove to be particularly interesting for polyatomic molecules.

ACKNOWLEDGEMENTS

The authors would like to thank Drs. J.R. Airey, T. Cool and W.S. Watt as well as the referee for their helpful comments on the manuscript.

REFERENCES

1. R.A. Toth, R.H. Hunt, and E.K. Plyler, J. Mol. Spectry 32, 85 (1969).

2. J. Tirschka and H. Salwen, J. Chem. Phys. 31, 218 (1959).

3. N. Djeu and S.K. Searles, to be published in IEEE J. Quantum Electronics, Oct. 1972.

4. N. Djeu, T. Kan and G.J. Wolga, IEEE J. Quantum Electronics 4, 256 (1968).

5. C.K.N. Patel, Phys. Rev. 141, 71 (1966).

6. D.H. Close, Phys. Rev. 153, 360 (1967).

7. M. Abramowitz and I.A. Stegun, Editors, Handbook of Mathematical Functions (National Bureau of Standards, Washington, D.C. 1964).

8. The lineshape function is sometimes expressed in an integral form such as found in A.C.G. Mitchell and M.W. Zemansky, Resonance Radiation and Excited Atoms (Cambridge University Press, London, 1961).

9. To simplify the discussion, we are considering only the fundamental transverse mode. For a detailed account of laser resonator modes, the reader is referred to R.J. Pressley, Editor, Handbook of Lasers (The Chemical Rubber Co., Cleveland, Ohio, 1971). For our purposes, it is also a good approximation to neglect cavity-pulling effects. See, for example, W.R. Bennett, Jr., Phys. Rev. 126, 580 (1962).

10. D.A. Draegert and D. Williams, J. Opt. Soc. Am. 58, 1399 (1968).

11. J.O. Hirschfelder, C.F. Curtiss, and R.B. Bird, Molecular Theory of Gases and Liquids (John Wiley and Sons, New York, 1967).

12. L.A. Young and W.J. Eachus, J. Chem. Phys. 44, 4195 (1966).

13. K. Cashion, J. Mol. Spectry 10, 182 (1963).

14. R. Herman and R.J. Rubin, J. Chem. Phys. 32, 1393 (1960).

15. G. Herzberg, Spectra of Diatomic Molecules (Van Nostrand Reinhold Co., New York, 1950).

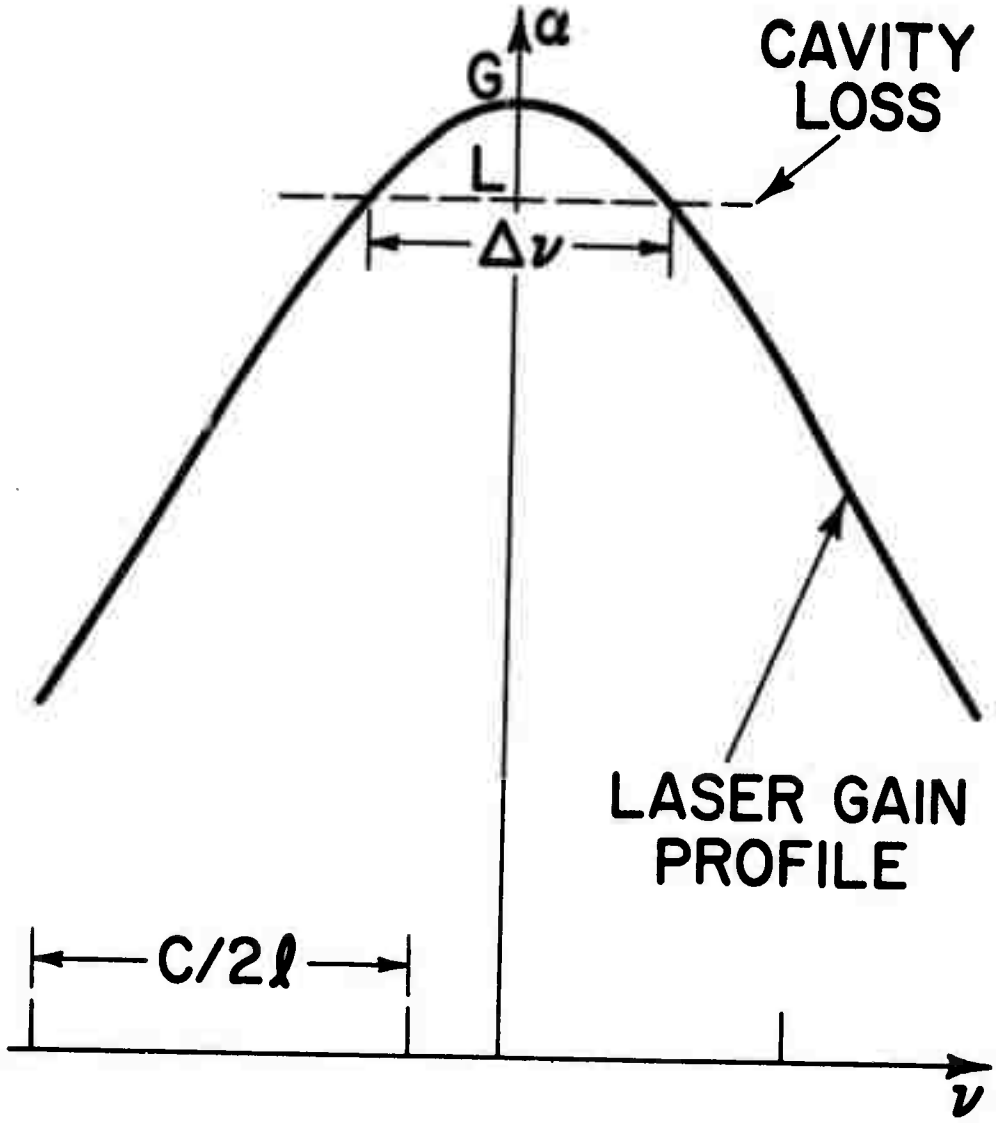

FIGURE 1

Illustration of single mode laser oscillation condition

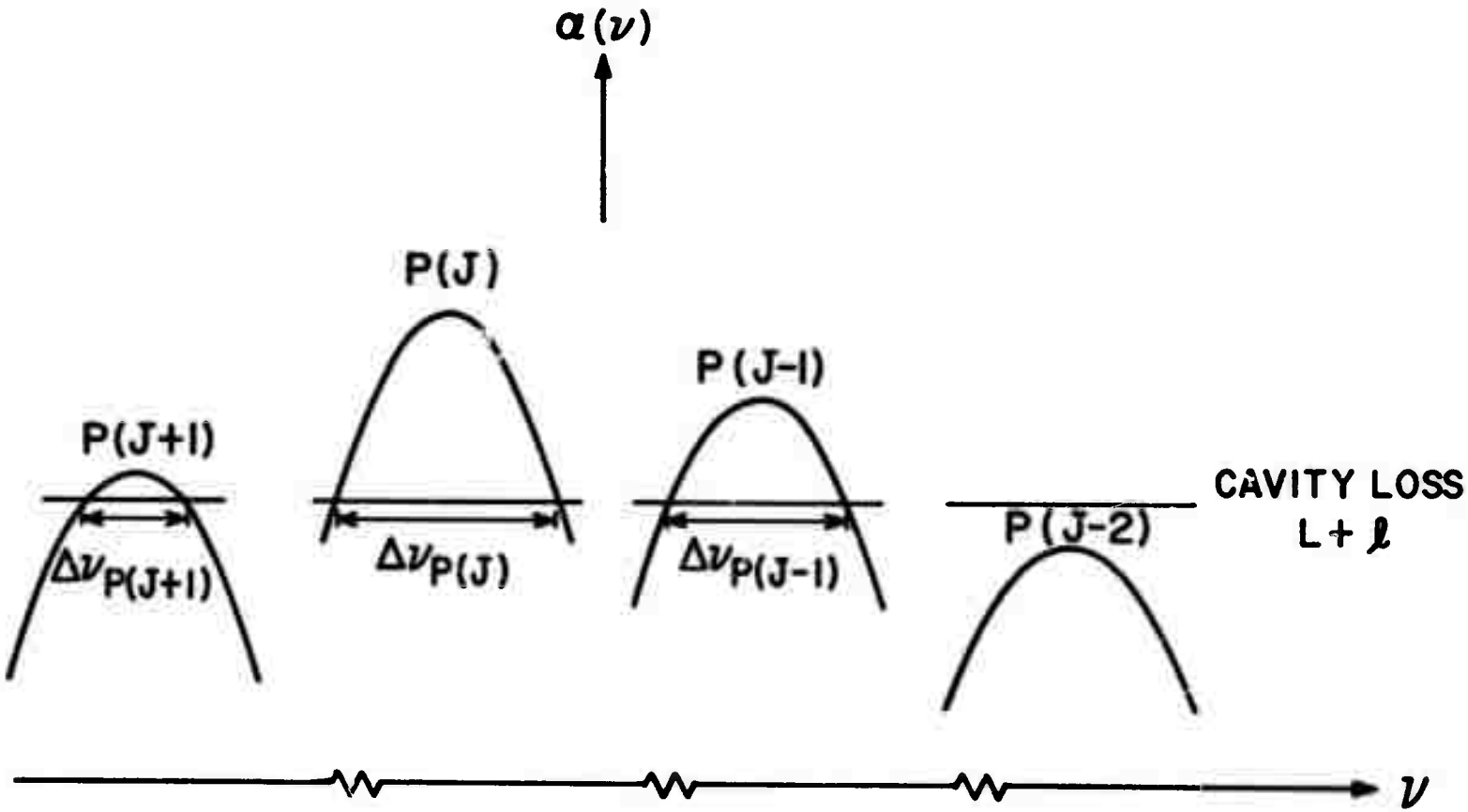

FIGURE 2

Illustration of laser oscillation ranges for a distribution of vibration-rotation transitions.

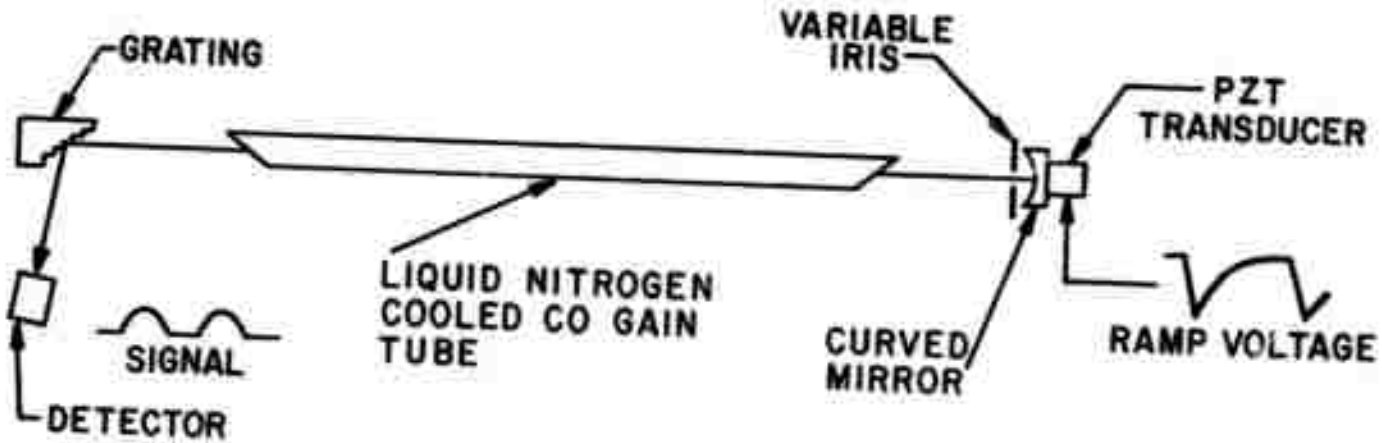

FIGURE 3

Schematic of apparatus

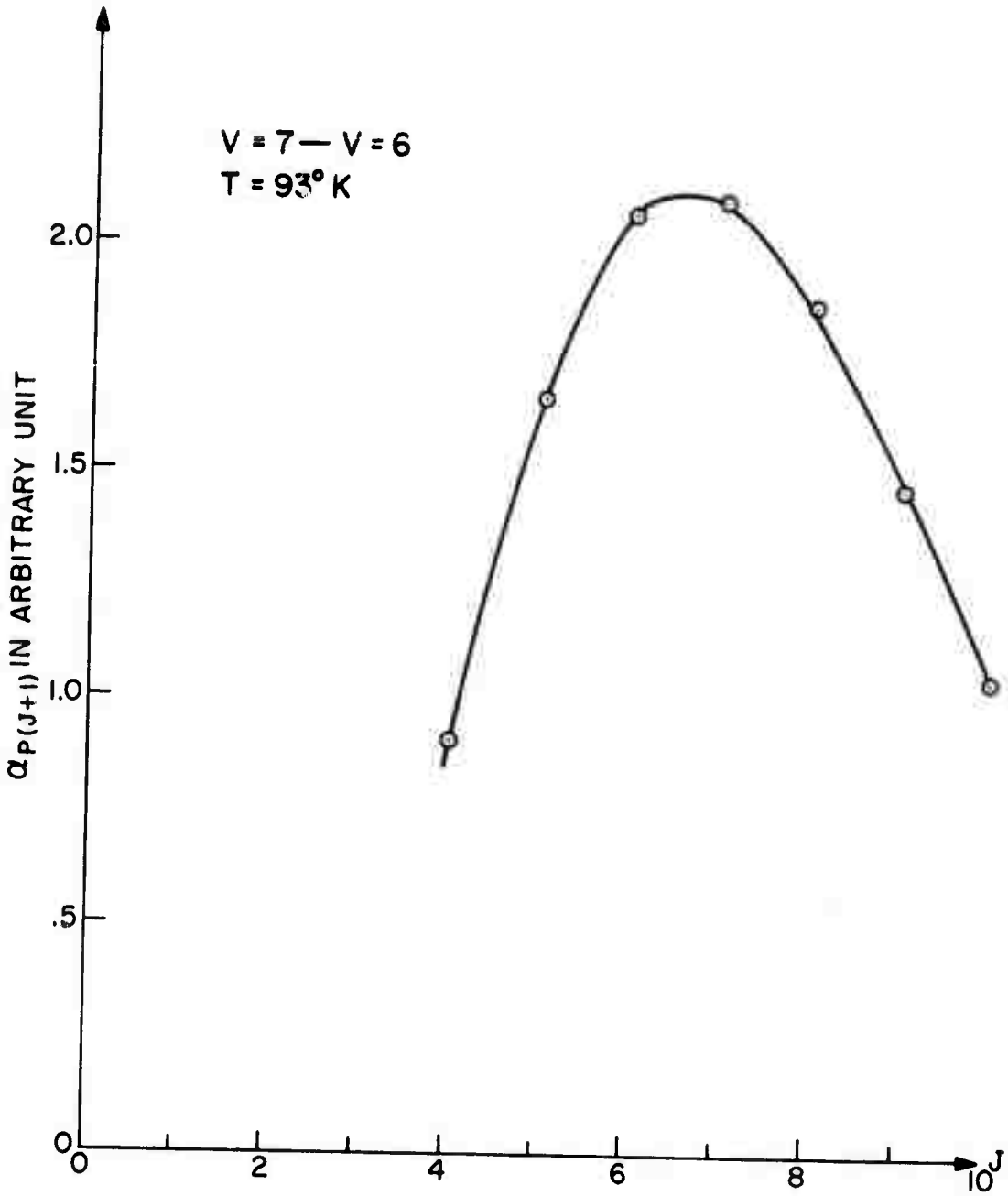

FIGURE 4

Experimental P branch linecenter gain distribution for $v = 7 \rightarrow v = 6$. The curve corresponds to a theoretical distribution with $T = 93°K$ and $N_7B_7/N_6B_6 = 0.792$.

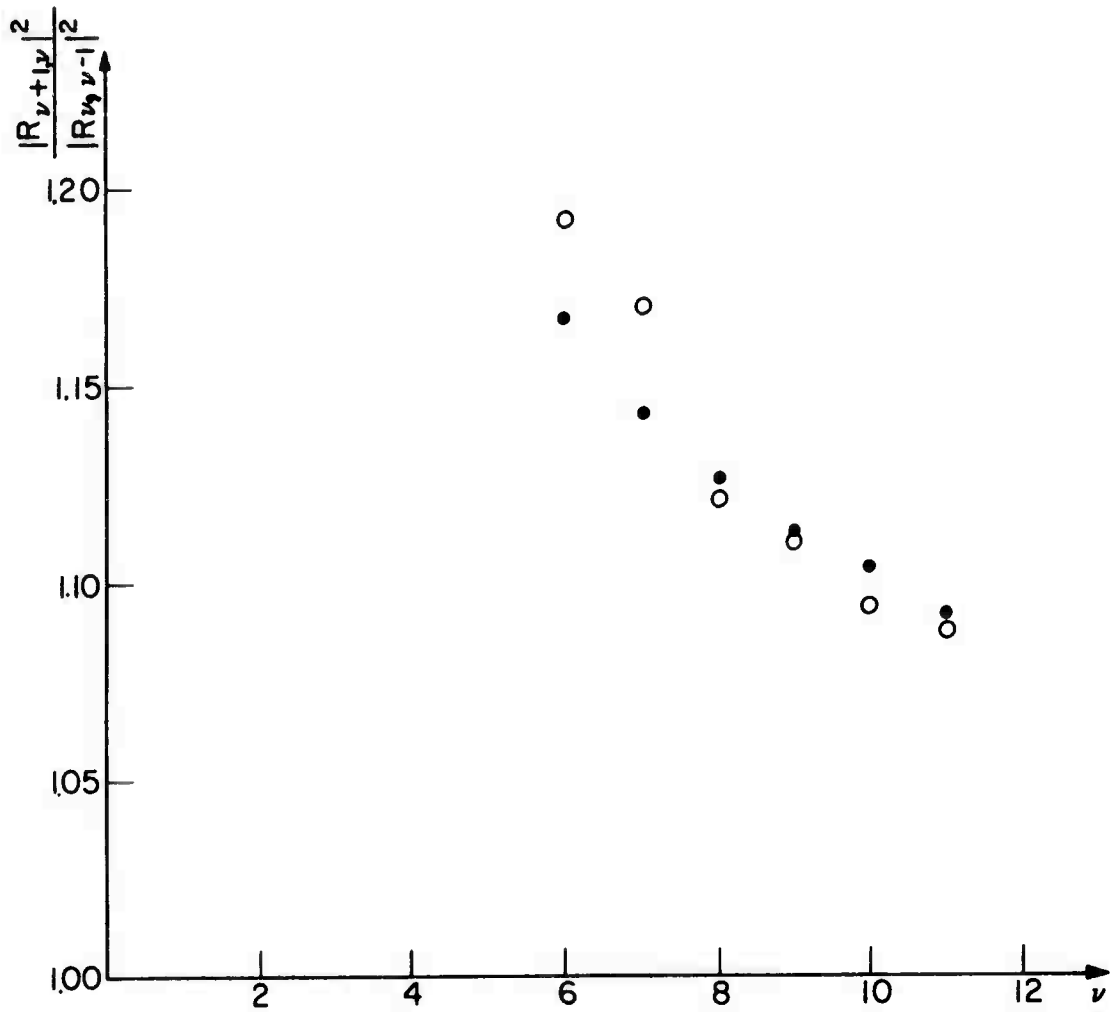

FIGURE 5

Ratio of matrix elements for adjacent CO fundamental bands as a function of v. Open circles are experimental values; dots are best theoretical fit.

TABLE 1

Experimental linecenter gain distributions. Results in the two columns are from two separate runs. Each set is on an arbitrary scale.

V+1→V	P(J)	$\alpha^{exp}_{P(J)}$	V+1→V	P(J)	$\alpha^{exp}_{P(J)}$
12→11	P(5)	0.890	9→8	P(5)	1.224
	P(6)	1.325		P(6)	1.834
	P(7)	1.483		P(7)	2.066
	P(8)	1.486		P(8)	2.094
	P(9)	1.235		P(9)	1.803
	P(10)	0.950		P(10)	1.425
	P(11)	0.669		P(11)	1.050
11→10	P(5)	0.995	8→7	P(5)	1.227
	P(6)	1.499		P(6)	1.897
	P(7)	1.740		P(7)	2.230
	P(8)	1.669		P(8)	2.215
	P(9)	1.364		P(9)	1.902
	P(10)	0.942		P(10)	1.481
	P(11)	0.712			
10→9	P(6)	1.612	7→6	P(5)	0.908
	P(7)	1.904		P(6)	1.660
	P(8)	1.833		P(7)	2.060
	P(9)	1.517		P(8)	2.092
	P(10)	1.060		P(9)	1.869
	P(11)	0.705		P(10)	1.465
				P(11)	1.047
9→8	P(5)	1.053	6→5	P(7)	1.318
	P(6)	1.725		P(8)	1.499
	P(7)	1.995		P(9)	1.509
	P(8)	1.991		P(10)	1.266
	P(9)	1.637		P(11)	0.945
	P(10)	1.165			
	P(11)	0.792			

TABLE 2

Matrix elements and corresponding Einstein A coefficients calculated from the wave function approximation using R_0^{4*} obtained from experimental results.

v	$\lvert R^v_{v-1}\rvert^2/\lvert R_0^{\ 1}\rvert^2$	$A^v_{v-1}/A_0^{\ 1}$
1	1.00	1.00
2	2.00	1.93
3	2.99	2.78
4	3.98	3.56
5	4.97	4.28
6	5.96	4.92
7	6.95	5.53
8	7.95	6.09
9	8.95	6.59
10	9.97	7.04
11	11.00	7.46
12	12.00	7.81

APPENDIX B

COLD CATHODE ELECTRON BEAM CONTROLLED CO_2 LASER AMPLIFIER*†

H.G. Ahlstrom and G. Inglesakis
Institute of Fluid Mechanics
Marseille, France

J.F. Holzrichter and T. Kan
Naval Research Laboratory
Washington, D.C. 20390

J. Jenson and A.C. Kolb
Maxwell Laboratories
San Diego, California 92123

ABSTRACT

A large area cold cathode (10 cm x 100 cm) electron gun has been constructed and used to control a CO_2 laser amplifier. Energy deposition of 226 J/liter in a time of 1 μsec has led to a gain of 4.9%/cm in an atmospheric pressure CO_2 laser mixture.

† To be published in Applied Physics Letters.

* This work was supported by the Advanced Research Projects Agency under ARPA Order 2062.

Recent experiments by Fenstermacher, Nutter, Leland and Boyer[1] and by Daugherty, Pugh, and Douglas-Hamilton[2] have shown that an electron beam will stabilize large volume CO_2 laser discharges. The electron guns for these experiments used thermionic emission from hot filaments in a diode[1] or tetrode[2] structure. Another possible source of electrons for laser control is the cold cathode. In contrast to the thermionic cathode which is capable of supplying moderate current densities ($< .1$ A/cm^2) for arbitrary pulse lengths, the cold cathode operates satisfactorily at high current densities (> 1 A/cm^2) and for time periods less than a few microseconds. A cold cathode electron gun is very simple in design, can be economical in certain applications, and is ideally suited for pumping laser amplifiers for an energy-storage mode of operation. Thus it is important to show that CO_2 laser media can be satisfactorily pumped under control of these high current density, short duration e-beams. We have constructed a large area (10 cm x 100 cm) planar cold cathode electron gun and have conducted preliminary experiments on the control of a discharge in a CO_2 laser amplifier.[3,4] Using a 3:½:1 mixture of $He:N_2:CO_2$ at atmospheric pressure, we have measured an unsaturated gain coefficient α of 4.9%/cm at 10.6 μ, for an energy input of 226 J/liter into the gas.

Work by Loda and DeHart[5] has demonstrated that large area cold cathodes (10 cm x 10 cm) can supply uniform electron current densities of 1 - 10 A/cm^2 at 200 keV for time durations of up to 5 μsec. These cathodes are in principle very simple. One merely applies a rapidly-rising voltage pulse to a conductor which has a sharp edge facing the anode. The most likely mechanism for diode operation begins with field emission from the regions of high field stress ($> 10^7$ V/cm) which are centered on sharp edges or whiskers. The rapid heating of these microscopic projections leads to their vaporization and the creation of a conducting plasma which serves as the source of electrons. This plasma, however, causes the impedance of the diode to collapse when it reaches the anode and short circuits the anode-cathode space. Before the impedance collapses the diode operates in a space charge limited mode[5] and the V-I relation approximately follows Child's law for a planar diode, $I = V^{3/2}/430d^2$, where d is the cathode-anode spacing in cm and V is the voltage on the diode in volts, and I is the current in amperes.

Our 10 cm x 100 cm cold cathode was constructed from strip razor blade material, in order to enhance plasma formation at the edge. The 10 cm long blades were oriented transverse to the axis of the gun and placed on .050" centers. The blades were rounded on the corners and held in a smoothly shaped holder which was mounted in the horizontal plane 5.5 cm from the foil support structure (see Fig. 1) on specially designed Teflon insulators. The diode was connected to a six-stage Marx generator, which erected to 200 kV in a time of 100 ns and had an output capacity of 0.05 μF. The $L\frac{di}{dt}$ voltage drop in the cable and cathode inductance reduced the cathode voltage by 44 kV. This yielded,

after 0.3 μsec, a current of 4 A/cm^2 which agrees with the calculated space-charge limit. If the transmission factor of the foil (.0015" Aℓ) and support structure are taken into account, one would observe a peak current density of $\sim$ 3 A/cm^2 in the laser gas. The experimental current density is estimated to be 0.3 to 0.8 A/cm^2 from the gas conductivity[1] and from Faraday cup measurements. The deviation from simple geometric transmission through the foil support structure is most likely caused by large transverse moments imparted to the electrons upon emission from the razor blade edges. This is supported by the results of J.C. Martin[6], which indicate that the half angle of electron emission from a razor blade cathode is about 45°.

Electron beam uniformity measurements are required to complete the studies of these electron guns. Moreover, higher diode voltages should be used to enhance the cathode plasma formation process and ensure good uniformity of emission. Measurements on the impedance collapse of the diode indicated that the plasma closed toward the anode at a rate of about 4 cm/μsec. This is greater than the rate measured by Loda and DeHart which is $\sim$ 1.5 cm/μsec.

The laser plasma was generated at atmospheric pressure between a 10 cm x 100 cm Aℓ anode and stainless steel wire cathodes (see Fig. 1). The electrode spacing for most experiments was 5.0 cm. The gas was contained in a plexiglass box which had been lined with absorbing material on the inside surface to prevent parasitic oscillation. In addition, the NaCl windows were canted in opposite directions and the Aℓ anode was sandblasted to prevent specular reflection. A sealed-off probe-laser utilizing an invar cavity was operated at 10.6 μ [P(18) to P(22)] to probe the amplifying medium. The probe beam was directed through the amplifier box, into a screen room, and on to an Au:Ge detector that was cooled to 77°K. The detector, bias circuit, and oscilloscope system had a risetime faster than 1 μsec, and the system was measured to be linear over the dynamic range of the gain measurements. The laser frequency was brought to line center with a piezoelectric translator; no beam wander due to the e-beam produced plasma was evident.

Figure 2 shows the gain coefficient plotted as a function of electrical energy deposited into the gas. In the insert of Figure 2 is a typical oscillogram showing the time history of the sustainer current pulse and development of the optical gain. Notice that the gain peaks in the afterglow of the sustainer discharge. Variations in the energy deposition into the laser plasma were achieved by changing the E/P ratio for a fixed pumping time of typically $\sim$ 1 μsec. The peak gain was measured for an E/P ratio of 6.6 kV/cm. Extrapolating from Fenstermacher's data[1], a 0.5 A/cm^2 electron beam will control about 39 A/cm^2 of sustainer current (E/P $\simeq$ 5.0 kV/atm-cm). This is in substantial agreement with our results. Under these conditions, sustainer energy is delivered to the gas at the rate of 190 J/liter/μsec. Limitations of charge storage in the Marx bank driving the diode

precluded investigations where the conductivity of the plasma was maintained for times greater than 1 μsec. The optical energy-storage efficiency as reflected by the gain is lower than that observed by Fenstermacher et al.[1] This may be due to the different rates of energy deposition in the two devices. The scatter in the data is most likely due to a reduction in the e-beam range in the gas as the cathode voltage dropped and to random nonuniformities in the e-beam as the diode impedance collapsed. Since the probe laser sampled only a very small volume, any deviation in the pumping rate over this volume shows up in the total small signal gain.

The results of these experiments indicate that the cold-cathode electron gun should offer a relatively simple means of controlling large-volume gas lasers. This method is particularly useful in situations where rapid, high current pumping is desirable (<2 - 3 μsec), as is the case in CO_2 amplifiers designed for nanosecond pulse amplification. At the measured gain of 4.9% cm^{-1}, 5 to 6 joules of optical, 10.6 μ energy is stored in the medium which can be extracted in a nanosecond pulse.

ACKNOWLEDGEMENTS

We would like to acknowledge the contributions of K. Fertl, D. Adcock, N. Leech, W. Whitney and D. Shores to this experiment.

REFERENCES

1. C.A. Fenstermacher, M.J. Nutter, W.T. Leland and K. Boyer, Appl. Phys. Letters 20, 56 (1972).

2. J.D. Daugherty, E.R. Pugh, and D.H. Douglas-Hamilton, Paper T1, 24th Annual Gaseous Electronics Conference, Oct. 5-8, 1971, Gainesville, Florida.

3. H.G. Ahlstrom, G. Inglesakis, J.F. Holzrichter, T. Kan, J. Jansen, and A.C. Kolb, "Current, Voltage and Gain Measurements in a High Current Electron Beam CO_2 Laser", 3rd Conference on Chemical and Molecular Lasers, St. Louis (May 1972).

4. G. Loda, "Measurements on a High Power 10 μ Atmosphere CO_2 Discharge Laser", Bull. Am. Phys. Soc. 17, 681 (May 1972).

5. G. Loda and T. DeHart, "Investigation of Pulsed Cold Cathode Electron Guns for Use as a Laser Discharge Sustainer", Physics International Report No. PIFR-326.

6. J.C. Martin, unpublished notes.

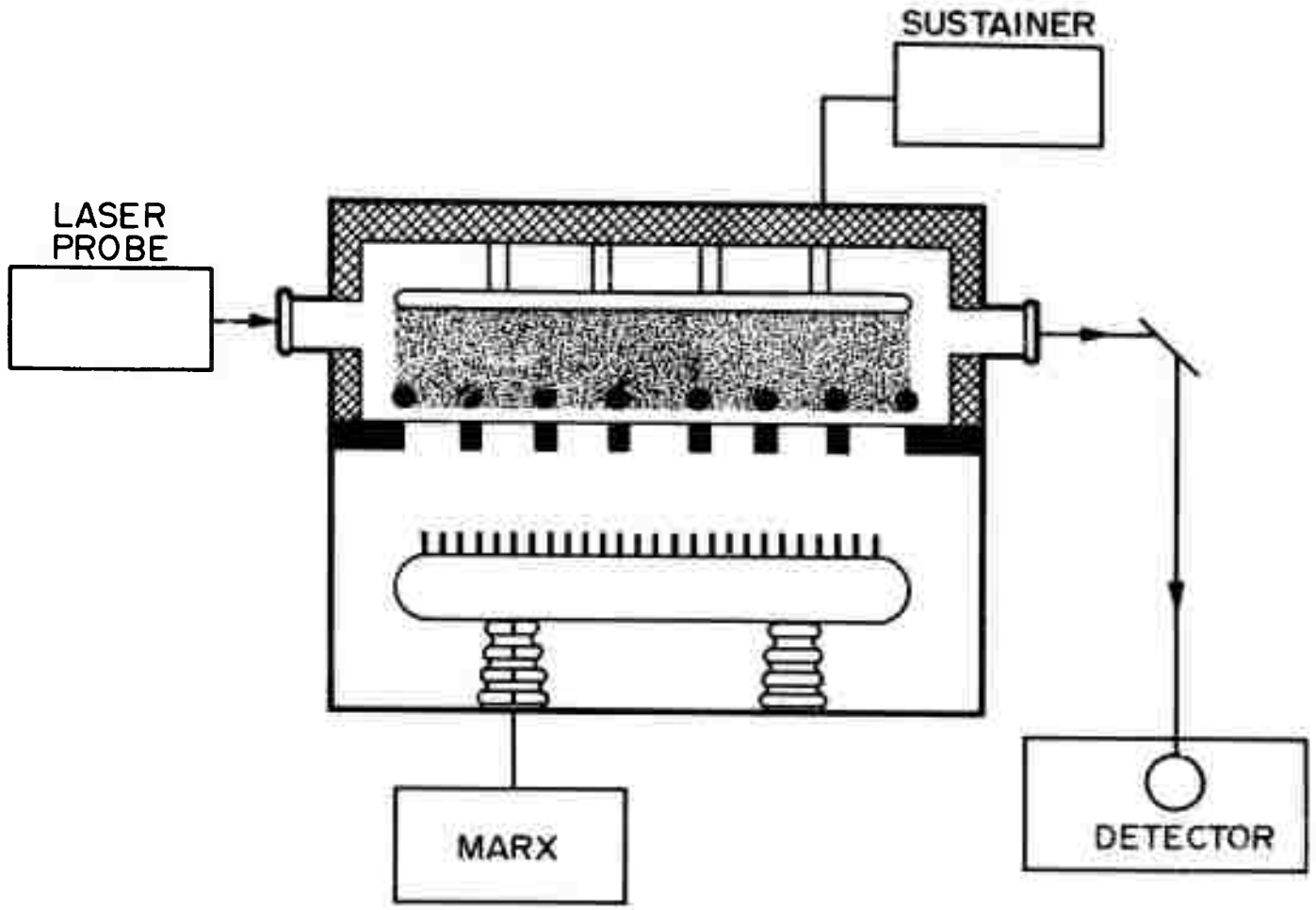

FIGURE 1. Schematic diagram of experimental apparatus

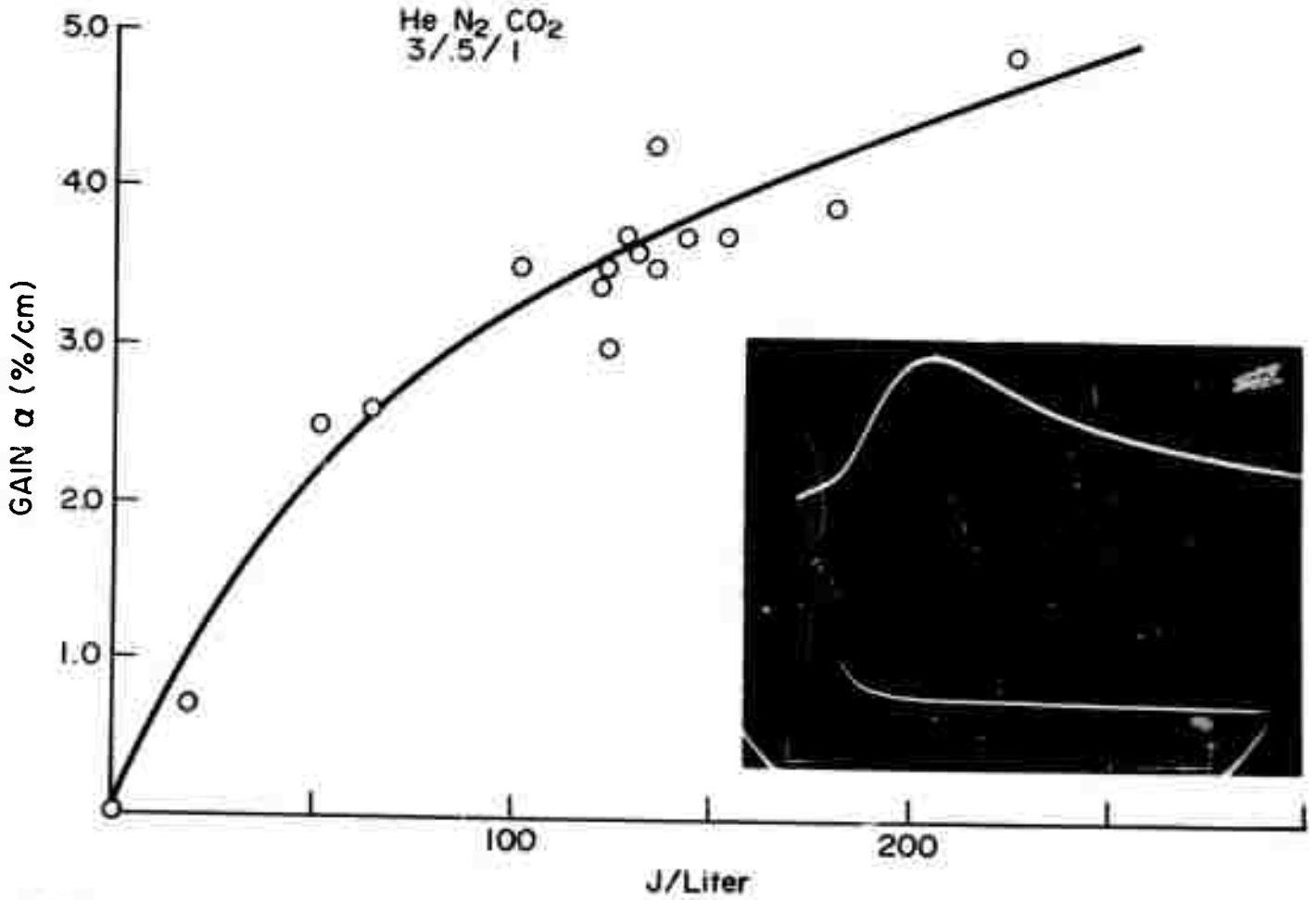

FIGURE 2. Gain coefficient as function of energy deposition into gas. Insert shows a typical oscillogram. Top trace is gain pulse and bottom trace is sustainer current, 3.4 kA/cm. Sweep speed was 1 μs/cm.

APPENDIX C

DAMAGE MEASUREMENTS WITH SUBNANOSECOND PULSES*

John M. McMahon

Naval Research Laboratory
Washington, D.C. 20390

1. Introduction

There is currently a great deal of interest in generating intense subnanosecond pulses for laser CTR applications as well as for other purposes. Success in construction of relatively efficient solid state lasers which generate terawatt (or higher) level pulses and which operate reliably for many shots will require either that the pulse shape and intensity be tailored in time and spatial extent such that non-linear effects do not predominate or that geometries be chosen in which these effects can reasonably be expected not to occur.

Disc amplifiers, for example, appear to be relatively immune to self focusing (if only in that the surfaces will damage first). They however are somewhat unattractive from an efficiency and convenience standpoint compared to a solid rod system.

We have investigated the self focusing problem for three laser glasses in common use (Owens-Illinois ED-2; Soveril MG 915 and Schott LG-56). Measurements of N_2 are reported on unpumped rods for pulse durations between 20 psec and 250 psec. Measurement techniques for subnanosecond pulses are not presently as quantitative as might be desired. Pulse duration measurements by non-linear optical techniques may lead to erroneous results unless great care is taken. Energy measurements are complicated by plasma formation in the calorimeter at very low levels compared to q switched pulses ($\simeq$ 50 mJ/cm^2 on carbon) which reduces the signal to noise ratio to (typically) less than 20:1 and there are difficulties in measuring near and far field intensity distributions with a high precision and wide dynamic range at 1 μm.

2. Measurement of N_2 in Laser Glasses

In the 1970 ASTM symposium, J. Davit[1] of CGE and M. Duguay and J. Hansen[2] of BTL reported on measurements on N_2 for several glasses by various methods. Duguay and Hansen reported some measurements at $\sim$ 8 psec on BK-7 and LASF-7 glasses and Davit on tests done at 2 nsec on LG-56 and MG-915 glasses. While BK-7 might be expected to behave in a similar fashion to the laser glasses Davit tested, the value of N_2 was about an order of magnitude larger than the BTL value. This suggests the possibility that for very short pulses N_2 might be

*This work was supported by the Advanced Research Projects Agency under ARPA Order 2062.
Paper presented at the 4th ASTM-NBS Symposium on Damage in Laser Materials, Boulder, Colorado, June 14-15, 1972.

smaller due to mechanisms important on the nanosecond time scale not being able to respond to short pulses. Another possibility was that since neither author used a laser which produced a time band width limited pulse, both measurements could be consistent with a model in which some of the pulse energy is in very short temporal spikes.

For the measurements reported here we used a mode locked Nd:YAG oscillator-amplifier which has been described elsewhere.[3] This system produces a TEM_{00} spatial mode output single pulse with an energy adjustable from 1-200 mJ in a pulse whose width can be adjusted from 20 psec to 1.3 nanoseconds by the use of transmission etalons in the cavity. Our measurements and those of Carmen and co-workers at LLL indicate that the pulse is essentially time-bandwidth limited[4] with a smooth Gaussian spectral and temporal output. Figure 1 shows the geometrical arrangement of this device.

For the trapping measurements the beam was propagated ~ 3 meters to get rid of near field Fresnel fringes and the pattern checked and found to be a Gaussian down to below the e^{-3} points. The beam was then run through a sample rod and the trapping length noted from the side during 10-20 shots for each sample. In all cases the start of the filament was characterized by the emission of blue light (presumably from plasma breakdown in the track). This was somewhat enhanced in the ED-2, presumably due to the ultraviolet pumping the cerium which then fluoresced in the region of 4000-5000 Å.

Table 1 lists the geometries and absorption coefficients of the samples tested. The Soveril glass tested was a rod made by the old process and had a significantly higher absorption coefficient than MG 915 made by the continuous flow process. The LG 56 rod was supplied by CGE with the NRL VD 640 and had a low absorption coefficient for LG-56. We initially questioned whether this was LG 56 or LG 630 and were assured by CGE that it was LG 56.

In the actual sequence of experiments the laser was tuned to run at a given pulsewidth and then the samples were each irradiated for 10-20 shots and the mean trapping length, peak energy density, pulsewidth and spatial distribution determined. The laser was then tuned to the next pulsewidth and the sequence repeated. Table 2 shows the results for pulse durations of 20 psec and 250 psec. The pulse peak powers and beam parameters were $P_o = 8 \times 10^{10}$ W/cm^2, b = 1.1 mm and $P_o = 1 \times 10^{10}$ W/cm^2, b = 1.5 mm, respectively.

The difference in beam parameter was caused by the beginning of focusing in the YAG preamplifiers which was not severe enough to noticably perturb the temporal or spectral structure of the pulse. The cone angle of the self-phase modulated light from the samples was ≃ 0.1 radian at 250 psec and ≃ 0.25 radian at 20 psec. Typically 3-10 filaments would be formed which would traverse the length of the rod.

Table 3 gives trapping data on ED-2 for a somewhat more complete set of experiments. Data sets were run for 20 psec, 125 psec and 250 psec "clean" pulses and also for a pulse 125 psec long with the etalon misaligned to give two spectral components of equal intensity. These interfered giving a peak intensity ~ four times the intensity for a non-structured pulse. This caused a reduction in trapping length of a factor of two.

Table 4 gives the calculated value of N_2 for the glasses tested with an estimated absolute accuracy of ±40%. The value of BK-7 should be taken as a upper limit since $\ell_{sample} \simeq z_{foc}$.

3. Discussion of the Results

The data all showed an excellent agreement with Kelley's formula for the parametric variation of self focusing length[5]

$$z_{foc} = \frac{b}{4} \left(\frac{N_o}{N_2}\right)^{\frac{1}{2}} \frac{1}{E} \quad . \qquad (1)$$

Additionally, over the range of temporal values tested N_2 for a particular glass was found to be sensibly constant.

It was additionally shown that N_2 will follow temporal structure on the pulse. If we had assumed our structured pulse to be smooth, an N_2 value four times the observed value would have been obtained.

Under a given set of conditions there did appear to be small but experimentally significant differences in self focusing length. That there is a difference between ED-2 and LG-56 is not too surprising since the two are dissimilar glasses, but the difference between the LG-56 and MG-915 is surprising, since they are essentially the same glass. These may be related to the difference in absorption coefficient of the two glasses.

4. Systems Considerations

Based upon the values of N_2 reported here there appear to be no fundamental difficulties in amplifying pulses to high energies if the trapping length is long compared to the amplifier length and the pulse is temporally and spatially smooth. Unfortunately, these conditions are rarely met (for more than a few shots).

Dust particles on surfaces can provide nuclei for wavefront disturbances which can then cause trapping in the next stage. Shot by shot this damage can then propagate through the system. This problem can be minimized if the amplifiers are spaced in the far field of any filaments generated in the previous amplifier.

TABLE 1

SAMPLES TESTED

GLASS TYPE	ℓ(cm)	γ(cm^{-1})
ED-2	30	3×10^{-3}
MG-915 (cast)	30	7.5×10^{-3}
LG-56	50	3×10^{-3}
BK-7	6	3×10^{-3}

TABLE 2

RELATIVE DATA ON TRAPPING LENGTH

TYPE	Z(250 psec)	Z(20 psec)
ED-2	24 ± 1	6.6 ± 1
MG-915	24 ± 1.5	6.1 ± 1
LG-56	21 ± 1.5	5.6 ± 1
BK-7	--------	6 + *

* The 6 cm sample only trapped occasionally (≃ 30% of shots) and within 1 cm of the surface.

TABLE 3

TRAPPING DATA ED-2

t(psec)	P_o(W/cm^2)	b(mm)	Z(cm)
20	8×10^{10}	1.1	6.6 ± .5
125	1.2×10^{10}	1.2	18 ± 2
250	1×10^{10}	1.5	24 ± 1
125*	4.8×10^{10}	1.2	9.2 ± 1.6

* Etalon misaligned to cause temporal beats with a four-fold enhancement of peak power.

TABLE 4

N_2 VALUES (esu)

BK-7	6×10^{-14}
ED-2	$(7 \pm 3) \times 10^{-14}$
MG-915	$(7 \pm 3) \times 10^{-14}$
LG-56	$(8 \pm 3) \times 10^{-14}$

It is also generally very difficult to avoid Fresnel fringes in the beam pattern. Based on the experiments of Guiliani,[6] a Fresnel fringe itself may be expected to have a high threshold for trapping (since it would be a one dimensional process). However, in a circularly symmetric beam, the Fresnel fringes may accentuate damage by moving energy into the beam center where it may tend to form an intensity spike. We have seen such a spike forming at times and we understand that Bettinger[7] at CGE has seen such a spike form and then self-focus. This effect seems to be somewhat diminished if any apertures in the system are non-concentric.

Operating the CGE VD 640 amplifier train with 250 psec pulses outputs of 50-60 joules have been achieved with little or no degradation over ≃ 100 shots. A limited number of shots have been run at levels of 90-100 shots. No degradation has been observed to date.

REFERENCES

1. J. Davit, NBS Special Publication 341, (1970) pp 37-44.

2. M.A. Duguay and J.W. Hansen, NBS Special Publication 341, (1970) pp 45-50.

3. J. Emmett et al, "Disc Lasers", IEEE Int. Quantum Electronics Conference, Montreal, Canada, May 1972.

4. R. Carmen, IEEE Int. Quantum Electronics Conf., Montreal, Canada, May 1972.

5. P.L. Kelley, Physical Review Letters, 15, 26 (1965), p. 1005.

6. M. Guiliani, IEEE Int. Quantum Electronics Conference, Montreal, May 1972.

7. J. Bettinger, Private Communication.

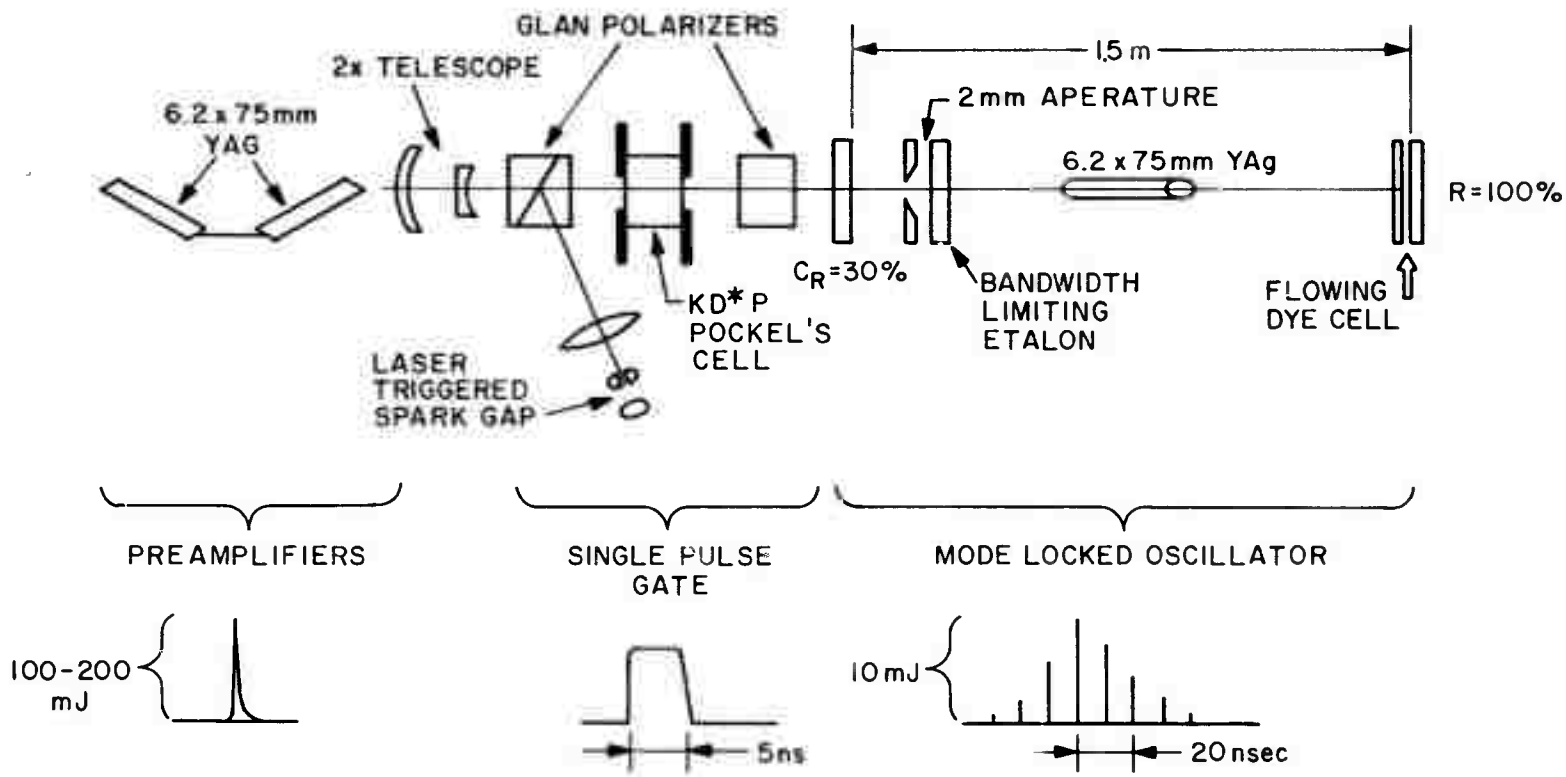

Nd:YAG SHORT PULSE GENERATOR

APPENDIX D

REFLECTIVITIES OF OWENS ILLINOIS LASER GLASSES WITH DIFFERENT SURFACE PREPARATIONS

J.F. Holzrichter

Naval Research Laboratory
Washington, D.C. 20390

1. INTRODUCTION

Recent studies of the construction of large laser systems have pointed out the need for careful consideration of amplified spontaneous emission and self-oscillation within the laser medium itself. These effects can seriously reduce the efficiency of the laser system by extracting energy from the gain medium in undesirable modes. Proposals for large Nd^{3+} doped glass laser amplifiers are suggesting glass disks of up to 25 cm in major diameter and up to several cm thick. Internal "whisper" modes within these disks and amplification of spontaneously emitted light that is scattered off of the edges or surfaces of the disks can seriously reduce their energy storage capability.

We have made some simple measurements on the internal scattering efficiency of rough ground, polished, coated surfaces of 1% Nd-Owens Illinois ED-2 laser glass. These measurements have been made using an integrating sphere technique. They point out the wide variation in scattering efficiency of glass surfaces as a function of angle and surface preparation. These measurements in conjunction with recent computer codes that can trace rays in arbitrary geometries with arbitrary absorption coefficients (including gain) can be used to estimate the extent of the above problems.

2. MEASUREMENT TECHNIQUE

Figure 1 shows the technique that was used to measure the internal reflectivity of various surfaces. The incoming laser beam enters the small integrating sphere (a ping-pong ball painted with $BaSO_4$ paint) and scatters off of both glass surfaces. We are interested only in the scattering from the rear surface. The front surface reflection is allowed to escape from the sphere through a small hole that is suitably positioned and the rear surface reflection scatters within the sphere. After the first bounce off of the sphere, the interior of sphere is uniformly illuminated and subsequent ray trajectories are statistically identical. This is independent of the specular or diffuse nature of the surface reflectivity. The germanium photodiode (Electro-Nuclear No. 653) is pointed so that only scattered light is received. It detects the relative amount of scatter from various glass samples. The sphere can be calibrated by using a $BaSO_4$ surface to provide

total diffuse scattering. The incoming laser beam is chopped at 200 Hz with a tuning fork modulator and the modulated signal from the photodiode is detected with a lock-in amplifier. A 1.15 micron He-Ne laser was used because of its availability and because most scattering and absorbing processes in the materials that we have examined are essentially independent of wavelength in the 1.06 to 1.15 micron region.

The linearity of the system was verified with known attenuators and the scattering accuracy was verified by comparing the front surface Fresnel reflection from a piece of ED-2 glass to a $BaSO_4$ covered plate. The 6% reflectivity agrees with the Cary 14 measurement of 5.5%.

An error is introduced in that diffusely scattered radiation from the rear surface that is below the critical angle will be trapped within the glass. The extent of this effect can only be estimated in the present system and is discussed in Section 3. Care must be taken to ensure that only laser radiation that is scattered from the back surface is measured. A slight amount of scattering of the front surface reflected beam from the edge of the exit hole could lead to erroneous results. Effects to reabsorption of scattered light by the test surface, and from non-specular scattering from the front surface have not been considered. These effects would be small.

3. EXPERIMENTAL RESULTS

The data presented in the following Table (Table 1) was taken with the experimental apparatus that was discussed in Section 2. The samples were 0.63 cm thick slabs of Owens Illinois ED-2 glass that were smooth ground (22 μ Al_2O_3 abrasive) one side and smooth polished (pell polish) on the other. Sample No. 2 was coated with Owens Illinois black glass on the ground surface. Sample No. 1 was not coated at all, and Sample No. 3 was smooth polished on both sides and then coated on one side with the Owens Illinois black glass. On this sample there was no diffuse reflection. The incident beam was 13° from the normal. The reflectivities are corrected for the front surface Fresnal losses.

The black glass coating is black "solder" glass that was specially developed for the purpose of cladding ED-2 laser glass. It has no Owens Illinois designation to date.

TABLE I

SAMPLE NO.	REFL. (μ VOLTS) SIGNAL	% REFL. COMPARED TO $BaSO_4$	% REFL. CORRECTED FOR CRITICAL ANGLE EFFECTS
$BaSO_4$	4200	100%	100%
1. Smooth Grnd. No coating	100	2.6%	6.5%
2. Smooth Grnd. O.I. Coating	45	1.2%	2.7%
3. Smooth polish O.I. Coating	10	0.27%	0.27%
Front surface refl.	220	5.2%	5.2%
Smooth grnd. to laser beam	390	9.2%	9.2%

The data is reproducible to within ± 10%, and on measurements that can be checked with the Cary 14, the agreement is good. However, the corrected data depends on the surface being Lambertian. Angular measurements indicate that at normal incidence this may be reasonable, however, this data is certainly less accurate, probably ± 25%.

The amount of light that can escape from a Lambertian surface inside a medium of higher index is restricted by total internal reflection at low angles.

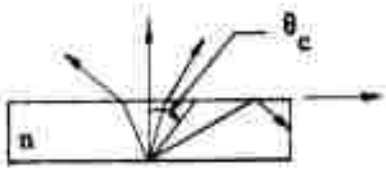

$$\theta_c = \sin^{-1} \frac{1}{n}$$

If the light is conducted out of the measuring region and completely reabsorbed as in our system, the detected signal must be corrected for the lost light. This effect is non-negligible.

For a Lambertian surface that scatters as $\cos\theta$:

$$\frac{I_{out}}{I_{in}} = \sin^2 \theta_c = .41\Big|_{n=1.56} .$$

The detected signals from the diffuse absorber are corrected by multiplying column 3 by 2.4 and are placed in column 4 of Table I.

Low Angle Scattering

Additional data on the low angle scattering efficiency is presented in Table II. This data was taken by comparing the reflected light to the incoming laser light as measured directly with the integrating sphere. See Figure 2. The laser polarization was perpendicular to the plane of incidence.

TABLE II

Scatter from Following Sample	Raw Signal μ Volts		Percent Trans. As Function of Internal Angle From Surface (Corrected for Fresnel Losses)	
	Angle	Signal	Angle	Refl.
Laser Signal		50		100%
Attenuation thru 2 surfaces		44		88%
No. 3 Smooth polish	1.6°	33	1.6°	74% spec.
O.I. black glass	3.2°	25	3.2°	54% spec.
	6.4°	17	6.4°	38% spec.
	9.5°	12	9.5°	27% spec.
No. 2 Smooth grind	3.2°	21	3.2°	47% mostly spec.
O.I. black glass	6.4°	12	6.4°	27% mostly spec.
Smooth polish	3.2°	35	3.2°	79% mostly spec.
ED-2 surface	6.4°	39	6.4°	85% mostly spec.

In this configuration, light that is scattered at large angles will not be detected and this can lead to some errors. The data in the last column for a polished ED-2 surface should be 100%, because the beam would undergo total internal reflection. This indicates that some light has not been accounted for. The data in this table show that at low angles, irrespective of the surface preparation the reflectivities are high.

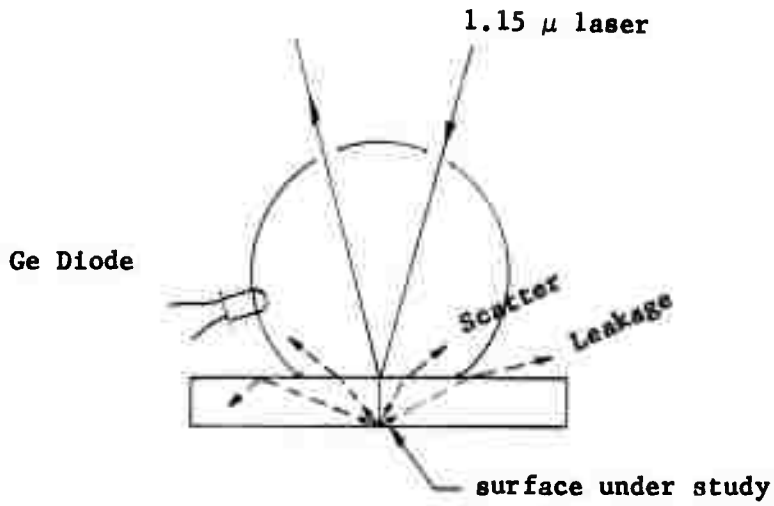

FIGURE 1

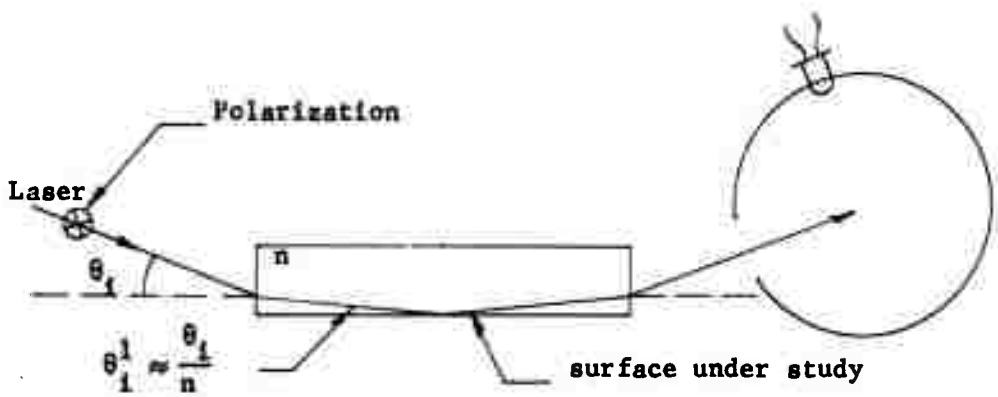

FIGURE 2

APPENDIX E

DISC LASER TEST RESULTS

John M. McMahon
John L. Emmett
John Holzrichter
John B. Trenholme

March 1972

Naval Research Laboratory
Washington, D.C. 20390

Introduction

Successful predictive design of large aperture disc amplifiers requires a thorough knowledge of the operative physics in several areas which are not normally too important in solid rod laser amplifiers. Conversely, a disc amplifier represents a geometry in which the relevant physics can be studied with a higher degree of certitude.

These effects of special moment for disc amplifiers can be ranked in order of importance;

(1) free lasing and/or superfluorescence in the discs,

(2) since one pumps through the faces, any active (i.e. pumped) losses will be present to a much more severe extent than in a rod amplifier,

(3) damage to the discs due to the intense optical radiation of the flashlamps.

During the past nine month period we have explicitly investigated the first two categories of effects and perforce the third. To assist in this effort we have employed several powerful computational tools as well as reasonably standard experimental techniques. The Monte-Carlo optical pumping code (ZAP) has been used to predict the energy storage and a modified code used to perform superfluorescence calculations, quasi-analytic models have been used to predict free lasing thresholds.

Experimentally, the VD 640 glass laser was first used for gain measurements both with long (30 nsec) and short (250 psec) pulses. This was not too satisfactory for several reasona; the spatial profile was not too uniform and the other demands for the use of the laser system made it difficult to prosecute the experiments with as much vigor as might have been desired. The delivery of a Chromatix Model 1000 C Nd:YAG laser in December eased this restriction and additionally offered much greater flexibility in the type of experiments which could be pursued.

Free Lasing and Superfluorescence Results

Early experiments with the French laser as the pump laser showed no gain anomolies as long as the rough ground edges of the discs were isolated from the gold plated holder by a black anodized copper strip (a first attempt to paint the edges black was unsuccessful since the paint disintegrated in a few shots). The operation was restricted to < 55% of the maximum bank energy by the facts that we had only 15 lamps in these tests and also that the trigger isolation capacitors then used disintegrated at 18-19 kV.

In December operation with the Chromatix laser and a full system revealed that the gain did not materially increase above the level previously reached as the pump energy was increased to 150 kJ. This was not expected at that level because of free lasing or superfluorescence, so a set of experiments was prosecuted to determine whether or not some active loss was dominating. This investigation is described in the next section in more detail. It had convincingly negative results which left only free lasing and/or superfluorescence as the possible mechanisms.

Several alternate edge treatments had been under consideration for some time and a black solder glass (G9000) developed by Owens-Illinois was chosen as a more likely candidate than the two ceramic glazes which were also formulated for several reasons:

(1) a lower firing temperature resulting in less chance of having to reanneal the discs;

(2) an index of refraction more nearly matching the index of ED-2 (1.7 vs 1.56).

This coating was applied to eight (8) discs and an identical sequence was run from 25 - 72 % of the bank energy using the Chromatix laser to produce a 1 kW, 200 nsec probe pulse every 20 μsec during the pump pulse. Figure 1 shows the peak small signal gain coefficient/disc as a function of the edge treatment. Two subsidiary experiments are included one, with pyrex glass shields in place and one with the black copper strips removed. In the former case the peak gains were essentially the same with and without the shields; in the latter case, fluorescence probes revealed that even at the lowest operating voltage at which the lamps would trigger (10 kV), the rolloff occurred. By extrapolating the fluorescence back to a well behaved region the estimate shown in Fig. 1 was obtained.

The analysis codes strongly suggested that the problem was relaxation oscillations in the discs rather than superfluorescence and the relative levels at which oscillation commenced with and without the black copper strips tended to strongly reinforce this conclusion. Figures 2 and 3 show data which compares the gain as a function of time

for the black glass coated discs with the case with copper strips. The fluctuations in the gain values were marginally statistically significant and much more suggestive of the energy storage in an oscillator near threshold than a system being depumped by superfluorescence.

The results with the black glass edge are in excellent agreement with ZAP and the superfluorescence code predicts a rolloff of only $\sim 3\%$ (which is included in Figure 1) due to superfluorescence at full energy. Figure 4 shows that the full data set with the black glass. It is also predicted that the discs will not oscillate below e^2 gain with this coating. There are however two caveats at this time; the coating appears to be damaged to some degree by ultraviolet from the flashlamps and perfect adhesion of the coating to the discs was not found so the full predicted gain may not be feasible. The first problem is being investigated now and the second is relevant to larger systems; this system will operate with the present coating.

Active Loss Investigation

Earlier results on rod amplifiers at NRL, AFWL and AO had suggested the possibility of active losses playing some role at high pump energy densities and when the gain rolloff was discovered this possibility was pursued.

Operation with pyrex shields revealed the same rolloff occurring at essentially the same level and ruled out ultraviolet lamp emission below 3000 Å. A concurrent experiment in which the transverse gain through the center of the disc was measured showed the same roll off and argued against the cerium in the ED-2 playing any dominant role since then it would have been a surface effect (because of the large absorption cross-section) and the gain through the center of the disc would have continued to rise.

The possibility of a broad band transient color centering was ruled out by spectrally tuning the Chromatix laser to 1.12 mμ and .946 mμ. In both cases there was no effect to a precision of $\pm .002\ cm^{-1}$. This left only the possibility of an excited state absorption in the neodymium system itself. This was checked by performing the small signal gain measurement at 1.052 μ, 1.064 μ, 1.074 μ and 1.079 μ and comparing the relative magnitude of the gain coefficients at the other wavelengths to $\alpha_{1.06\ \mu}$ and normalizing the measurements to Duston's fluorescence data on Ed-2. This is shown in Figure 5. In all cases the gain rolled over at $\sim 50\%$ pump energy. Figure 4 shows this data. At the inversion level achieved ($\sim .42\ J/cm^3$) this data and the highest level data shows that if there is any excited state absorption it must:

(1) have a spectral shape very similar to the fluorescence curve which would be fortuitous, or

(2) have a peak magnitude $< 1\%/cm$.

It appears that an excited state absorption (if it occurs), is not a particularly significant mechanism for disc amplifiers since high energy densities compared to those projected are required for it to play a significant role. It should be noted that there is no basic inconsistency between this conclusion and observations on rod amplifiers as they were at much higher stored energies. The superlinearity of the earlier NRL and AFWL results however suggests that they were contaminated by superfluorescence.

Damage to Disc Surfaces

In conversations with LASL representatives and John Meyers of Owens Illinois it appears that LASL has seen massive surface damage to discs and that one possibility is that the cerium oxide powder Owens Illinois favors for final polishing forms an amalgam with the glass with a very high ultraviolet absorption coefficient. In the course of reviewing why we had not seen such an effect we found that

(1) eleven of the sixteen NRL discs were repolished with Linde B abrasive after the black paint disaster,

(2) the remainder had to be repolished after a subsequent flashlamp explosion.

In approximately 350 shots to date on the disc amplifier we have observed the following phenomena on a less spectacular but persistent fashion,

(1) any unremoved polishing compound will be burned into the surfaces,

(2) we have had a problem with gold from the mounts flecking off and being deposited on the surfaces. This seems to have been caused by improper surface preparation before plating and after ~ 200 shots this effect has disappeared,

(3) in several discs internal bubbles have appeared which are not oriented along the optic axis but rather follow skew paths rather as if they were there initially and irradiation has increased the size to a noticable extent,

(4) random small damage spots apparently caused by dust particles.

None of these effects have had any significant effect on the laser performance of the device but they are cosmetically unpleasing.

Summary of Results to Date

The dominant problem in the operation of the NRL system has been shown to be pre-lasing of the discs off the disc edge. It appears that

the black glass coating Owens Illinois has developed will suffice to permit operation of this device at up to the design levels.

Projected Experimental Program (6/30/72)

(1) Check geometrical sealing of ZAP program.

(2) Check gain to full pump energy.

(3) Look for excited state absorption at higher inversions.

(4) Run to full energy (400 - 500 J) with 250 psec pulses.

(5) Measure pump uniformity by doing x-y scan with Chromatix laser.

DISC LASER

V(kV)	$\alpha\ell$(disc)	$\alpha\ell$(11)	N(J/cm^3)	ϵ(%)	ϵ^1(%)*
10	.1025	1.130	.316	1.14%	1.24%
12	.1375	1.516	.436	1.09%	1.185%
14	.1613	1.78	.498	.915%	.995%
16	.185	2.04	.575	.81%	.88%
17	.193	2.14	.595	.75%	.816%

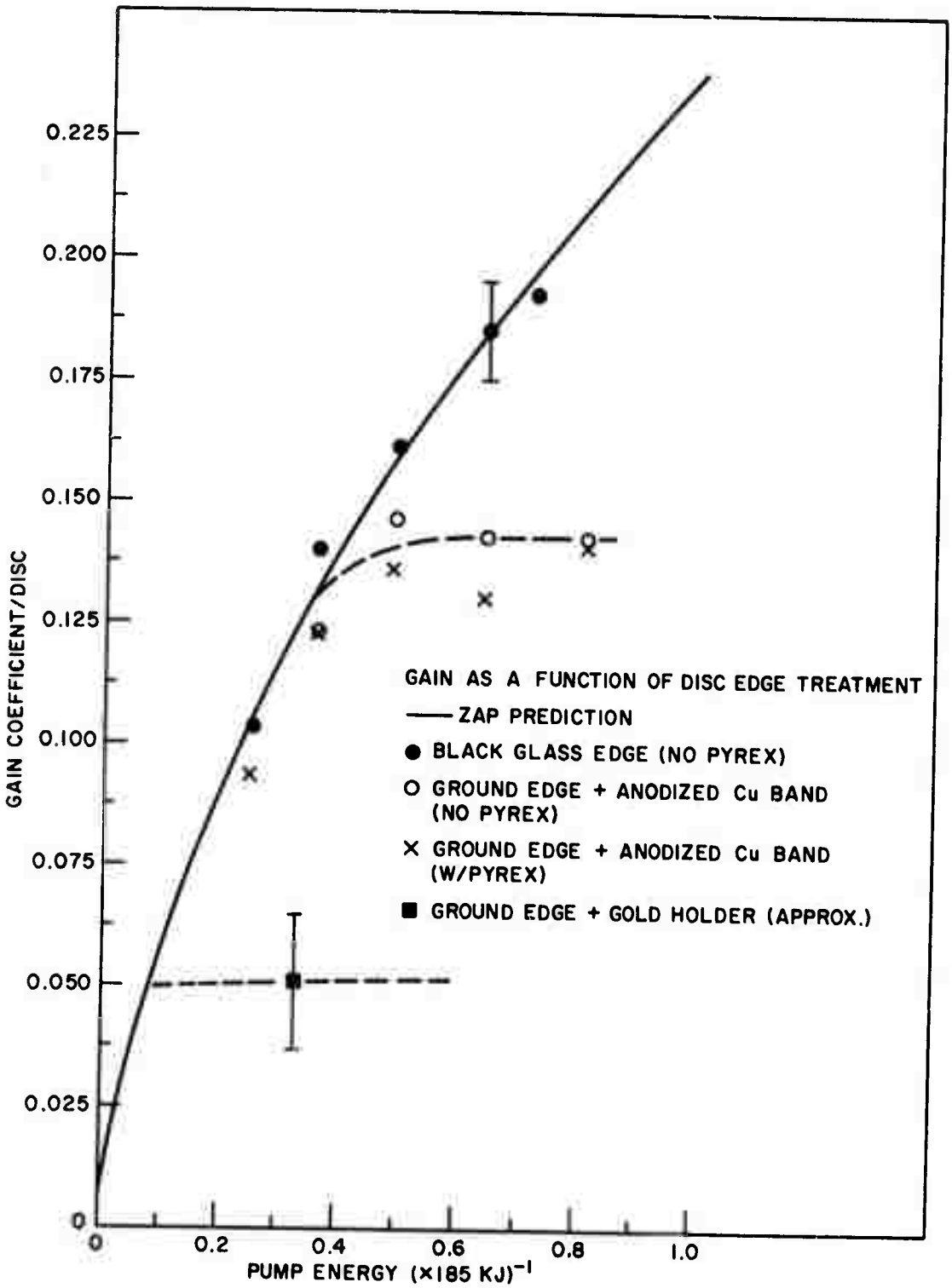
GAIN AS A FUNCTION OF DISC EDGE TREATMENT
ZAP PREDICTION
BLACK GLASS EDGE (NO PYREX)
GROUND EDGE + ANODIZED Cu BAND (NO PYREX)
GROUND EDGE + ANODIZED Cu BAND (W/PYREX)
GROUND EDGE + GOLD HOLDER (APPROX.)
GAIN COEFFICIENT/DISC
0.225
0.200
0.175
0.150
0.125
0.100
0.075
0.050
0.025
0
0.2
0.4
0.6
0.8
1.0
PUMP ENERGY (×185 KJ)$^{-1}$

FIGURE 1

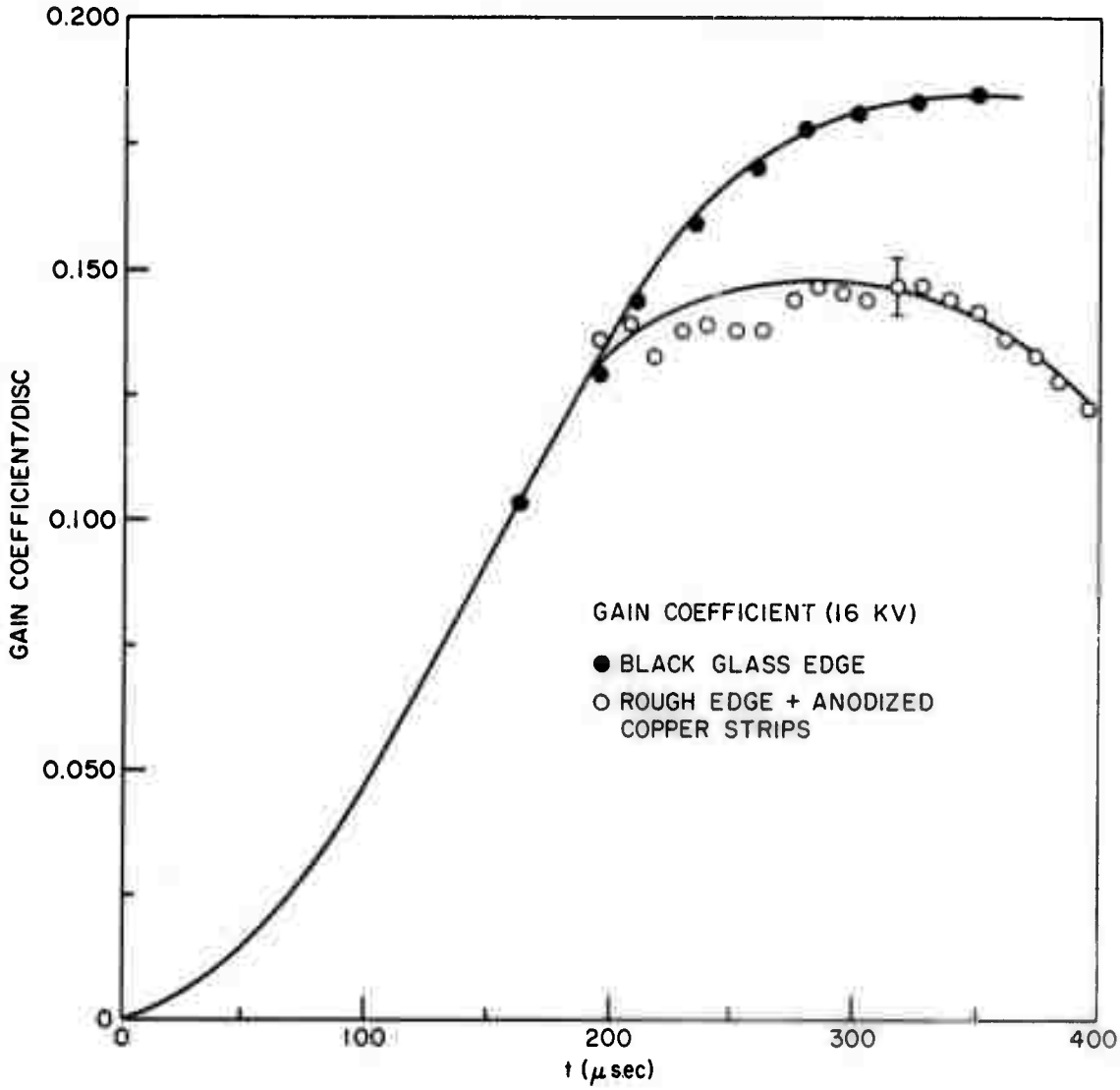
0.200
0.150
0.100
0.050
0
GAIN COEFFICIENT/DISC
0
100
200
300
400
t (μsec)
GAIN COEFFICIENT (16 KV)
● BLACK GLASS EDGE
O ROUGH EDGE + ANODIZED COPPER STRIPS

FIGURE 2

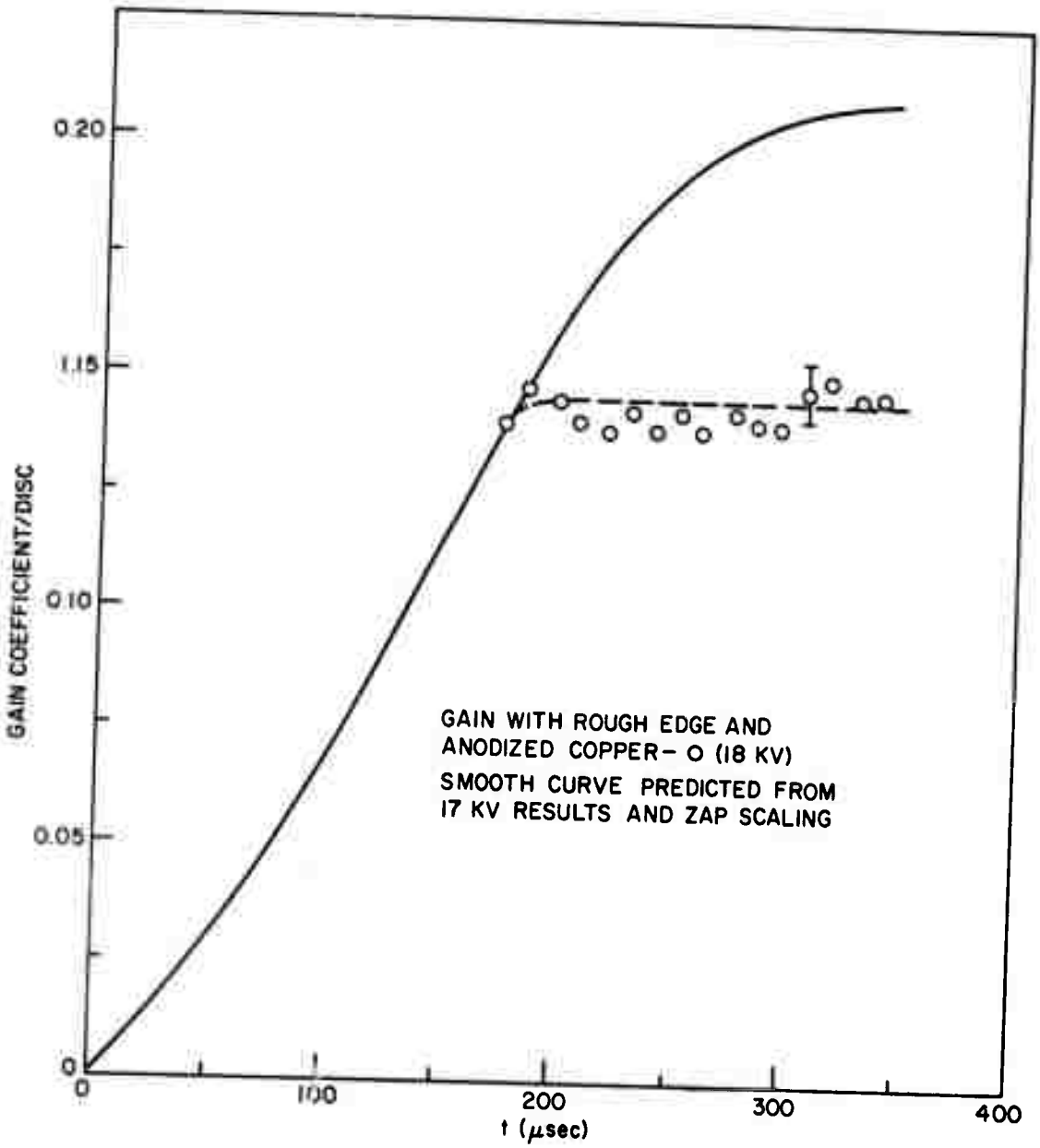
0.20
1.15
0.10
0.05
0
GAIN COEFFICIENT/DISC
GAIN WITH ROUGH EDGE AND
ANODIZED COPPER- O (18 KV)
SMOOTH CURVE PREDICTED FROM
17 KV RESULTS AND ZAP SCALING
0
100
200
300
400
t (μsec)

FIGURE 3

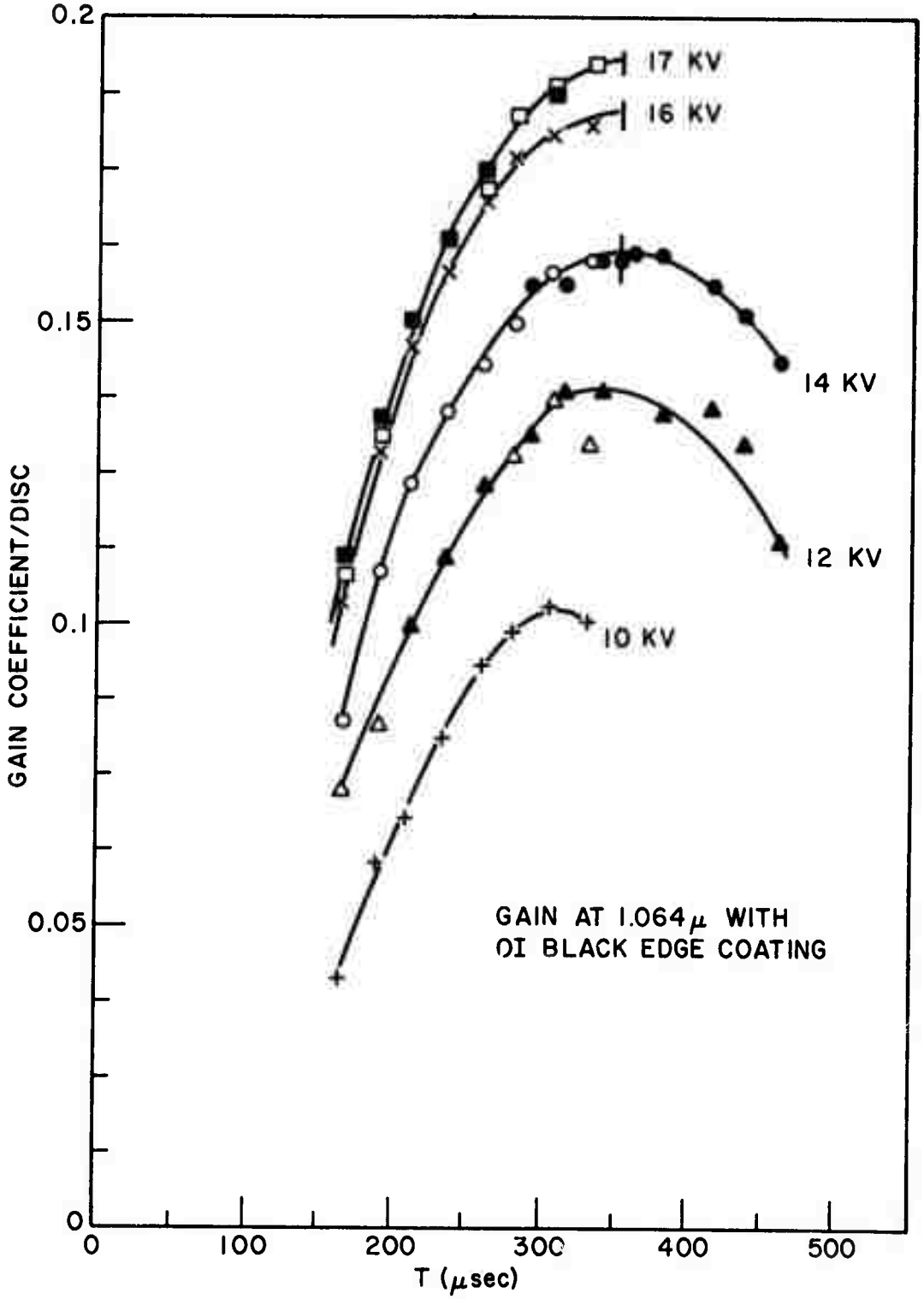
0.2
0.15
0.1
0.05
0
GAIN COEFFICIENT/DISC
17 KV
16 KV
14 KV
12 KV
10 KV
GAIN AT 1.064μ WITH
OI BLACK EDGE COATING
0
100
200
300
400
500
T (μsec)

FIGURE 4

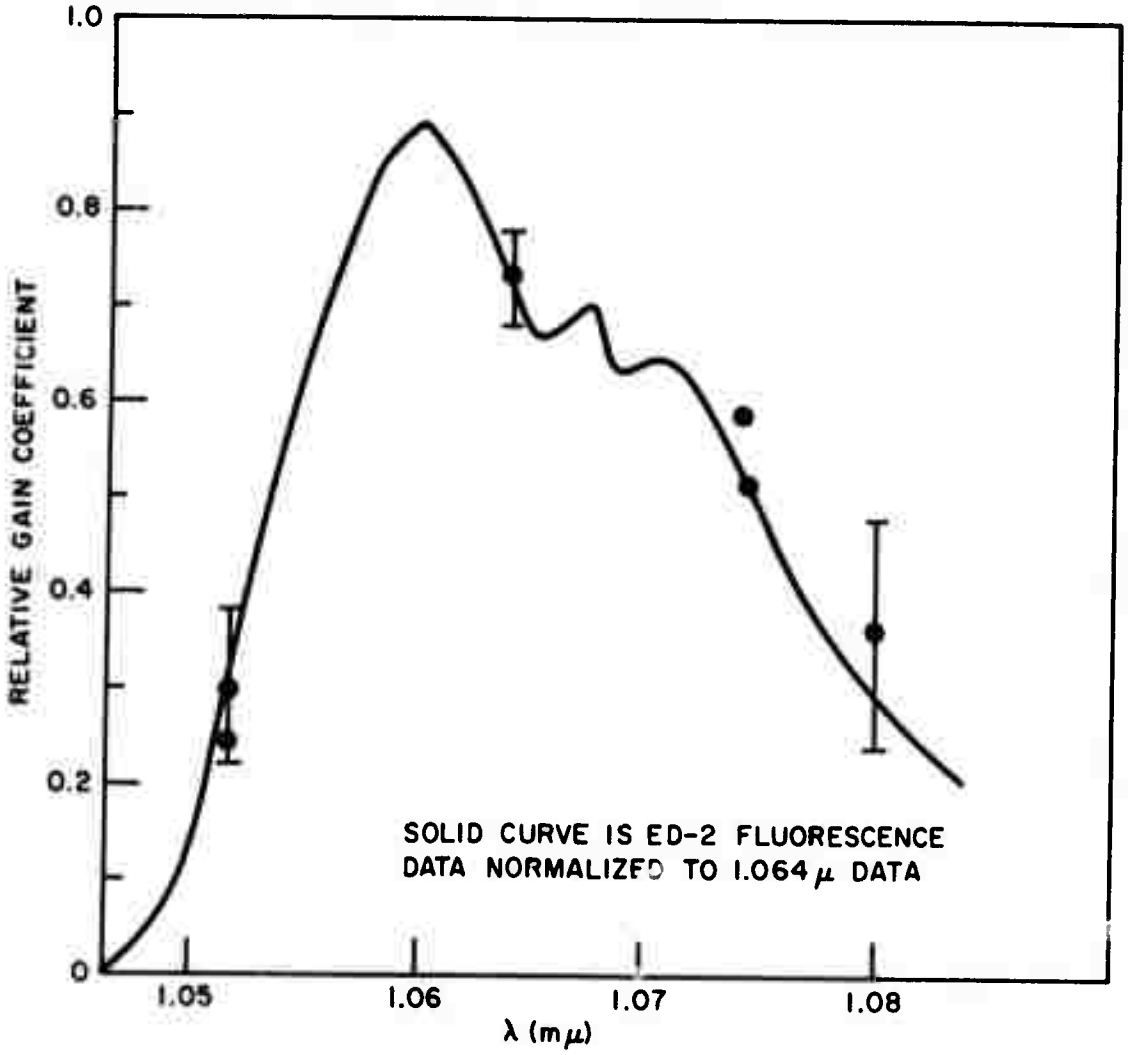
1.0
0.8
0.6
0.4
0.2
0
RELATIVE GAIN COEFFICIENT
1.05
1.06
1.07
1.08
λ (mμ)
SOLID CURVE IS ED-2 FLUORESCENCE
DATA NORMALIZED TO 1.064 μ DATA

FIGURE 5

Appendix F

NRL Memorandum Report 2480

Fluorescence Amplification and Parasitic Oscillation Limitations in Disc Lasers

JOHN B TRENHOLME

Laser Physics Branch

Optical Sciences Division

July 1972

NAVAL RESEARCH LABORATORY
Washington, D.C.

Approved for public release; distribution unlimited.

TABLE OF CONTENTS

I. INTRODUCTION 1

II. FLUORESCENCE AMPLIFICATION 2

A. Fluorescence Amplification in a Sphere 4

1. Single-Wavelength Calculation 4

2. Lorentzian Line Profile 8

3. Gaussian Line Profile 12

4. Summary of Analytic Sphere Results 13

5. Monte Carlo Calculation 14

B. Circular Disc 16

1. Analytic Approximation: Thin Disc, Low Gain 16

α. Radiation Below the Critical Angle 18

β. Radiation Above the Critical Angle 24

γ. Total Result 28

2. Monte Carlo Calculation 30

C. Elliptical Disc 35

D. Discussion 37

III. PARASITIC OSCILLATION 40

A. Lossless Modes in a Circular Disc 42

B. Lossy Modes in a Circular Disc 48

C. Combined Oscillation Diagram 51

D. Parasitic Oscillation with a Rough Edge 52

E. Discussion 55

IV. EFFECTS ON PUMPING..... 57

A. Fluorescence Amplification..... 57

B. Parasitic Oscillation..... 60

V. CONCLUSIONS..... 60

ABSTRACT

In disc laser amplifiers, the achievable inversion (and thus the gain and energy output) is limited by fluorescence amplification and parasitic oscillation. In this paper, analytic results and Monte Carlo calculations of both these effects are presented for spheres, circular discs, and elliptical discs. The effects of gain, fluorescence line profile, refractive indices, and disc thickness on fluorescence amplification are presented. The loss rate is seen to increase rapidly above an across-diameter gain of exp (5) or so, independent of thickness. Parasitic oscillation is analyzed as a function of edge and face index ratios, and of edge roughening. Above exp (3) gain, parasitic suppression is difficult, even with a rough edge. Parasitics thus appear to present more difficulties than fluorescence amplification. The effects of both processes on peak inversion achieved during a pumping pulse are also presented. In conclusion, the maximum practical size of Nd^{3+} glass laser discs is estimated to be about 30 cm due to the effects of parasitic oscillation and fluorescence amplification.

Authorization

NRL Problem K03-08.502

Project No. ARPA Order 2062

This is a final report on one phase of the problem; work is continuing on other phases.

I. INTRODUCTION

Multi-disc laser amplifiers are presently of interest in the production of high-energy light pulses for the generation of dense, high-temperature plasmas for x-ray generation and controlled thermonuclear reactions. Disc amplifiers, as compared to rod amplifiers, have the advantages of more uniform pumping, easy heat removal, small size of individual glass pieces, and less susceptibility to self-trapping. However, the design of these amplifiers must be carefully carried out if costly and time-consuming mistakes are not to be made.

One of the problems which must be understood before disc amplifier design is undertaken is that of fluorescence amplification[1-9] (sometimes called amplified spontaneous emission, superfluorescence, or - incorrectly[10] - superradiance). Fluorescence amplification makes energy storage in lasers more and more difficult as the inversion level rises. Section II of this paper is a discussion of analytical and Monte Carlo calculations of the limitations due to fluorescence amplification in various geometrical shapes relevant to the disc laser problem, and of the effects of varying size, shape, gain, refractive index, and line profile.

Another problem which arises in disc amplifier design is parasitic oscillation. Such oscillation sets a sharp upper limit to the achievable inversion, and often is a more serious problem than fluorescence amplification. In Section III of this paper, parasitic oscillation limits to achievable gain in a single disc will be calculated as a function of the reflections due to the refractive indices of a disc and its surroundings, and as a function of the edge roughness of the disc.

Both fluorescence amplification and parasitic oscillation act to limit the maximum practical size of the discs in a disc amplifier, since both processes get worse as a disc becomes larger (assuming constant inversion density). Accurate analysis of both effects is therefore required to determine the exact limitations on size and gain.

II. FLUORESCENCE AMPLIFICATION

Many materials, when properly pumped, exhibit fluorescence (the spontaneous emission of photons). The fluorescence arises when the upper level of the fluorescent transition is populated by the pumping process, and radiative transitions to the lower level take place. Once the pumping is turned off the fluorescence usually decays exponentially with a time constant called the fluorescent lifetime τ. An exponential decay implies that the process is linear - that is, that the fluorescence is linearly proportional to the population in the upper level.

Suppose, however, that the pumping was so intense that an inversion exists; the population in the upper level is greater than the population in the lower level. The pumped material then exhibits optical gain at the transition frequency, and may be used to amplify light in a laser amplifier or oscillator. However, the fluorescence continues under conditions where gain exists; in fact, the processes of spontaneous emission (fluorescence) and stimulated emission (gain) are inextricably interconnected. This means that fluorescent light, once emitted within the volume of the material, will be amplified before it reaches the edges. This increases the effective fluorescence loss rate, which is the same as decreasing the instananeous

fluorescent lifetime. Because the gain, and thus the added loss, now depends on the inversion level, the fluorescent decay process is no longer linear. Instead, the decay rate becomes faster as the inversion level increases. This fluorescence amplification problem is especially severe in large laser systems, since the long path lengths available lead to large total gain and thus large amounts of fluorescence amplification.

So far we have considered what happens when the pumping is over. However, the fluorescence and gain processes also exist during the pump pulse. If the fluorescence amplification is negligible, so that the system is linear, then doubling the pumping amplitude will double the inversion. In general, the peak inversion will be linearly proportional to the pump pulse amplitude. This proportionality will be destroyed if gain exists in the material. In the presence of fluorescence amplification, equal increments of pumping will yield smaller and smaller inversion (and gain) increases, because the decay rate per unit of inversion will increase with the inversion. The details of pumping in the presence of fluorescence amplification are studied in Section IV.

In this section we will consider only single-pass fluorescence amplification. That is, the edges of the discs will be assumed to be totally absorbing, so that once the fluorescent light hits an edge it is not reflected back into the disc again. This is the best possible edge condition for an amplifier, since if the disc edge is not perfectly black the light will be reflected back into the disc and excite further stimulated emission, thus increasing the fluorescence loss rate. We are therefore

calculating an upper bound on gain due to the effects of fluorescence amplification, since any actual disc will return some reflected light, thus increasing the loss rate and decreasing the gain. We here limit ourselves to the black-edge case because once light is reflected from the edges oscillation will occur at some gain level and a different method of analysis must be used to find this level (see Section III).

A. Fluorescence Amplification in a Sphere

We first calculate the stimulated emission in a sphere, not because sphere lasers[11] are of interest but because an exact analytical calculation is possible in this case. In addition, the sphere forms a simple system in which to demonstrate the effects of line shape.

1. Single-Wavelength Calculation

Consider a laser material in the shape of a sphere. We will assume that a spatially uniform inversion exists throughout the sphere, and make a calculation of the instantaneous rate of fluorescence amplification. The inversion causes the material to have a gain coefficient α, such that the intensity of a pencil of light rays increases as $P = P_o \exp(\alpha \ell)$, where ℓ is the path length along the ray direction. Suppose that spontaneous emission releases a power of I per unit volume. If the sphere has a diameter D, the total spontaneous emission is $I \pi D^3/6$. We will calculate the amount by which this spontaneous emission is amplified.

Introduce a system of spherical coordinates centered on the surface of the sphere (Fig. 1). The angle ϕ is measured from the sphere diameter, and θ gives the rotation around the diameter. The distance r is measured

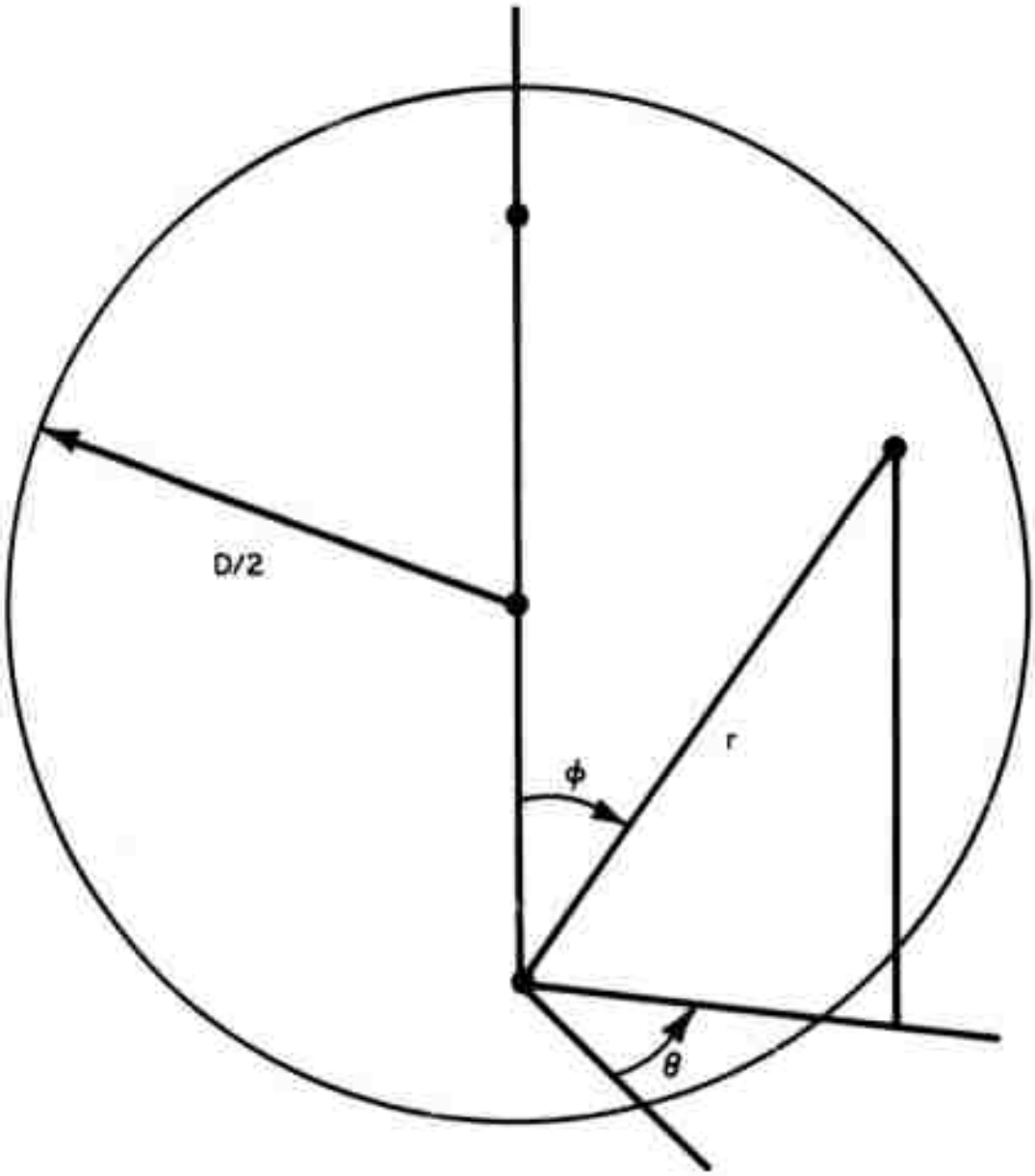

Fig. 1 - Coordinate system for the analysis of fluorescence amplification in a sphere of diameter D. The origin is at the sphere's south pole.

along the direction defined by θ and ϕ. The element of volume in these coordinates is $r^2 \sin\phi \, dr \, d\theta \, d\phi$, and the fluorescence from this volume is $I \, r^2 \sin\phi \, dr \, d\theta \, d\phi$. We assume that this fluorescence is emitted isotropically. An element of sphere surface of area dS at the origin of coordinates will intercept a fraction of the fluorescence equal to the projected area of dS in the direction of the volume element ($dS \cos\phi$) divided by the area of a sphere centered on the volume element and passing through the origin ($4 \pi r^2$). However, the fluorescence will be amplified by a factor $\exp(\alpha r)$ before it reaches dS. Thus dS will intercept a total radiation (spontaneous plus stimulated) of

$$\frac{I}{4\pi} \exp(\alpha r) \cos\phi \sin\phi \, dr \, d\theta \, d\phi \, dS.$$

Now integrate this expression over the volume of the sphere to find the total flux on the area dS:

$$dP = \frac{I \, dS}{4\pi} \int_0^{2\pi} d\theta \int_0^{\pi/2} d\phi \int_0^{D\cos\phi} dr \, e^{\alpha r} \cos\phi \sin\phi$$

$$= \frac{I \, dS}{2} \int_0^{\pi/2} d\phi \int_0^{D\cos\phi} dr \, e^{\alpha r} \cos\phi \sin\phi$$

$$= \frac{I \, dS}{2\alpha} \int_0^{\pi/2} d\phi \left(e^{\alpha D\cos\phi} - 1\right) \cos\phi \sin\phi \quad .$$

With the change of variable $u = \cos\phi$, the flux becomes

$$dP = \frac{I\ dS}{2\alpha} \int_0^1 du\ u \left(e^{\alpha D u} - 1\right)$$

$$= \frac{I\ ds}{2\alpha} \left\{ e^{\alpha D} \left[\frac{1}{\alpha D} - \frac{1}{(\alpha D)^2} \right] + \frac{1}{(\alpha D)^2} - \frac{1}{2} \right\} .$$

By symmetry, all elements of the sphere surface receive the same flux, so the total emission hitting the sphere surface is

$$P = \frac{I\ \pi\ D^2}{2\alpha} \left[\frac{e^{\alpha D}}{\alpha D} \left(1 - \frac{1}{\alpha D}\right) + \frac{1}{(\alpha D)^2} - \frac{1}{2} \right] .$$

To find the amount M by which the original spontaneous emission has been multiplied, divide by the total spontaneous emission $I\ \pi\ D^3/6$ and find

$$M = \frac{3}{2\beta} \left[\frac{2e^{\beta}}{\beta} \left(1 - \frac{1}{\beta}\right) + \frac{2}{\beta^2} - 1 \right] ,$$

where we have introduced the variable $\beta = \alpha D$. Note that β is the log of the gain straight across the sphere. The ratio of stimulated to spontaneous emission is

$$A = \frac{3}{2\beta} \left[\frac{2e^{\beta}}{\beta} \left(1 - \frac{1}{\beta}\right) + \frac{2}{\beta^2} - 1 \right] - 1 .$$

Our calculation has been for a single value of α. However, in actual laser materials the fluorescence and gain are distributed in wavelength according to some line profile, with values from zero to the peak value being represented. The effective values of the spontaneous emission multiplier M and the stimulated-spontaneous ratio A are therefore found by averaging the single wavelength values over the line. From the viewpoint of fluorescence amplification, the worst possible case would be a flat-topped or rectangular line profile, since in that case the line average is equal to the peak value. For more realistic line profiles, in which values less than the peak are represented, the line average is less than the peak α by an amount which depends on the line shape.

It should be noted that $M = 1 + A$ for any line shape, since by definition $M = (J + K)/J = 1 + J/K$ and $A = J/K$, where J is the spontaneous radiation and K is the stimulated radiation.

2. Lorentzian Line Profile

Let us, for example, calculate the values of M and A for a Lorentzian line profile. The gain (and the fluorescence, which has the same line shape) have the form

$$\alpha = \frac{\alpha_p}{1 + \frac{2(\lambda - \lambda_o)}{W}^2} .$$

where α_p is the gain at the peak of the line, λ_o is the center wavelength and W is the full width at half maximum.

Since all that matters when averaging over a line is the fraction of the line representing different values of α, we need to find a function which gives this amplitude weighting. For any symmetric shape of α, we have

$$M = \frac{\int_{-\infty}^{+\infty} \alpha\, M\, d\lambda}{\int_{-\infty}^{+\infty} \alpha\, d\lambda}$$

$$= \frac{\int_{0}^{\alpha_p} \alpha\, M \frac{d\lambda}{d\alpha}\, d\alpha}{\int_{0}^{\alpha_p} \alpha \frac{d\lambda}{d\alpha}\, d\alpha} .$$

Introducing the variable $x = \alpha/\alpha_p$, we have

$$M = \int_{0}^{1} M\,(\alpha_p)\ \rho_L(x)\ dx$$

where the Lorentzian weighting function $\rho_L(x)$ is given by

$$\rho_L(x) = \frac{\alpha \frac{d\lambda}{d\alpha}}{\int_{0}^{\alpha_p} \alpha \frac{d\lambda}{d\alpha}\, d\alpha}$$

$$= \frac{\frac{1}{\sqrt{x(1-x)}}}{\int_{0}^{1} \frac{dx}{\sqrt{x(1-x)}}} .$$

Since the integral in the denominator is the beta function $B(\frac{1}{2},\frac{1}{2}) = \pi$, we have

$$\rho_L(x) = \frac{1}{\pi\sqrt{x(1-x)}} \quad .$$

The line-averaged value of the stimulated/spontaneous ratio is given by

$$A_L = \int_0^1 A\left(\alpha_p x\right) \rho_L(x)\, dx$$

$$= \frac{3}{2\pi}\int_0^1 dx \left[\frac{2e^{\beta x}}{\beta^2 x^2}\left(1 - \frac{1}{\beta x}\right) + \frac{2}{\beta^3 x^3} - \frac{1}{\beta x}\right] \frac{1}{\sqrt{x(1-x)}}$$

where $\beta = \alpha_p D$. Unfortunately, the various terms of the integrand lead to (cancelling) infinities. We therefore calculate A_L by a less direct method.

Firstly, we determine the power series expansion of A by expanding the exponential and combining terms. We find

$$A = \frac{3\beta_\lambda}{8} + \frac{\beta_\lambda^2}{10} + \frac{\beta_\lambda^3}{48} + \frac{\beta_\lambda^4}{280} + \ldots\ldots$$

$$= \sum_{n=1}^{\infty} \frac{3\beta_\lambda^n}{(n+3)(n+1)!}$$

where $\beta_\lambda = \alpha D$.

Then the line average is

$$A_L = \frac{3}{\pi}\int_0^1 dx \left[\sum_{n=1}^{\infty} \frac{\beta^n x^{n-\frac{1}{2}}}{(1-x)^{\frac{1}{2}}\,(n+3)(n+1)!}\right] .$$

We reverse the order of summation and integration, and use the fact that the integral over x is a beta function to find

$$A_L = \frac{3\beta}{16} + \frac{3\beta^2}{80} + \frac{5\beta^3}{768} + \frac{\beta^4}{1024} + \cdots\cdots$$

$$= \sum_{n=1}^{\infty}\left[\frac{3\beta^n}{(n+3)(n+1)!}\prod_{r=1}^{n}\left(\frac{2r-1}{2r}\right)\right] .$$

Since the series must be summed numerically to find the A_L corresponding to some specific β, the error due to truncating at any n must be known. Let the relative error due to ignoring terms beyond m be ϵ_m, so that

$$A_L = \left(\sum_{n=1}^{m} a_n\,\beta^n\right)\left(1 + \epsilon_m\right)$$

where

$$a_n = \frac{3}{(n+3)(n+1)!}\prod_{r=1}^{n}\left(\frac{2r-1}{2r}\right) .$$

Then we have

$$\epsilon_m = \left(\sum_{n=m+1}^{\infty} a_n \beta^n\right) \Big/ \left(\sum_{n=1}^{m} a_n \beta^n\right) \quad .$$

As m becomes large, the ratio of successive coefficients of β in the expansion of A_L becomes

$$\frac{a_{n+1}}{a_n} = \frac{(n+3)(2n+1)}{(n+4)(n+2)(2n+2)} \rightarrow \frac{1}{n + \frac{7}{2}} \quad .$$

We therefore have an upper limit to the truncated part of the series:

$$\sum_{n=m+1}^{\infty} a_n \beta^n < \sum_{n=0}^{\infty} a_{m+1} \beta^{m+1} \left(\frac{\beta}{m+9/2}\right)^n = \frac{a_{m+1} \beta^{m+1}}{1 - \frac{\beta}{m+9/2}} \quad .$$

Therefore

$$\epsilon_m < \frac{a_{m+1} \beta^{m+1}}{\left(1 - \frac{\beta}{m}\right) \sum_m}$$

where $\sum_m = \sum_{n=1}^{m} a_n \beta^n$.

3. <u>Gaussian Line Profile</u>

We may find the effect of a Gaussian line profile having the form

$$\alpha = \alpha_n \, 2^{-4\left(\frac{\lambda - \lambda_o}{W}\right)^2}$$

by the same method used for the Lorentzian line. In this case, the amplitude weighting function is

$$\rho_G(x) = \frac{1}{\sqrt{-\pi \ln x}}$$

and term-by-term integration of the series expansion of A yields

$$A_G = \frac{3\beta}{8\sqrt{2}} + \frac{\sqrt{3}\,\beta^2}{30} + \frac{\beta^3}{96} + \frac{\beta^4}{280\sqrt{5}} = \ldots\ldots$$

$$= \sum_{n=1}^{\infty} \frac{3\beta^n}{(n+3)(n+1)!\,\sqrt{n+1}} \quad .$$

In this case, as in the Lorentzian one, the ratio of successive coefficients approaches $n + 7/2$ as $n \to \infty$, and so the truncation error limit given for the Lorentzian line profile also applies to the series expansion of A for a Gaussian line profile.

4. Summary of Analytic Sphere Results

Table I gives numerical values of the ratio of stimulated to spontaneous radiation A as a function of β (the log of the across-sphere gain at the line peak) for flat-topped, Gaussian, and Lorentzian line profiles of the gain coefficient. For small values of β, we see that A is linearly dependent on β with a coefficient which depends on the line shape. The rise of A with β becomes faster as β approaches unity, and is very fast for values of β much greater than one. We shall see later that this behavior is typical of any shape of laser material. The fact that decay rates rise sharply for $\beta > 1$ means that pumping becomes more and more difficult in this region.

TABLE I

Ratio of stimulated to spontaneous radiation A in a sphere as a function of the log of the across-sphere gain at the line peak β for flat-topped, Gaussian, and Lorentzian line profiles.

β	A_{FLAT}	A_{GAUSS}	A_{LORENT}
.01	.003760	.002657	.001879
.02	.007540	.005326	.003765
.05	.01900	.01340	.009470
.1	.03852	.02710	.01913
.2	.07917	.05543	.03905
.5	.2153	.1484	.1040
1.	.5000	.3352	.2326
2.	1.396	.8790	.5980
5.	12.97	6.491	4.153
10.	593.6	206.8	123.4
20.	3.457×10^{6}	8.097×10^{5}	4.670×10^{5}
50.	6.097×10^{18}	8.778×10^{15}	4.992×10^{17}
100.	7.984×10^{39}	8.055×10^{38}	4.562×10^{38}

5. Monte Carlo Calculation

The amount of fluorescence amplification in a sphere was also calculated by means of a Monte Carlo optical power flow program. Since analytical results are available in the case of a sphere, it may seem pointless to duplicate the results with an approximate method. However, the Monte Carlo

program can be used with geometric shapes of arbitrary complexity. Thus it is much more general in its application than analytic methods, but of course any such program should be checked in a geometry where the results are known. This is the reason for its use in the case of a sphere.

The Monte Carlo program is called ZAP. It traces optical power flow in systems which are made up of segments bounded by planes, spheres, cylinders, cones, conic surfaces, and so forth, or in combinations of such segments. The material in the segments is specified by its refractive index and absorption (or amplification) coefficient. The system surfaces may have constant or angle-varying reflection, both specular and scattering. Each optical ray carries with it up to two hundred wavelength intervals. The bulk and surface properties of the system may vary with wavelength, and the optical power in each wavelength interval will change according to the system properties at its particular wavelength. Rays are started at random from specified sources (surface or volume) with given initial wavelength distributions of power, and traced through the system to find the deposition or extraction of power in all the system elements. A ray cut-off scheme is used which assures that ray truncation error is small without wasting time following weak rays. ZAP was designed for accurate modelling of laser pump cavities (a job it does well), but it is also well suited to the calculation of fluorescence amplification in arbitrary geometries.

The sphere geometry was specified to ZAP, and runs of 2500 rays were made for various values of β to achieve an accuracy of two or three percent. The rays were started at random throughout the sphere, to correspond to uniform inversion. All rays hitting the sphere surface were totally absorbed.

Runs were made for a flat-topped line (one wavelength), for a line with a Gaussian profile, and for a line with a Lorentzian profile. The Gaussian and Lorentzian lines were modelled by dividing a line profile into equal intervals of wavelength. The gain coefficient and starting power in each wavelength interval were then taken proportional to the value of the gain coefficient at the center of the interval. It is necessary to go a large distance out on the tail of the Lorentzian line in order to get a proper weighting of low values of the gain (recall that the Lorentzian amplitude weighting function approaches infinity as the amplitude approaches zero). The final result, with the above number and spacing of wavelengths, is about 1% high for a sphere when the calculation is exact. To this systematic error, the Monte Carlo method adds the previously mentioned random error of 2 or 3%.

A comparison of the analytic and Monte Carlo results for a sphere is shown in Fig. 2. The agreement is quite satisfactory, since the exact result lies within the Monte Carlo error limits in all cases.

B. Circular Disc

We will now consider the case of a circular disc, which is of considerably greater practical interest. We will first perform an approximate analytic calculation which is exact for infinity thin discs at low gain, and then find the results for thick discs and/or high gain by the Monte Carlo method.

1. Analytic Approximation: Thin Disc, Low Gain

Consider the spontaneous fluorescence emitted from a small element of volume in a circular disc with a totally absorbing edge. Some of the radiation will strike the edge directly, while the rest will hit the faces. Both components will be amplified as they travel. The radiation which goes to

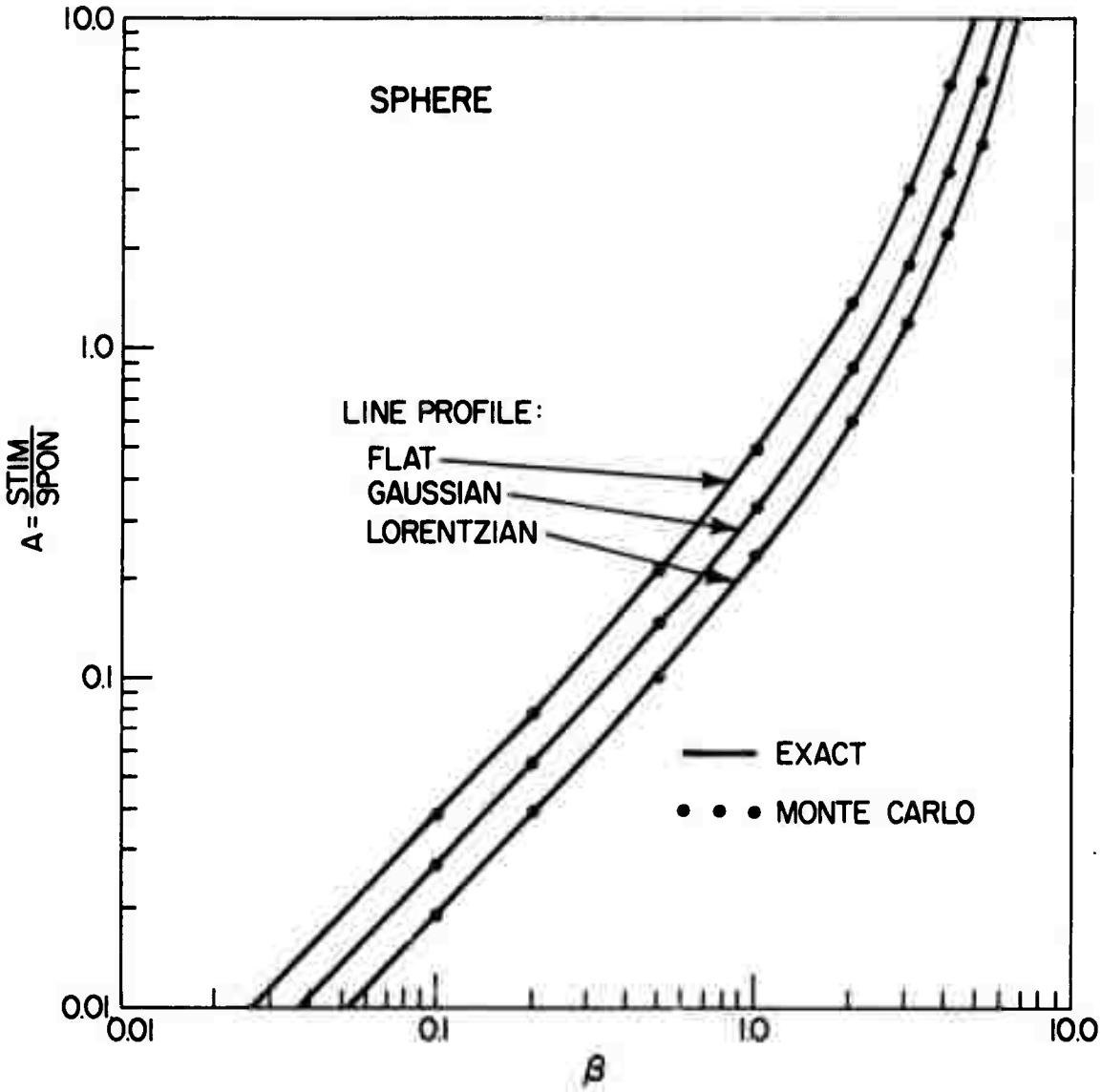

Fig. 2 - Analytic and Monte Carlo values for the ratio A of stimulated to spontaneous loss as a function of the product β of the gain coefficient and diameter for a sphere. Curves are shown for three different line profiles of the gain coefficient.

the faces can be further separated into two parts. Some will strike at less than the critical angle for total internal reflection, in which case most will be transmitted and a small fraction ($\sim$ 5%) reflected back into the disc. Some will strike at more than the critical angle, and will be totally reflected back into the disc. This totally reflected component will continue to bounce back and forth between the faces until it finally strikes the black edge. The path length for this process is the same as if the radiation had gone straight to the continuation of the edge beyond the faces (Fig. 3). Thus there are two parts of the circular disc gain calculation: the radiation below the critical angle, and that above the critical angle.

α. Radiation below the critical angle

Consider a circular disc of diameter D and thickness L. A volume element at a distance r from the disc center emits a pencil of radiation at an angle ϕ from the normal to the disc (Fig. 4). The distance from the point of emission to the edge is ℓ; the ray travels a distance $\ell \csc \phi$ before it hits the edge. Note that this result is independent of the position along an axis normal to the disc faces (the z-position) of the emitter. The distance ℓ depends on the angle θ from a disc radius through the emitting element to the emitted pencil. From Fig. 5 we see that

$$\ell = \sqrt{\left(\frac{D}{2}\right)^2 - (r \sin \theta)^2} - r \cos \theta \ .$$

The radiation is multiplied by a factor of exp ($\alpha \ \ell \csc \phi$) as it travels to the edge; we recall that α is the gain coefficient in the material.

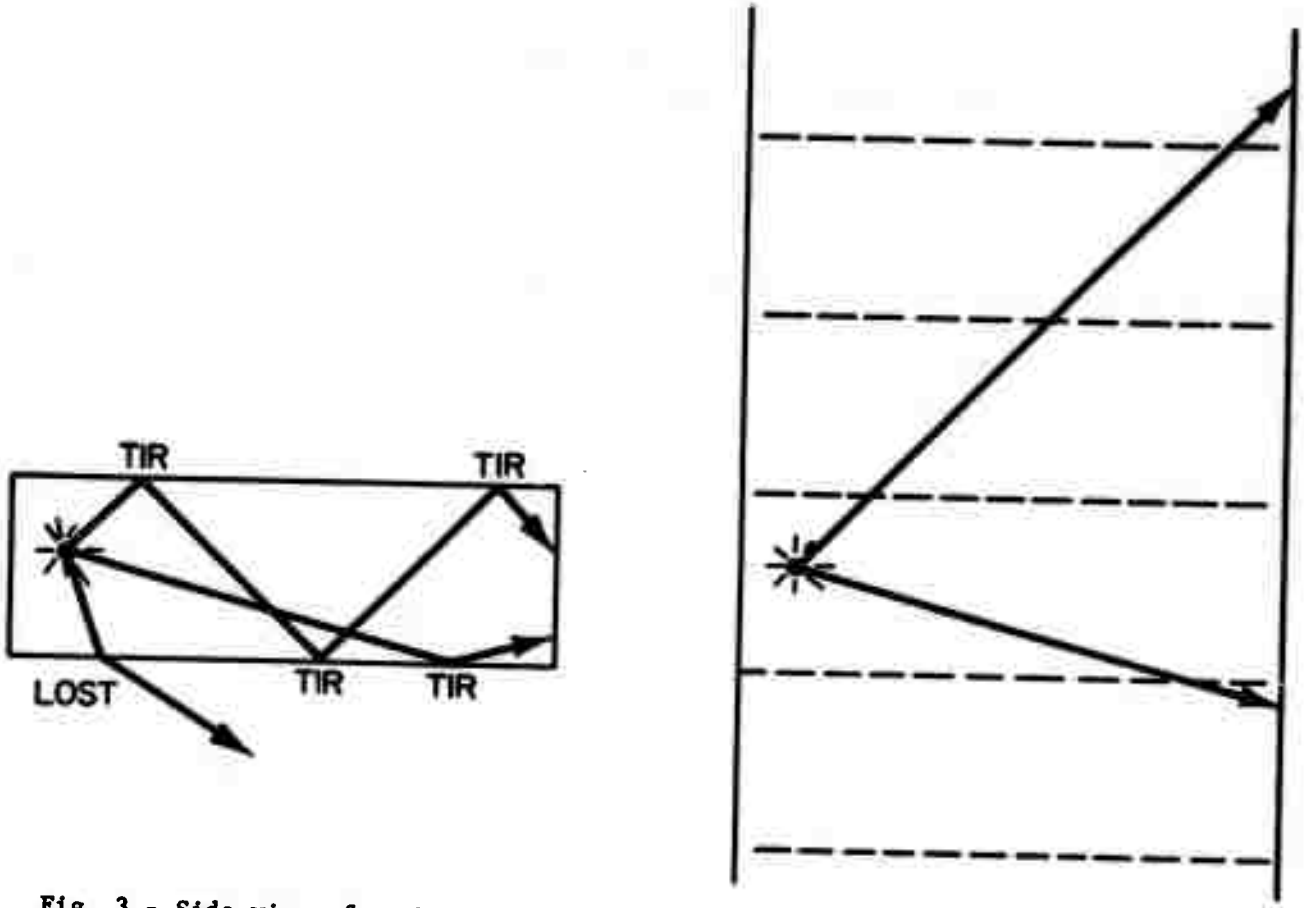

Fig. 3 - Side view of paths of rays which are trapped by total internal reflection in a circular disc. The paths are equivalent to straightline paths in an infinite cylinder, formed by multiple reflections of the disc in its faces.

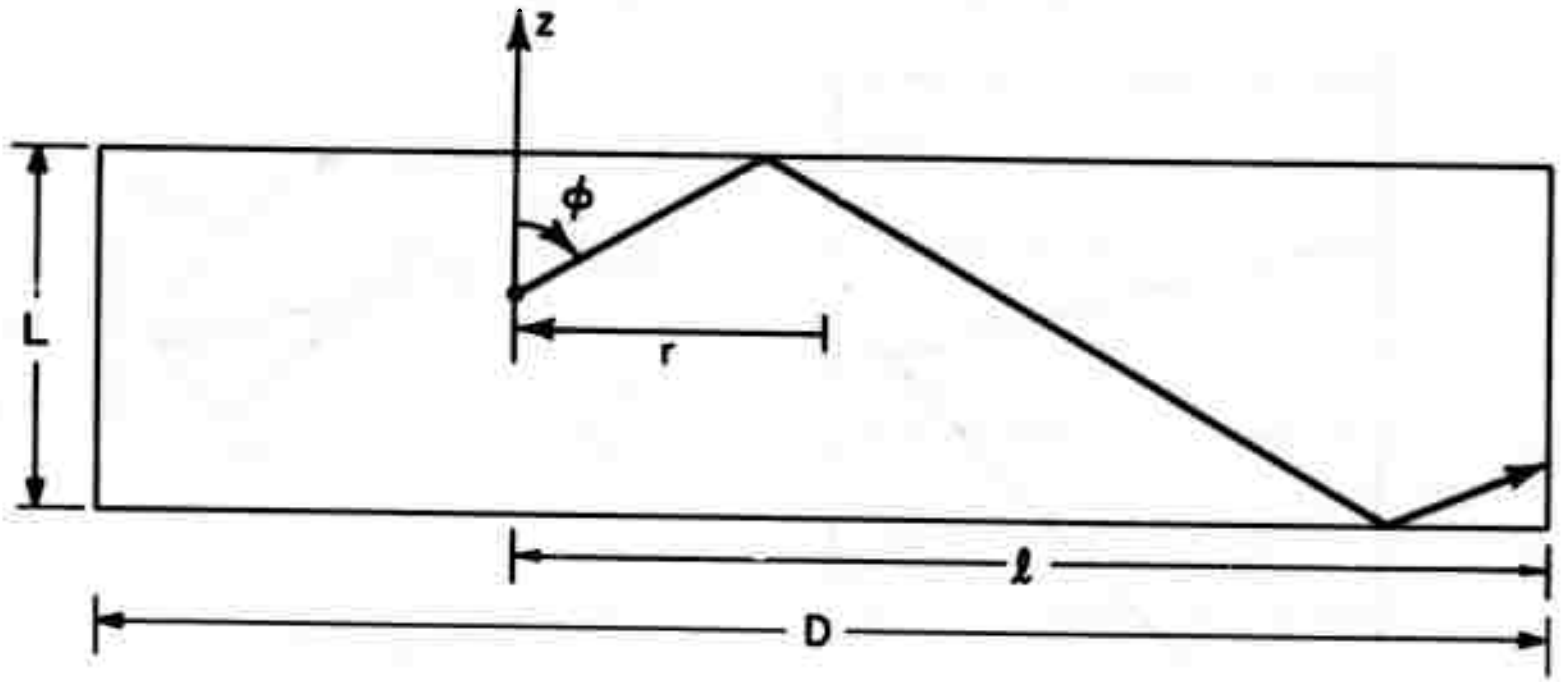

Fig. 4 - Details of the path of a ray which is trapped by total internal reflection in a circular disc. See text.

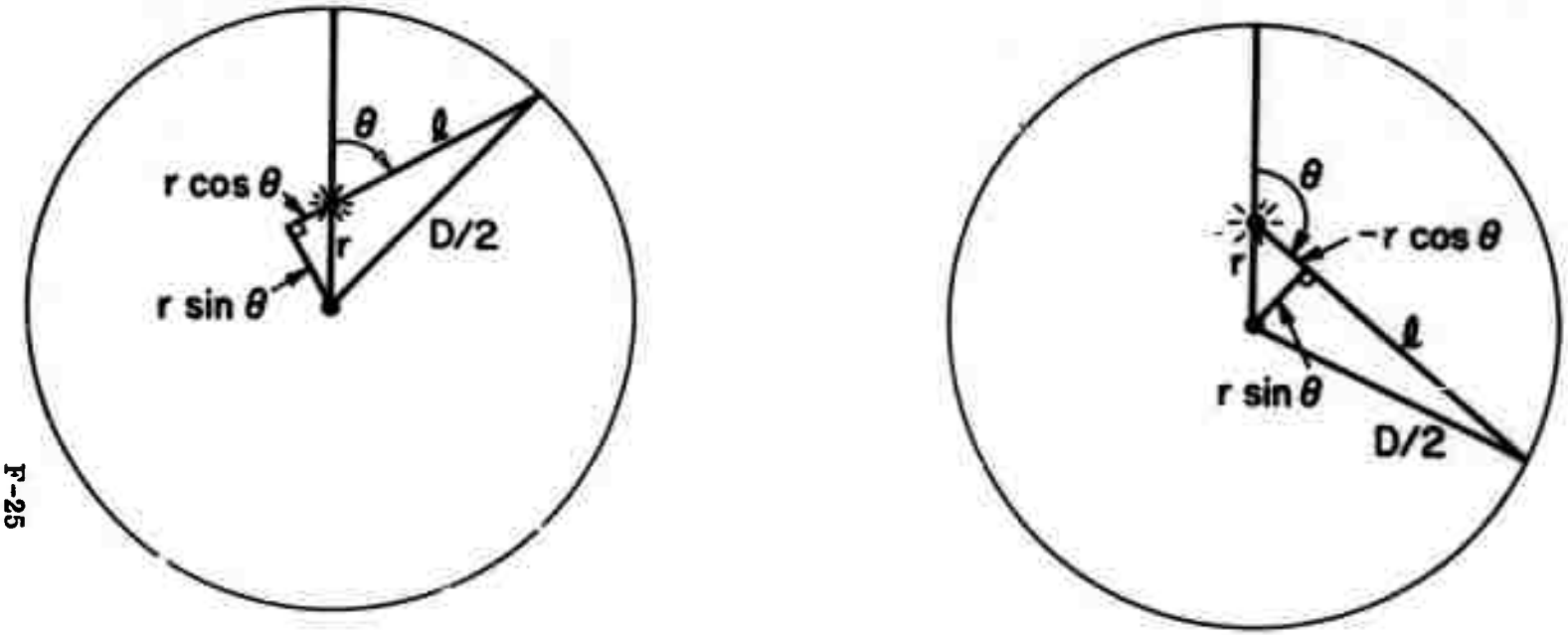

$$(r\cos\theta + \ell)^2 + (r\sin\theta)^2 = (D/2)^2$$

$$\ell = \sqrt{(D/2)^2 - (r\sin\theta)^2} - r\cos\theta$$

Fig. 5 - Geometry for the calculation of the distance from the point of emission to the disc edge. The formula is the same for $\theta < \pi/2$ and $\theta > \pi/2$, as shown.

We must integrate over the disc volume (i.e., over r) and over solid angle. The fractional disc volume at radius r is $8r\,D^{-2}\,dr$, and the fraction of solid angle at θ, ϕ is $(4\pi)^{-1}\sin\phi\,d\theta\,d\phi$. The angle ϕ varies from θ_c to $\pi-\theta_c$, where θ_c is the critical angle, but by symmetry we can take twice the integral from θ_c to $\pi/2$. Likewise we may take twice the integral from 0 to π for θ. The above-critical-angle integral for the ratio M of total to spontaneous emission is then

$$M_1 = \frac{8}{\pi D^2}\int_0^{D/2} dr \int_{\theta_c}^{\pi/2} d\phi \int_0^{\pi} d\theta\; r \sin\phi \exp\left[\frac{\alpha\left(\sqrt{\frac{D^2}{4} - r^2\sin^2\theta} - r\cos\theta\right)}{\sin\phi}\right].$$

This is somewhat clarified by use of the dimensionless variable $u = 2\,r/D$, whence

$$M_1 = \frac{2}{\pi}\int_0^{1} du \int_{\theta_c}^{\pi/2} d\phi \int_0^{\pi} d\theta\; u \sin\phi \exp\left[\frac{\alpha D\left(\sqrt{1 - u^2\sin^2\theta} - u\cos\theta\right)}{2\sin\phi}\right].$$

For the low gain condition $\alpha D \ll 1$, we can expand the exponential in its power series and produce a simpler integral:

$$M_1 = \frac{2}{\pi}\int_0^{1} du \int_{\theta_c}^{\pi/2} d\phi \int_0^{\pi} d\theta\; u \sin\phi \left[1 + \frac{\alpha D\left(\sqrt{1 - u^2\sin^2\theta} - \cos\theta\right)}{2\sin\phi} \pm \ldots\right].$$

The first term in the series yields the simple result $\cos\theta_c$, but the second term is more difficult. Sin ϕ cancels in numerator and denominator, so the ϕ integral is just $(\pi/2 - \theta_c)$, leaving

$$M_1 = \cos\theta_c + \frac{\alpha D}{\pi}\left(\frac{\pi}{2} - \theta_c\right)\int_0^1 du \int_0^\pi d\theta\, u\left(\sqrt{1 - u^2 \sin^2\theta} - u\cos\theta\right).$$

In the θ integral, the $\cos\theta$ portion integrates to zero, leaving twice the complete elliptic integral of the second kind

$$2E\left(u^2\right) = \int_0^\pi d\theta\left(\sqrt{1 - u^2 \sin^2\theta}\right).$$

so that

$$M_1 = \cos\theta_c + \frac{2\alpha D}{\pi}\left(\frac{\pi}{2} - \theta_c\right)\int_0^1 du\, u\, E\left(u^2\right)$$

which by the change of variable $q = u^2$ becomes

$$M_1 = \cos\theta_c + \frac{\alpha D}{\pi}\left(\frac{\pi}{2} - \theta_c\right)\int_0^1 dq\, E(q)$$

thus yielding the final result

$$M_1 = \cos\theta_c + \frac{\alpha D}{\pi}\left(\frac{\pi}{2} - \theta_c\right)\left(\tfrac{1}{2} + G\right) \pm \ldots$$

where $G = .9159656 \cdots$ is Catalan's constant.

β. Radiation above the critical angle

Let us follow the radiation emitted at above the critical angle for total internal reflection by a volume element at distance b from the disc face (Fig. 6). Starting at angle ϕ from the normal to the face, the ray travels a distance b sec ϕ before it hits the face. The relative strength is now exp (α b sec ϕ). A fraction T is transmitted through the face and (for our purposes) lost, while (1-T) is reflected and crosses the disc. The path length to the opposite face is L sec ϕ (recall that L is the disc thickness), and so the reflected ray is amplified by exp (α L sec ϕ). It then again loses a fraction T to the outside, and (1-T) recrosses the disc, is amplified, and is partially transmitted and partially reflected. The bouncing process continues until the ray hits an absorbing edge. Let the relative strength at the first encounter of the face be P = exp (α b sec ϕ), and define the gain on a pass all the way across the disc to be K = exp (α L sec ϕ). Then the ray strength is as follows (Fig. 7):

1	at the start
P	at the initial face intercept
P(1-T)	after the first reflection
P(1-T)K	after crossing to the opposite face
$P(1-T)^2K$	after the second reflection
$P(1-T)^2K^2$	after the second full crossing
$P(1-T)^3K^2$	after the third reflection
$P(1-T)^3K^3$	after the third full crossing

and so forth. The total amount radiated is then $PT + PT(1-T)K + PT(1-T)^2K^2 + PT(1-T)^3K^3 + \ldots$ which sums to $PT/[1 - (1-T)K]$ if we take an infinite number

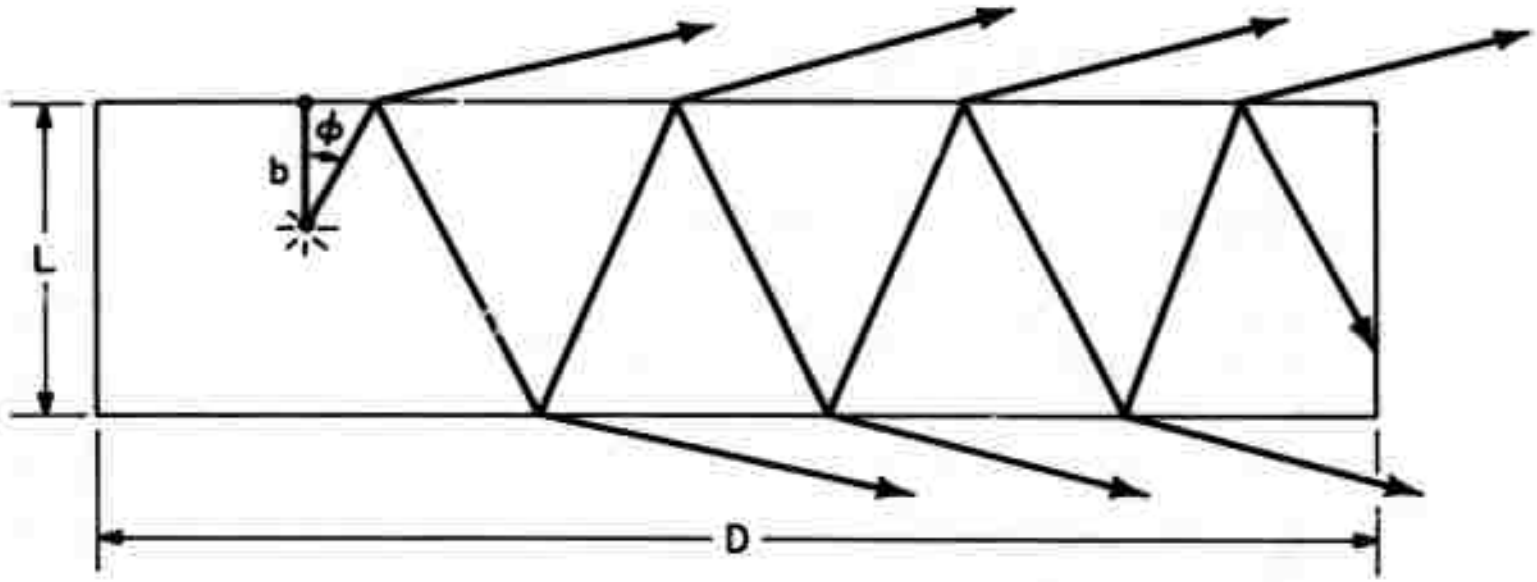

Fig. 6 - Path of a ray which is partially transmitted at the disc faces. The ray bounces from face to face, losing energy to the exterior on each reflection.

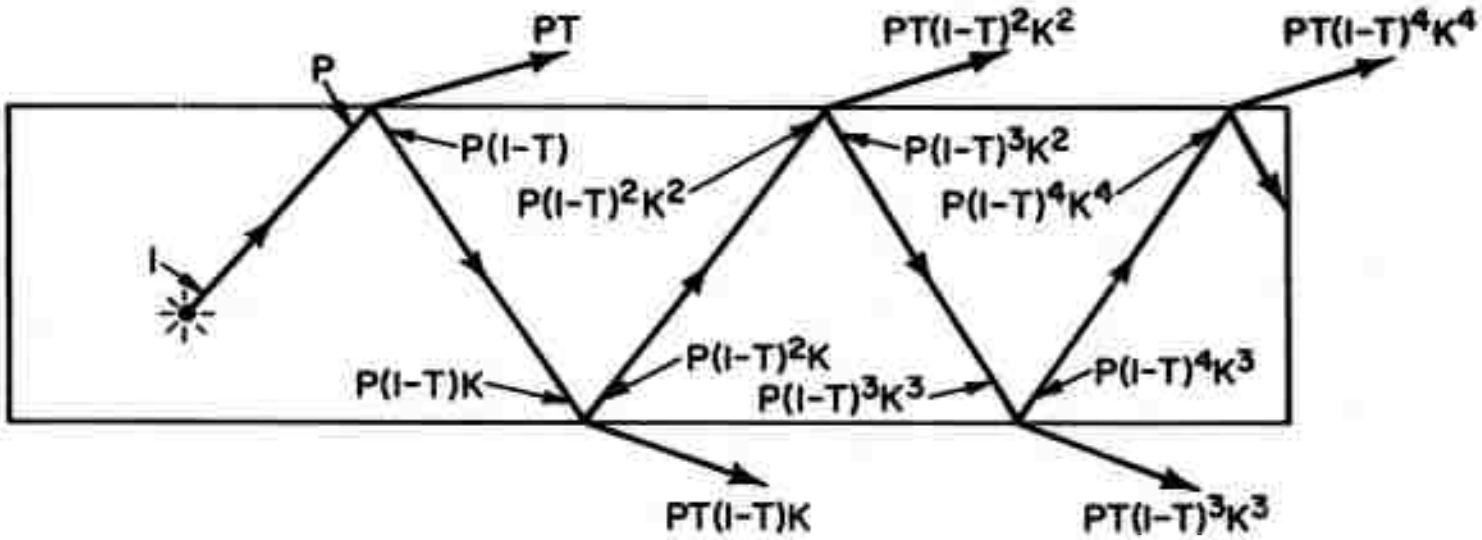

Fig. 7 - Amount of power in a partially reflected ray as a function of position. P is the power at the first reflection, T is the transmitted fraction at the surface, and K is the gain across the disc. See text.

of terms. Of course, the actual ray will terminate after a finite number of bounces, but the error in the infinite-bounce approximation is small as long as the gain across the disc times the reflectivity is small, in which case the ray strength is reduced to a negligible value in just a few bounces. This small-gain case is exactly the one we are calculating, so we will use the infinite-bounce approximation above, which overestimates the actual result.

We must integrate over angle and position to find the overall average gain. The fractional solid angle at angle ϕ is $\sin\phi\, d\phi/2$, and the fractional volume is db/L (note that the r and θ integrals have vanished because there is no r or θ dependence in the infinite-bounce approximation). Then the above-critical-angle radiation contributes approximately

$$M_2 \cong \frac{1}{L}\int_0^{\theta_c} d\phi \int_0^L db \; \frac{T \exp(\alpha\, b \sec\phi) \sin\phi}{1 - (1-T)\exp(\alpha\, L \sec\phi)}$$

where we have (by symmetry) taken twice the ϕ integral from 0 to θ_c rather than the integral from 0 to θ_c plus the integral from $\pi - \theta_c$ to π. For $\alpha L \ll 1$ we expand the exponentials in the integrand and divide to get

$$M_2 \cong \frac{1}{L}\int_0^{\theta_c} d\phi \int_0^L db \; \sin\phi \left(1 + \frac{\alpha b}{\cos\phi} + \frac{(1-T)\,\alpha L}{T\cos^2\phi} \pm \ldots\right)$$

$$= \int_0^{\theta_c} d\phi \; \sin\phi \left(1 + \frac{\alpha L\left(\frac{1}{T} - \frac{1}{2}\right)}{\cos\phi} \pm \ldots\right)$$

which integrates to

$$M_2 \cong \left(1 - \cos\theta_c\right) + \alpha L \left(\frac{1}{T} - \frac{1}{2}\right) \ln\left(\frac{1}{\cos\theta_c}\right) \pm \cdots \quad .$$

While performing this calculation we have made another approximation: we have assumed that the transmission T is independent of angle, and have ignored the fact that T depends on polarization. In actual fact, T decreases as ϕ approaches the critical angle, and more radiation returns to the disc to be amplified. If we use the normal-incidence value for T, this approximation underestimates the actual result, and (hopefully) tends to offset the overestimate due to the infinite-bounce approximation. In any case, both approximations get better as the disc gets thinner, since then even a ray starting near the edge takes many bounces to get to that edge, and the across-disc gain is low so even if a ray takes more bounces to exit than we calculate (due to greater reflectivity) the added radiation is small.

Y. Total Result

Adding together the results above and below the critical angle, we find that for low gain ($\alpha D \ll 1$ and $\alpha L \ll 1$) and thin discs we have

$$M \cong 1 + \alpha D \left(\frac{1}{2} - \frac{\theta_c}{\pi}\right)\left(\frac{1}{2} + G\right) + \alpha L \left(\frac{1}{T} - \frac{1}{2}\right) \ln\left(\frac{1}{\cos\theta_c}\right) .$$

This result is for one value of α, and thus corresponds to a flat line profile. Values of m corresponding to other line shapes may be calculated as in the sphere case.

With a Lorentzian line profile, the amplitude weighting function is $\rho_L(x) = \left[\pi\sqrt{x(1-x)}\right]^{-1}$. We can write M in the form $M = 1 + B\alpha(\lambda)$, where B is independent of λ. Then

$$M_L \cong \int_0^1 dx \; \frac{1 + B\,\alpha\,x}{\pi\sqrt{x(1-x)}}$$

$$= 1 + \frac{B\alpha}{\pi}\int_0^1 dx \; \sqrt{\frac{x}{1-x}}$$

$$= 1 + \frac{B\alpha}{\pi}\;\frac{\pi}{2}\,,$$

where α is now the gain coefficient at the line peak.

We thus have

$$M_L \cong 1 + \frac{\alpha}{2}\,B,$$

or

$$M_L \cong 1 + \alpha\,D\left(\frac{1}{4} - \frac{\theta_c}{2\pi}\right)\left(\frac{1}{2} + G\right) + \alpha\,L\left(\frac{1}{2T} - \frac{1}{4}\right)\ln\left(\frac{1}{\cos\theta_c}\right).$$

With a Gaussian line profile, $\rho_G = \left(\sqrt{-\pi\ln x}\right)^{-1}$ and we get

$$M_G \cong \int_0^1 dx \; \frac{1 + B\,\alpha\,x}{\sqrt{-\pi\ln x}}$$

$$= 1 + \frac{B\alpha}{\sqrt{\pi}} \int_0^1 dx \; \frac{x}{\sqrt{-\ln x}}$$

$$= 1 + \frac{B\,\alpha}{\sqrt{\pi}} \sqrt{\frac{\pi}{2}} \quad .$$

We thus have

$$M_G \cong 1 + \frac{\alpha}{\sqrt{2}} \; B,$$

or

$$M_G \cong 1 + \frac{\alpha D}{\sqrt{2}} \left(\frac{1}{2} - \frac{\theta_c}{\pi}\right)\left(\frac{1}{2} + G\right) + \frac{\alpha L}{\sqrt{2}} \left(\frac{1}{T} - \frac{1}{2}\right) \ln\left(\frac{1}{\cos\theta_c}\right) \quad .$$

Since the low-gain result in any geometry will always have the form $M = 1 + C\alpha$ or $A = C\alpha$ (where C is a constant depending on the geometry), the flat-topped, Gaussian, and Lorentzian lines will always have the low-gain ratios $2:\sqrt{2}:1$ exhibited for the sphere and cylinder.

2. <u>Monte Carlo Calculation</u>

ZAP was used to find the stimulated-spontaneous ratio A in circular discs. Again the inversion (and thus the gain coefficient) was assumed spatially uniform. The reflection at the face was taken as the average over polarization. In Fig. 8, we see the results for flat, Gaussian, and Lorentzian line profiles in discs whose thickness is 20% of their diameter.

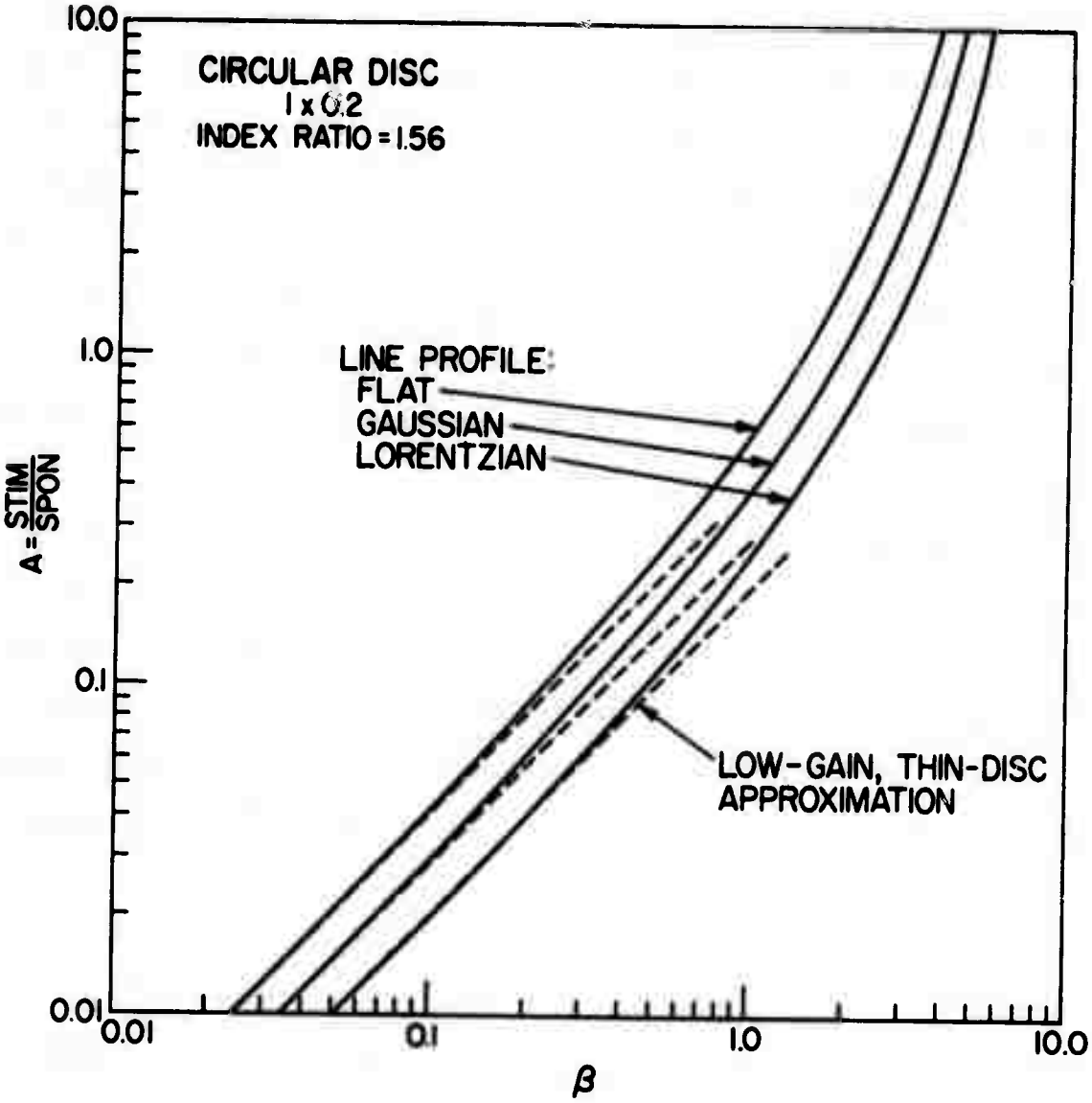

Fig. 8 - Monte Carlo values of the ratio A of stimulated to spontaneous loss as a function of the product β of the gain coefficient and diameter for a circular disc of thickness equal to 20% of its diameter. The ratio of the refractive index inside the disc to that outside the faces is 1.56. Curves are shown for three different line profiles of the gain coefficient. The low-gain, thin-disc approximation is shown for comparison.

The refractive index inside the discs was 1.56 times the index outside and the circular edge of the disc was totally absorbing. The A ratios are shown as a function of $\beta = \alpha D$, where α is the gain coefficient at the line peak and D is the disc diameter. Also shown is the small-gain, thin-disc approximation. The approximation is seen to be good below $\beta \cong .1$, even for discs this thick.

The A curves have the same general shape as the curves for a sphere, except for a faster rise when A is greater than one (this faster rise is due to the longer path available in the cylinder due to total internal reflection from the faces).

The amount of fluorescence amplification in a disc depends on the disc thickness and on the ratio of refractive indices inside and outside the sphere, as well as on the gain coefficient. As the cylinder index approaches the index of its surroundings, less and less of the light inside it undergoes total internal reflection, and A becomes lower. For exact index matching, no light returns into the disc and A has its minimum value. The variation of A with index ratio is shown in Fig. 9 for various values of β. The low-gain, thin-disc approximation is also shown in Fig. 9, and is seen to match the Monte Carlo results well except at low index ratios, where the angle for total internal reflection increases and the infinite-bounce approximation breaks down.

The Monte Carlo results for the variation of A with relative disc thickness are shown in Fig. 10. The values for $\beta = .1$ are compared to the low-gain, thin-disc approximation. The approximation is seen to be good to at least 80% disc thickness. The most interesting feature of these results

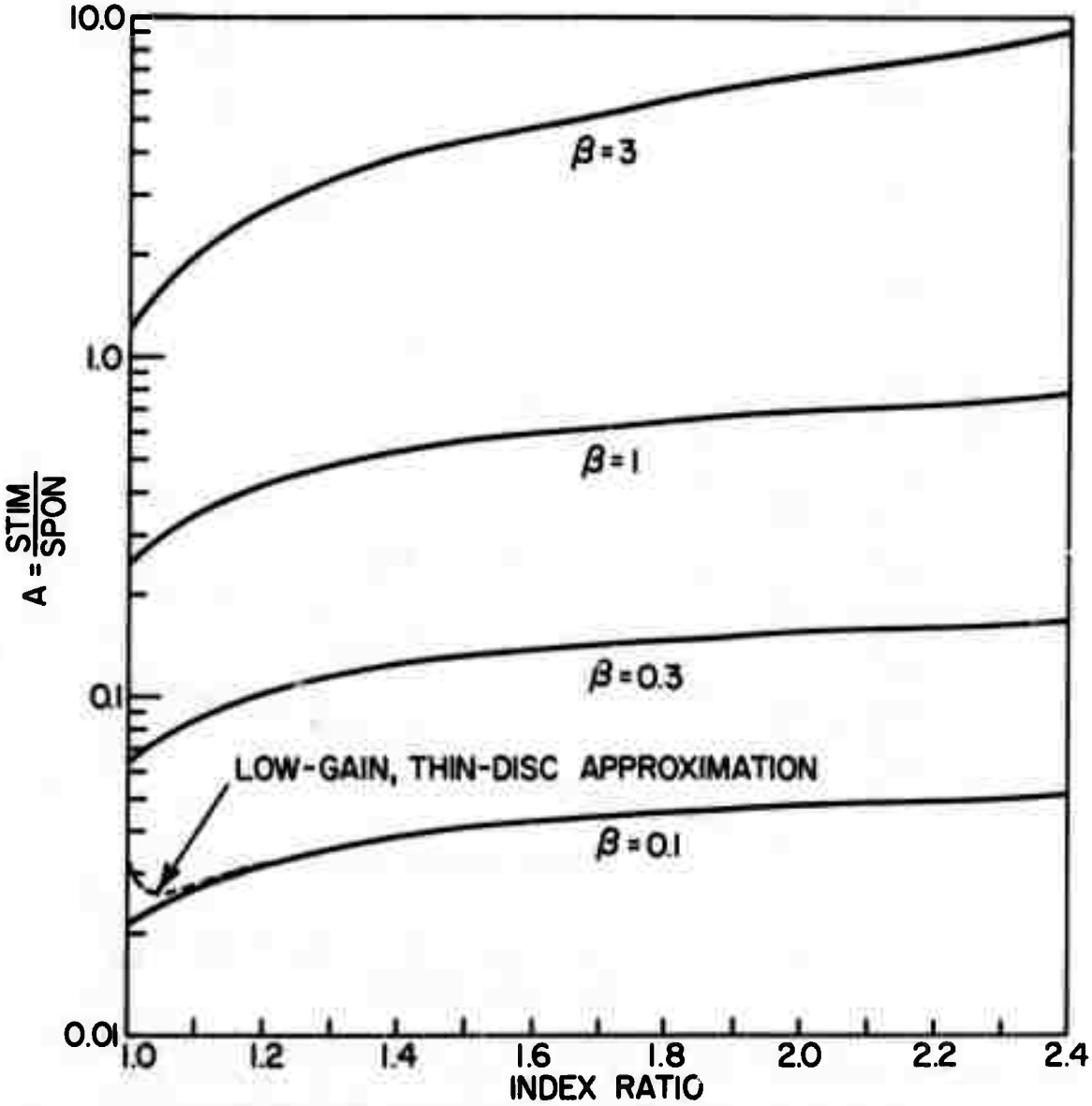

Fig. 9 - The effect of inside-outside refractive index ratio on the fluorescence amplification in a 20% thickness circular disc. The increase with index ratio is due to the greater fraction of radiation trapped by total internal reflection at higher ratio. The low gain, thin-disc approximation is compared to the $\beta = .1$ result, which it fits exactly except at low ratios.

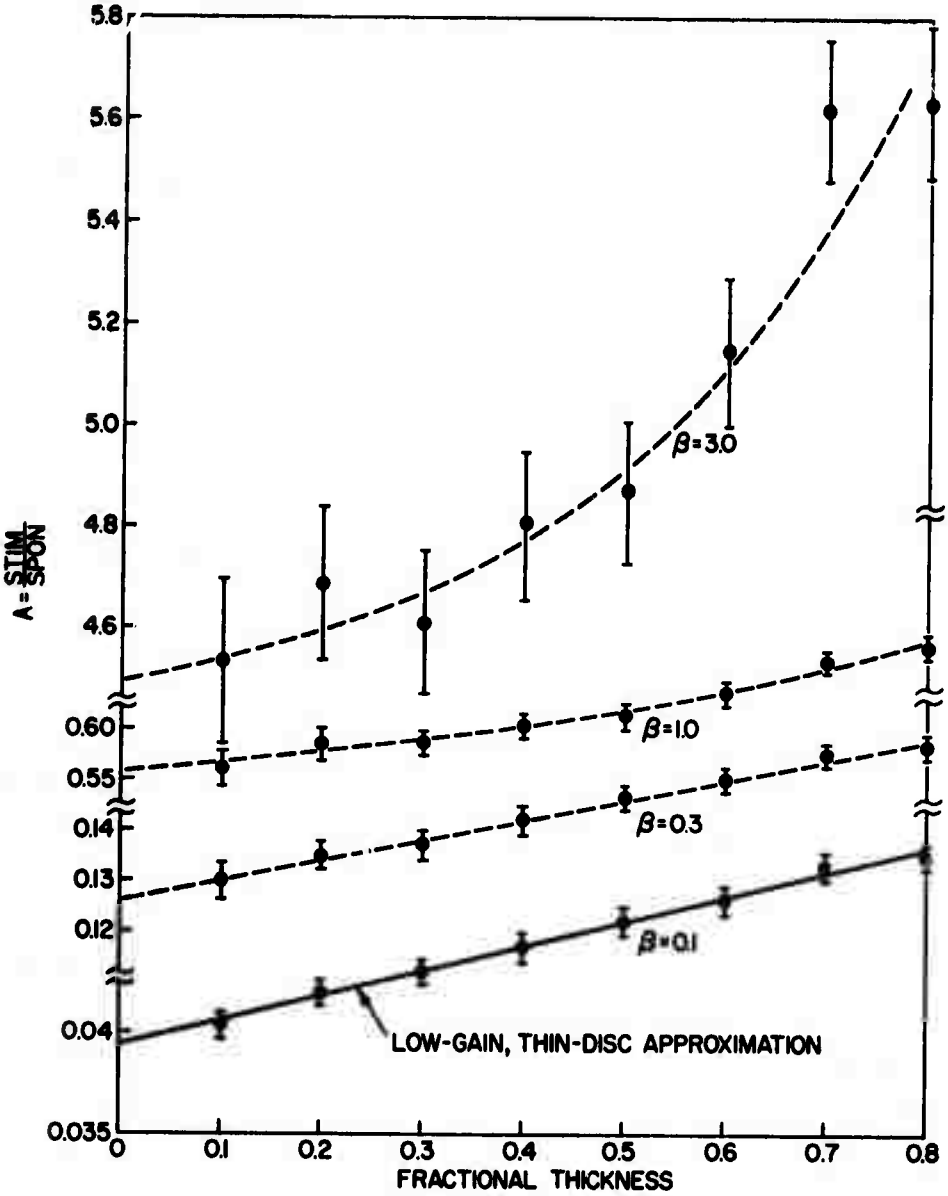

Fig. 10 - The fluorescence amplification in a disc of 1.56 inside-outside refractive index ratio as a function of the ratio of the disc thickness to its diameter. The increase is slow because the principal contribution is from rays undergoing total internal reflection, and this contribution is independent of thickness. The low-gain, thin-disc approximation is compared with the β = .1 result. Note broken vertical scale.

is the very slow increase of fluorescence amplification with disc thickness. This slow increase arises because much of the fluorescence amplification in a disc is due to rays which are totally reflected at the faces of the disc, and the contribution of such rays is independent of disc thickness. Since useful laser gain is roughly proportional to disc thickness, discs should be as thick as possible within the constraints of pumping uniformity, thermal distortion, self-trapping, and fabrication difficulty. There is also an obvious advantage in trading a thick, weakly-doped disc for a thin, highly-doped disc, since fluorescent lifetime usually decreases with doping.

C. Elliptical Disc

Analytical computation is difficult in the case of an elliptical disc, and unnecessary in light of the good fit of the Monte Carlo results to the sphere and circular disc cases. Therefore only Monte Carlo calculations were made in this case. The computations were for discs whose major and minor axes were in the ratio 1:0.5, which is typical of laser glass tilted at Brewster's angle in air if the beam is round. The thickness was 1/7 of the major axis, since this corresponds to an actual disc in use in a multidisc laser amplifier in our laboratory. Once more, the inversion was uniform, the inside-outside refractive index ratio was 1.56, and the curved edge was totally absorbing.

The ratio of stimulated to spontaneous radiation, A, is shown in Fig. 11 as a function of $\beta = \alpha D$, where D is the disc major axis. The results are about 70% of those for a circular disc of diameter equal to the ellipse major axis, for low values of β. As β increases, this fraction decreases.

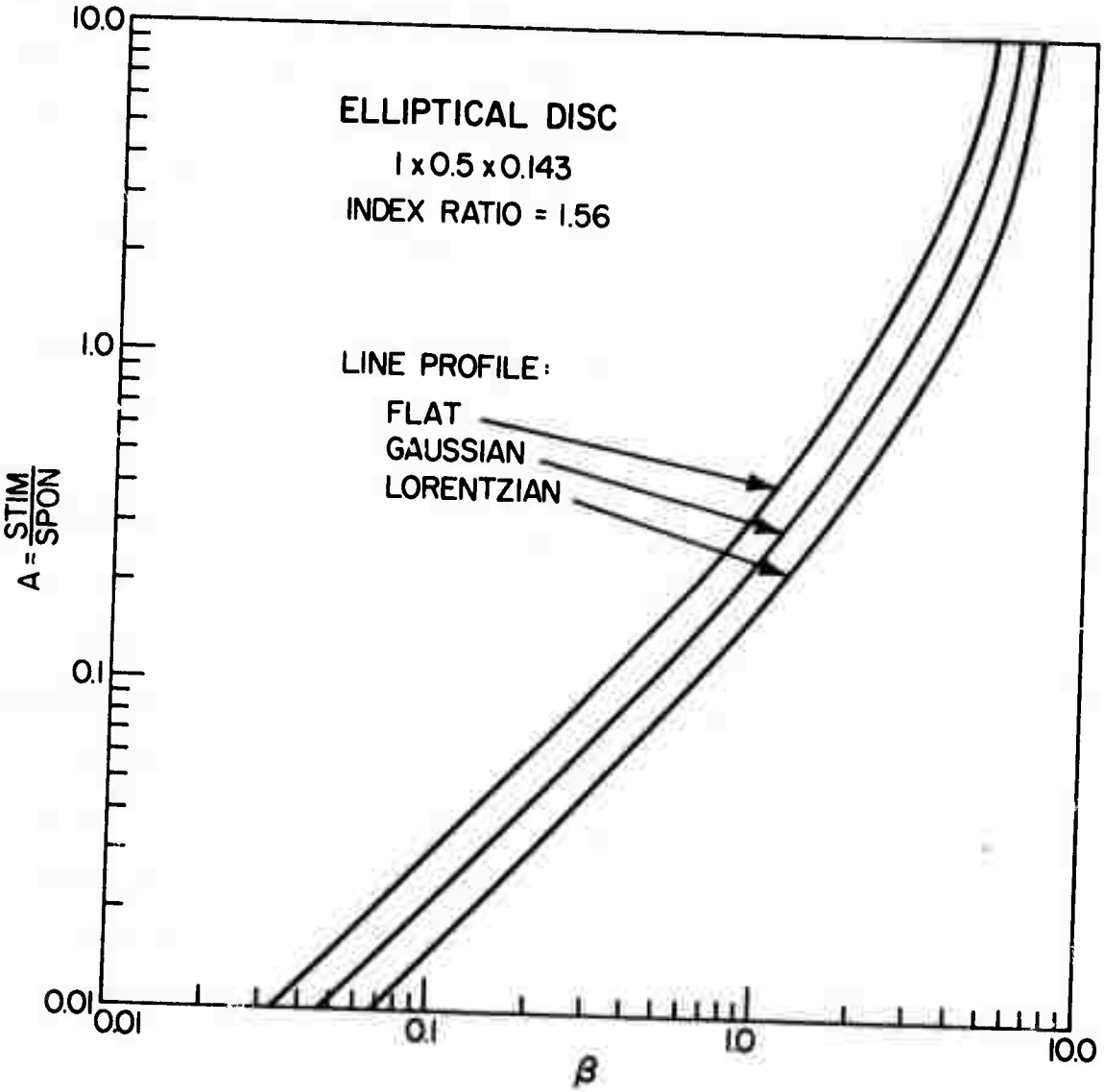

Fig. 11 - Monte Carlo values of the ratio A of stimulated to spontaneous loss as a function of the product β of the gain coefficient and major axis for an elliptical disc of minor axis 50%, and thickness 14.3%, of its major axis. The inside-outside refractive index ratio is 1.56. Curves are shown for three different line profiles of the gain coefficient.

The radiation absorbed by the disc edge and that exiting from the disc face were found separately in the elliptical disc calculations. These values are shown in Fig. 12 as a function of β. We see that the greater part of the stimulated radiation increase at high β goes to the disc edge, rather than to the disc face. In high energy systems, the edge absorber may thus have to withstand large loadings.

D. Discussion

We have studied the problem of fluorescence amplification, in which the fluorescence emitted by a material with optical gain is amplified by stimulated emission as it passes through the material, thus increasing the natural fluorescent loss rate. We have defined the ratio of total loss to fluorescence M and the ratio of stimulated to spontaneous loss A.

Fluorescence amplification causes pumping to become more and more difficult as the stored energy (and thus the gain) increases in a material. In effect, the energy decays with an instantaneous fluorescent lifetime given by τ/M, where τ is the natural or low-gain lifetime. This means that as the pump strength is increased, inversion will not increase in proportion. The resulting pump efficiency decrease is a slow function of the pump energy, rather than the abrupt upper limit due to parasitic oscillation (Section III). The exact details of the process depend on the geometry of the material and the fluorescent line shape, but in general pumping is quite difficult when the gain across the longest dimension of the material is about exp (5) $\cong$ 150 or more (we assume that the natural lifetime is not extremely long, so that its decrease by a factor of 10 is a serious problem). The effect of fluorescence amplification on pumping will be considered in detail in Section IV.

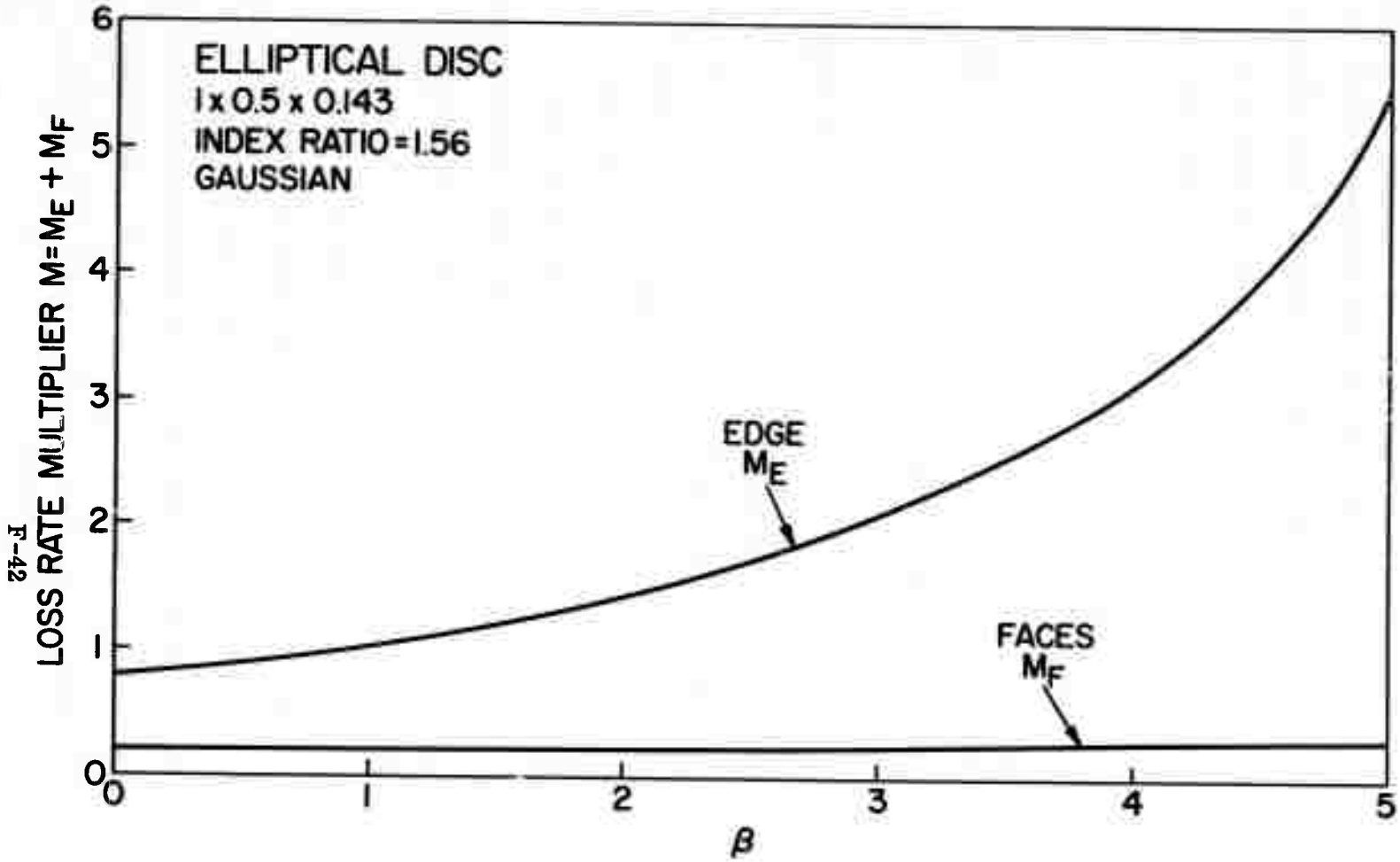

Fig. 12 - Amount of ratio M of total to spontaneous loss due to radiation absorbed at edge (M_E) and lost from faces (M_F) in an elliptical disc, as a function of β. Most of the increased loss due to fluorescence amplification is seen to go to the edge rather than out the faces.

The line shape of the fluorescent emission (and gain) is important because a line with broad, low wings has less fluorescence amplification than a more rectangular line, for the same peak value of the gain. For low gain, we have shown that the ratio A has the relative values $2:\sqrt{2}:1$ for flat (rectangular), Gaussian, and Lorentzian gain profiles; Monte Carlo calculations show that these relations are roughly maintained at higher gains. Actual laser materials often have complicated, multi-peaked line profiles, but in principle we could find the single-wavelength value A_λ for the geometry we are using and then (perhaps numerically) integrate this with the amplitude weighting function corresponding to the laser material we are using. In practice, it is undoubtedly sufficient to estimate where in the flat-Gaussian-Lorentzian family the actual line shape lies and to interpolate to find A for that line shape.

The geometry of the amplifying material strongly influences the amount of fluorescence amplification. In the simple case of a sphere, A and M depend only on the product of the gain coefficient α and the disc diameter D, and of course on the line shape. When we consider a circular disc, we find that A and M depend not only on αD, but also on the refractive index ratio between the inside and outside of the disc, and on the ratio of thickness to diameter of the disc. An index match between inside and outside is desirable since it leads to the least possible fluorescence amplification. However, in short-pulse high-power lasers the index-matching material may cause problems due to self-focusing damage, so this remedy is not always available. The fluorescence amplification is also least for vanishingly thin discs, but of course such discs have insufficient gain along the path of the actual laser pulse to even

overcome their own surface losses. Since the increase of fluorescence amplification with thickness is slow, it is not harmful to increase the disc thickness until it is limited by other considerations. For example, the deposition of pump energy changes with disc thickness, but this question is beyond the scope of this paper. An elliptical disc has the same type of index and thickness behavior as a circular disc, but the fluorescence amplification is somewhat less than in the circular case. Elliptical discs have the additional advantages of smaller size and hence lower cost (when compared to circular discs tilted at Brewster's angle to a circular beam) and closer coupling to the pump sources.

III. PARASITIC OSCILLATION

Parasitic oscillation takes place when a material with optical gain has in it (or through it) a light path which returns on itself. Under this condition, the material will break into oscillation when the gain is large enough to overcome the path losses. Such undesired oscillation will make it impossible to increase the stored energy in the oscillating volume, since once oscillation begins all further pumping is immediately converted into oscillating power and lost. If the mode of oscillation fills an appreciable fraction of the laser volume, it thus sets a sharp upper limit to the available stored energy, and therefore the gain. If the mode gain does not vary greatly with frequency across the gain line profile (or if it oscillates so rapidly as to effectively sample all values of gain in the line), then the place where oscillation will begin is the line peak. This means that the maximum

gain coefficient α determines the oscillation threshold, so that rectangular line profiles are the best from the view point of parasitic oscillation, since they maximize the available laser output at the onset of oscillation.

Parasitic oscillation cannot be calculated by ordinary Monte Carlo methods, since the power in oscillating modes typically flows in precise directions at any point in space. Unless the Monte Carlo algorithm is lucky enough to start a ray at exactly the correct position going in exactly the correct direction, it will not find the mode at all. Imagine, for example, the simple case of two reflecting plane mirrors 1 cm in diameter spaced 10 cm apart, with a laser material between them. In the case of such large mirrors, we can ignore diffraction and do a simple ray-tracing analysis. The mode occupies the whole volume between the mirrors, so the Monte Carlo method just has to get the angle right. In fact, however, there is only one exactly correct direction - the direction perpendicular to the mirrors. Rays at a small angle from the correct direction will bounce between the mirrors a number of times before they miss a mirror and exit from the system. On the average, a ray at an angle ϵ from the system axis will bounce N times, where N is given by

$$N \cong \frac{d}{2\ell\epsilon}$$

where d is the mirror diameter and ℓ is the inter-mirror distance. If the Monte Carlo method starts rays at random in angle, the probability of getting N or more bounces from a ray is

$$p(N) \cong \left(\frac{d}{4N\ell}\right)^2 \quad .$$

The rapid decrease of p as N increases means that a very large number of rays must be started to get a ray with many bounces. For our 1 cm by 10 cm resonator, we must start 16,000,000 rays (on the average) to get one with 100 or more bounces. Clearly, random-starting ray-tracing methods are not suitable for mode finding unless considerable modification is made to them. Without such modification, a Monte Carlo algorithm may give what seem to be perfectly reasonable results even in the presence of an oscillating mode above threshold.

Since our Monte Carlo program is unsuitable for the analysis of parasitic oscillation, a simplified analytic method was used instead. The method uses a simple ray-tracing viewpoint which ignores diffraction effects. In addition, phase is ignored and only amplitude is considered. Both these simplifications are justified on the basis that typical discs used in large lasers are very much larger than a wavelength, so that modes have low diffraction loss and close spacing in wavelength.

We will first consider lossless modes which rely on total internal reflection, then modes which have some loss and thus require gain in the laser material to achieve threshold, and finally the effects of a rough disc edge on the mode threshold.

A. Lossless Modes in a Circular Disc

It is possible for a mode which is totally lossless to exist in a circular cylinder because all reflections are by total internal reflection.

Consider, for example, the disc shown in Fig. 13. The disc faces are in contact with a medium with refractive index n_1, the disc itself has index n_2, and the (smooth) edge of the disc is clad with an absorbing material of index n_3 (we ignore any imaginary component of the absorber index). If the edge coating index n_3 is less than n_2, then total internal reflection is possible off the inside of the disc edge, and a ray can bounce losslessly around the disc perimeter in a plane parallel to the faces (Fig. 14). In addition, if the outside index n_1 is less than the disc index n_2, a ray can bounce from face to face of the disc by total internal reflection (Fig. 15).

In general, a ray may bounce off both the faces and the edge, and the ray path will be complicated (Fig. 16). We can describe such a path in terms of two angles: Ψ measures the angle of the ray from a disc diameter (Fig. 14), and θ measures the angle from a normal to the faces (Fig. 15). The angle of incidence on the faces is thus θ, and the angle ϕ of incidence on the edge obeys $\cos\phi = \cos\Psi \sin\theta$. Thus as θ becomes smaller, ϕ becomes larger. For a ray to be lossless, we must have both $\theta > \theta_c = \sin^{-1}(n_1/n_2)$ and $\phi > \phi_c = \sin^{-1}(n_3/n_2)$. This dual condition sets a lower bound on Ψ, since we must have $\cos\Psi < \cos\phi_c/\sin\theta_c$. Thus we must have

$$\Psi \geq \cos^{-1}\left[\frac{n_2}{n_1}\sqrt{1 - \left(\frac{n_3}{n_2}\right)^2}\right]$$

which implies that the lossless oscillation exists only outside a center portion of the disc of radius $R = D/2 \sin\Psi_o$, where Ψ_o is the minimum value of Ψ.

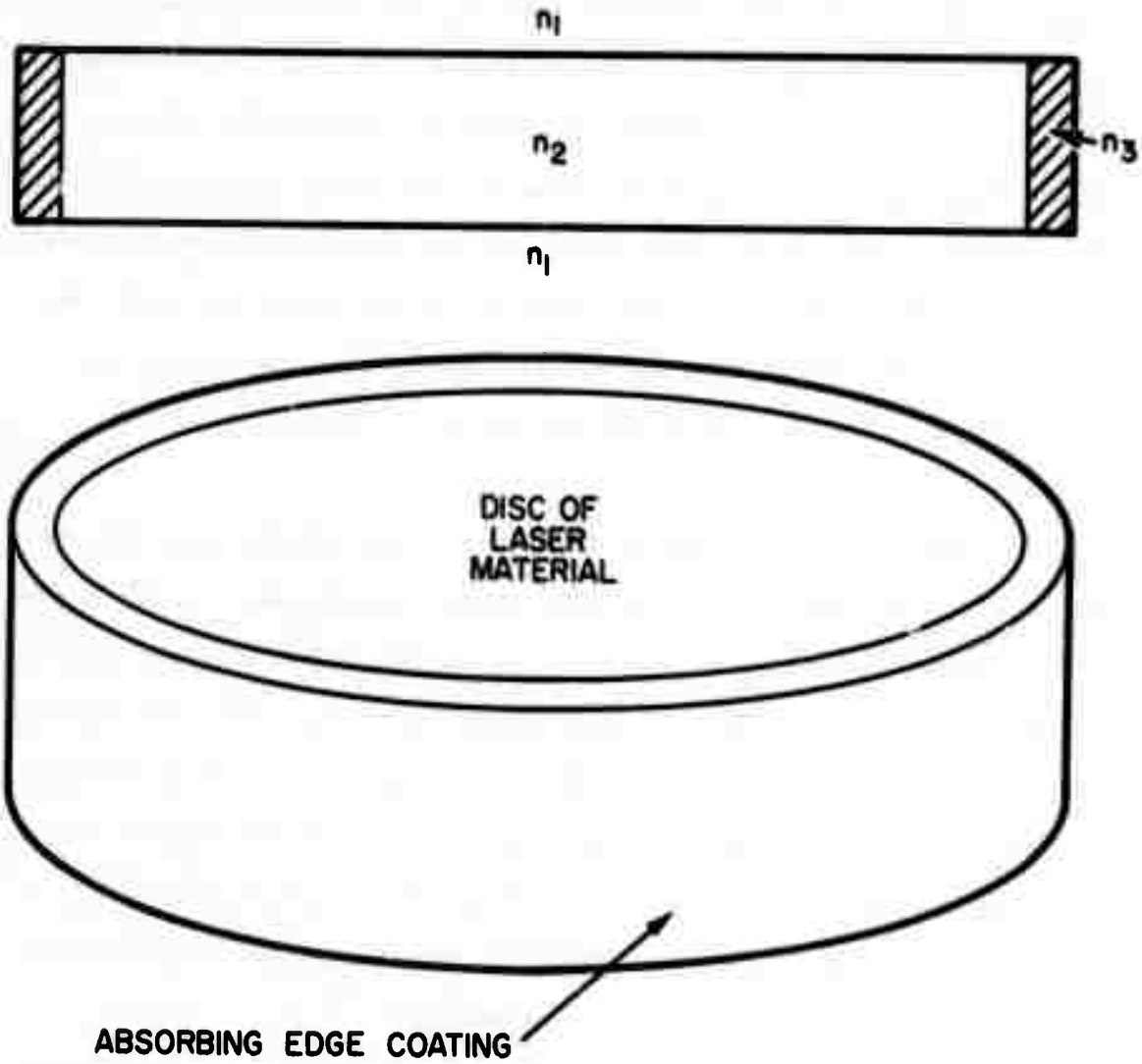

Fig. 13 - The disc configuration considered in the parasitic oscillation calculation. A circular disc of index n_2 is embedded in a material of index n_1. The edge of the disc is clad with an absorbing material of index n_3.

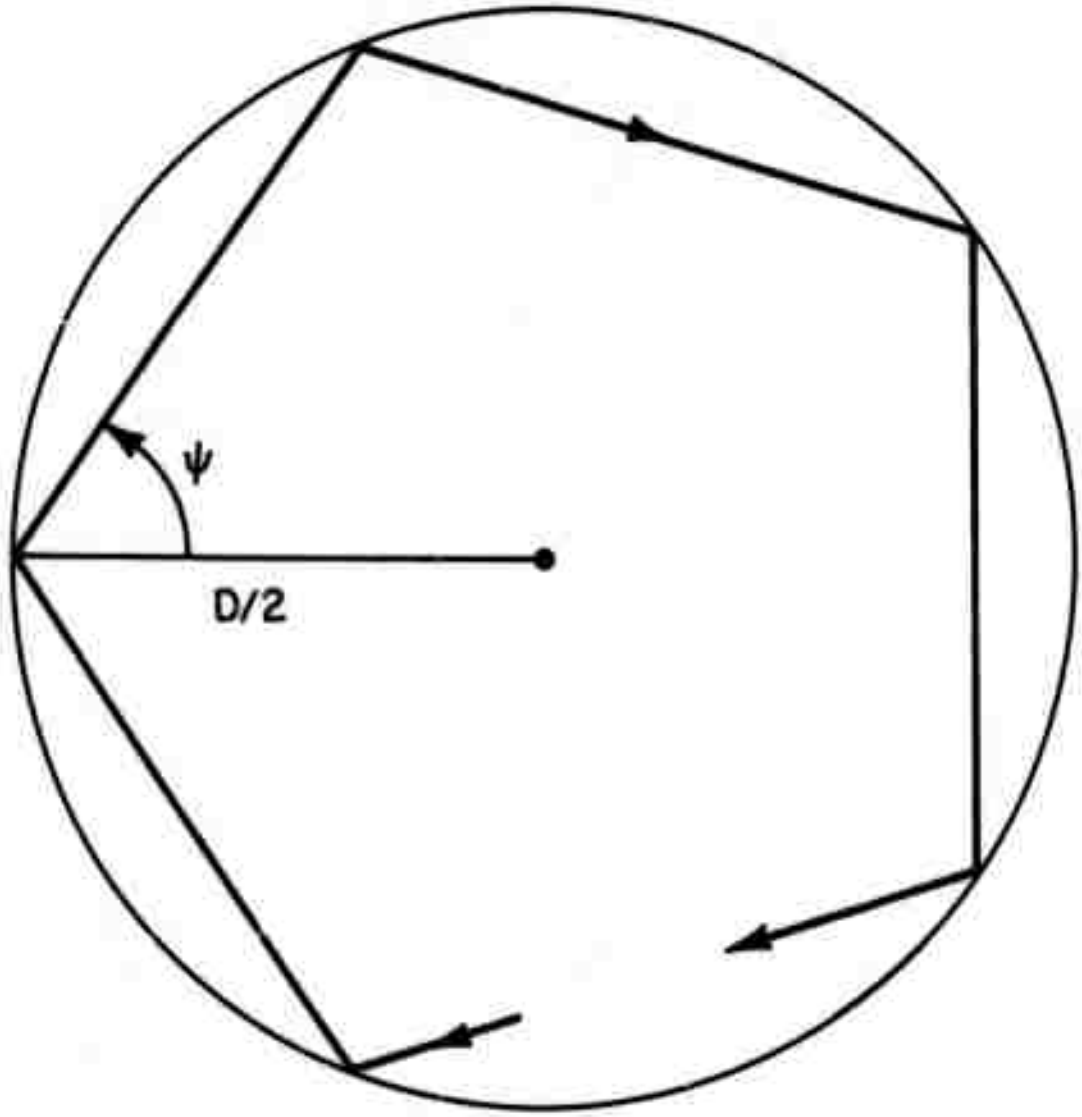

Fig. 14 - Typical lossless ray path possible if the disc index is greater than the edge-coating index. Total internal reflection takes place at the reflection points.

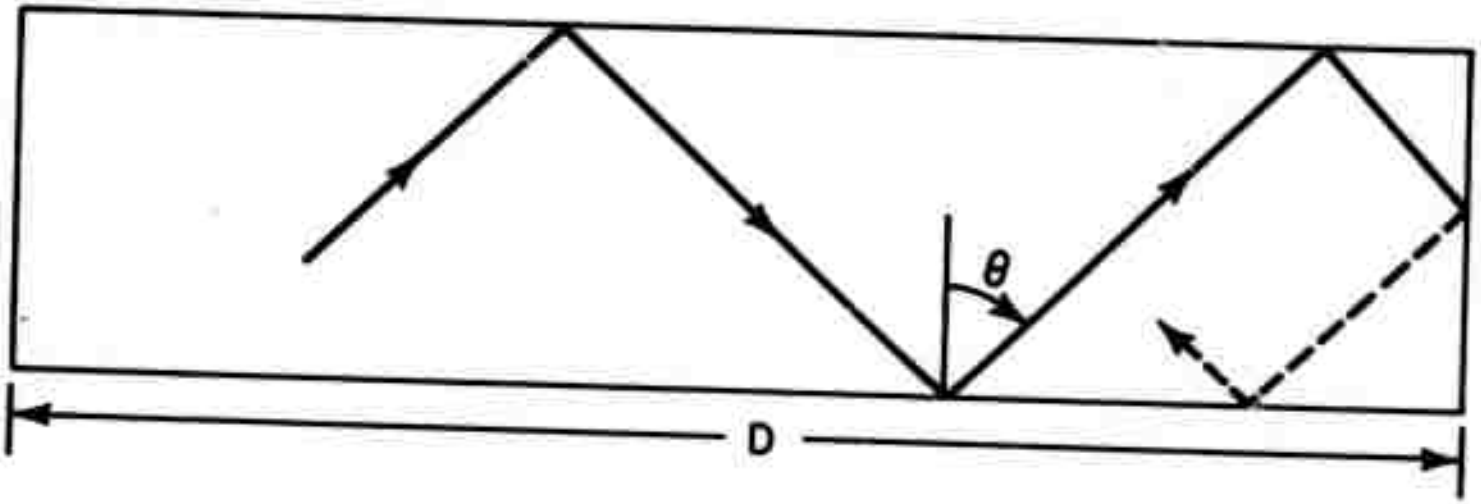

Fig. 15 - Typical ray path possible if the disc index is greater than the index of the surroundings. Total internal reflection takes place at the face reflections.

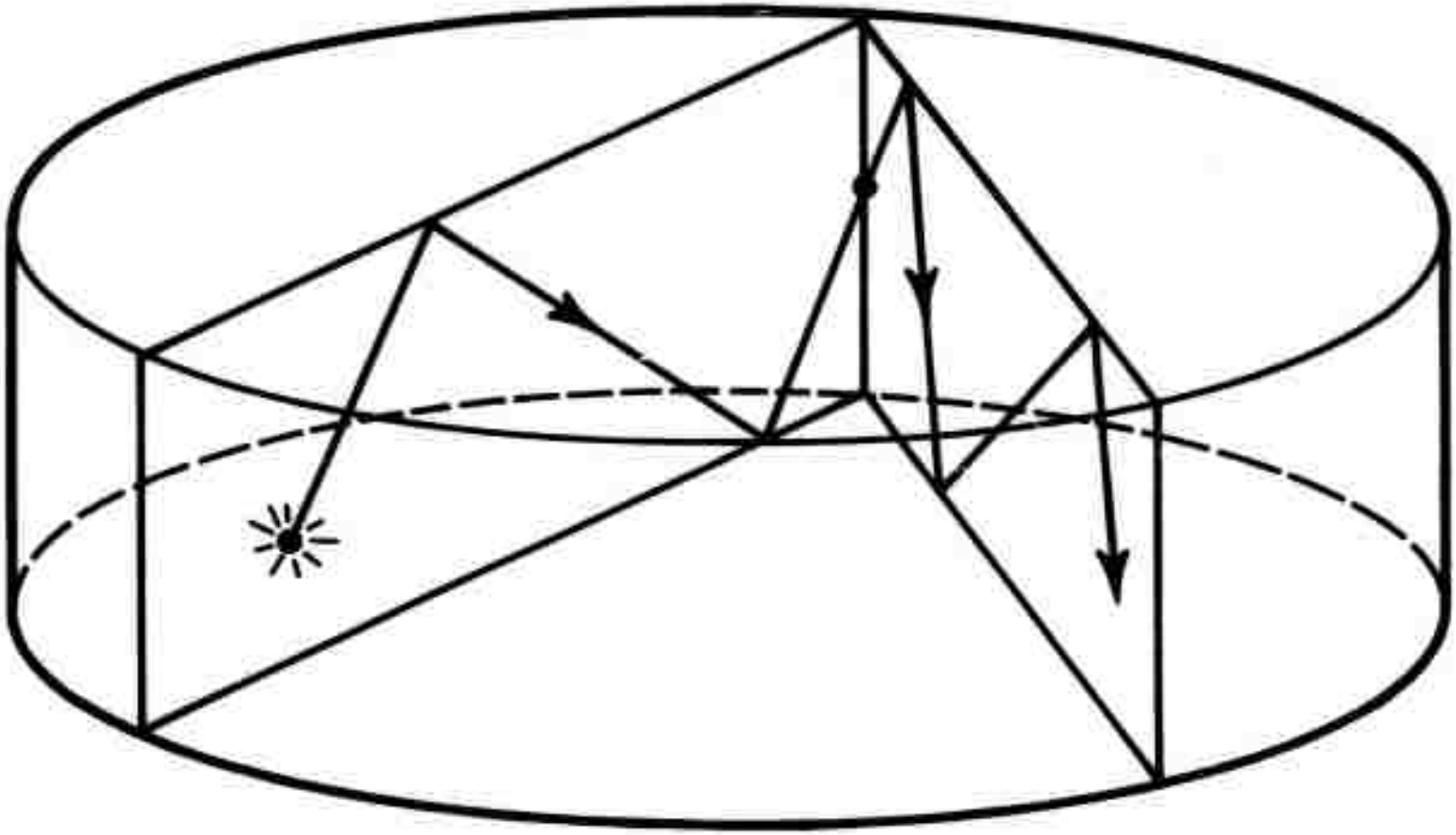

Fig. 16 - The path of a ray which bounces off both the faces and the edge. Between edge reflections, the path zig-zags in a plane perpendicular to the faces; the path changes to a new plane at each edge reflection.

We conclude that if the edge coating refractive index is less than the disc index lossless modes can exist in a circular disc. This means that as soon as there is any gain at all in the material oscillation will commence and further gain rise will be inhibited. The actual mode volume depends on the edge/disc and outside/disc refractive index ratios. It is clearly desirable to have the coating index larger than the disc index, since then lossless modes do not exist.

B. Lossy Modes in a Circular Disc

Even if there are no lossless modes in a disc, it will still oscillate on lossy paths if the gain is high enough. We wish to find the maximum gain achievable without parasitic oscillation, so we must find the mode with the least loss.

Consider a path which reflects off the disc faces by total internal reflection, but which has only partial reflection at the edge. We will use the same angles Ψ, θ as we used in the previous section to describe the ray. Let us assume that the edge reflection is given by R_σ, the larger of Fresnel's reflection coefficients. Then

$$R = \left[\frac{\sin(\phi - r)}{\sin(\phi + r)}\right]^2$$

where $r = \sin^{-1}(n_2/n_3 \sin\phi)$ and ϕ, as before, is given by $\phi = \cos^{-1}(n_1/n_2 \cos\Psi)$ when θ is equal to θ_c. The path length between edge bounces is $D \cos\Psi / \sin\theta_c = D\, n_2/n_1 \cos\Psi$, where D is the disc diameter. To oscillate, the net gain must be equal to unity, or

$$\left[\frac{\sin(\phi-r)}{\sin(\phi+r)}\right]^2 e^{\frac{\alpha D n_2}{n_1}\cos\Psi} = 1$$

where α is the gain coefficient at the line peak, $\phi = \cos^{-1}(n_1/n_2 \cos\Psi)$ and $r = \sin^{-1}(n_2/n_3 \sin\phi)$. We could now vary Ψ in this expression to find the minimum α required for oscillation, but it is sufficient to examine the behavior at $\Psi = 0$ and $\Psi = \pi/2$. Solving for αD, we have

$$\beta(\psi) = \alpha D = \frac{2n_1 \ln\left[\frac{\sin(\phi+r)}{\sin(\phi-r)}\right]}{n_2 \cos\Psi}$$

and

$$\beta(0) = 2\rho \ln\left(\frac{\sqrt{\sigma^2+\rho^2-1} + \rho}{\sqrt{\sigma^2+\rho^2-1} - \rho}\right)$$

where $\rho = n_1/n_2$ and $\sigma = n_3/n_2$, while

$$\beta(\pi/2) = \frac{4\rho^2}{\sqrt{\sigma^2 - 1}} \quad .$$

We have again used the variable $\beta = \alpha D$.

The calculation is only valid for $n_1 < n_2$ and $n_3 > n_2$, or $\rho < 1$ and $\sigma > 1$. In this region $\beta(0)$ is always less than $\beta(\pi/2)$, so we find that the lowest threshold modes are those in which the ray proceeds across a diameter of the disc, bouncing from face to face at the maximum angle which will produce total internal reflection. Such modes obviously fill the entire

disc volume. The threshold condition may be written

$$\beta_{CRIT} = \frac{2n_1}{n_2} \ln\left(\frac{\sqrt{n_1^2 - n_2^2 + n_3^2} + n_1}{\sqrt{n_1^2 - n_2^2 + n_3^2} - n_1}\right) .$$

Since the worst-case rays are those that travel diametrically across a circular disc, we expect the threshold for an elliptical disc of major axis equal to the disc diameter to be essentially the same as the circular threshold, since the same path is available. The surface curvature at the reflection points is of course larger in the elliptical case, but this should raise the threshold only slightly, since all it does is make the resonator somewhat more unstable.

In addition to the modes involving reflection off the edges, a relatively thick disc may also oscillate between its faces. The threshold for this process is easily calculated, since the face reflection at normal incidence is

$$R = \left(\frac{n_2 - n_1}{n_2 + n_1}\right)^2$$

and the gain from face to face is just exp (αL), e L is the disc thickness. We must have R exp(αL) = 1, or

$$(\alpha L)_{CRIT} = 2 \ln\left(\frac{n_2 + n_1}{n_2 - n_1}\right) .$$

Of course, this result also applies to elliptical discs.

C. Combined Oscillation Diagram

We may show the effects of both lossless and lossy modes on a single diagram in the ρ, σ plane (recall $\rho = n_1/n_2$ and $\sigma = n_3/n_2$). When lossless modes fill the disc from a radius R outward, we use

$$\cos\Psi = \frac{1}{\rho}\sqrt{1 - \sigma^2}$$

and

$$\sin\Psi = \frac{2R}{D}$$

to derive

$$\left[1 - \left(\frac{2R}{D}\right)^2\right]\rho^2 + \sigma^2 = 1 \quad .$$

Thus the locus of constant R in the ρ, σ plane is an ellipse. This result applies if $\rho < 1$ and $\sigma < 1$; if $\rho > 1$ then there is no total internal reflection off the faces and the answer becomes independent of ρ, since the oscillations lie in planes parallel to the disc faces and ignore the condition at the faces.

Lossy modes obey

$$\beta = 2\rho \ln\left(\frac{\sqrt{\sigma^2+\rho^2-1} + \rho}{\sqrt{\sigma^2+\rho^2-1} - \rho}\right) \quad ,$$

so we may draw loci of constant β in the ρ, σ plane to show how much gain may be achieved before oscillation commences. The lossy mode calculation is

valid if $\sigma > 1$ and $\rho > 1$, and again if $\rho > 1$ the expression becomes independent of ρ.

The diagram showing lines of constant oscillation-free radius R and lines of constant across-disc gain log β is shown in Fig. 17. From the view point of oscillation suppression, the best place to operate is with both edge and face index-matched, since oscillation is impossible under these circumstances. If other considerations make such operation undesirable, the degree of oscillation difficulty encountered with other choices of refractive indices is easily evaluated from the diagram.

D. Parasitic Oscillation with a Rough Edge

Since the oscillatory modes considered above rely on rays which follow specific paths, one method of reducing oscillation tendency would seem to be the roughening of the disc edge, so that an initially parallel beam would be smeared out in angle. This ought to remove much of the energy from the mode, thus increasing the loss. However, energy will also be scattered into the mode from rays initially not involved. Clearly, a quantitative analysis of this situation is required. Again a Monte Carlo approach is inapplicable, since a ray which is randomly scattered at the edge has the same low probability of getting into the high-gain region of the mode as was the case with specular modes. Of course, we expect the active mode volume in space and angle to be larger with a rough edge than in the specular case, but the amount by which this helps the Monte Carlo method is hard to estimate.

The rough-edge oscillation was therefore analyzed by a method related to the well-known method of analyzing modes in an optical resonator. An

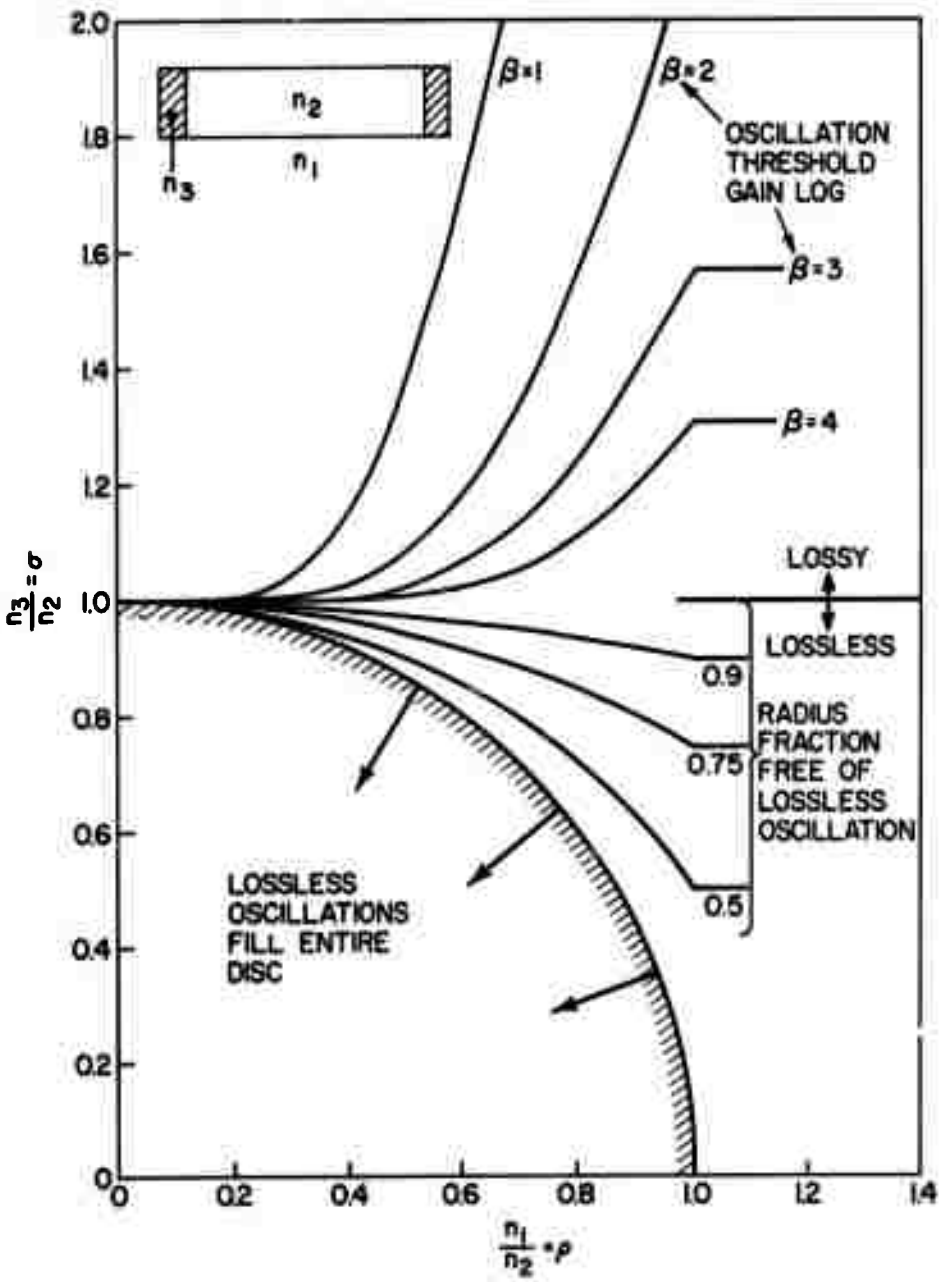

Fig. 17 - Combined diagram of lossless and lossy parasitic oscillation as a function of the index ratios of a circular disc. In the lower part of the diagram ($n_3/n_2 < 1$), the fraction of the disc free of lossless oscillations is shown. In the upper part ($n_3/n_2 > 1$), the β required to commence oscillation along lossy paths is shown. See text.

initial angular distribution of optical power was assumed at the disc edge, and the power was then transported across the disc (with gain), reflected with loss, and scattered in angle. In general, the distribution after this process was different, in both amplitude and shape, from the original distribution. The gain coefficient was adjusted after each iteration to keep the amplitude constant, and the process was reiterated until the angular distribution of power had reached an equilibrium state. After many such iterations, the gain had the value appropriate to the oscillation threshold, and the angular power distribution was that of the oscillating mode. Once again, diffraction and phase were ignored.

Since radiation which is totally internally reflected from the disc faces has much higher gain travelling across the disc than radiation which is only partially reflected, the power was assumed totally lost when it was partially reflected. With this assumption, all points on the disc edge are equivalent, and only the angle of the optical power is important (as opposed to its position). The hemisphere of possible angles was divided into sectors of equal solid angle, and the resulting matrix of powers was iterated as above. The edge roughening was simulated by taking the unit vector along the direction of the reflected ray, and adding to it a random vector with uniform distribution throughout a sphere of radius $F \cos\theta$, where $F \leq 1$ and θ is the angle from the reflected ray to the normal. The resulting vector was then renormalized to unity. Various amounts of surface roughening were simulated by varying F from zero (specular reflection) to one (very rough). The edge reflectivity R was independent of angle.

The increase in threshold due to increasing F is shown in Fig. 18 for various values of the edge reflectivity. There is obviously improvement over the specular case, but it is not as great as might be expected. From a practical viewpoint, it is very hard to reduce the reflectivity of a rough surface to the low values achievable by index-matching a smooth surface, because of the many pits and cracks in a rough edge. Therefore one should be cautious when attempting laser improvements by edge roughening.

E. Discussion

We have shown that lossless modes exist for certain refractive index ratios between the inside, outside, and edge of a circular disc. Even if these modes are suppressed by proper choice of the indices, lossy modes will still exist. Such modes place an upper limit on gain, since once the gain reaches the mode threshold for oscillation, no further gain increase is possible in the mode volume. Highest gain is achieved for close index matching between the disc and the material in contact with its faces, and between the disc and the absorbing coating on its edge. We have shown what gain is possible if proper matching is not feasible for reasons not connected with oscillation.

Even if the absorbing material on the edge is a good index match to the disc, there may be areas of less-than-perfect adhesion, or chips and cracks in the disc edge. Such flaws will have reflection larger than the coating-disc interface, and in practice will make the achievement of very high absorption at the edge difficult. If the higher-reflectivity flaws are small,

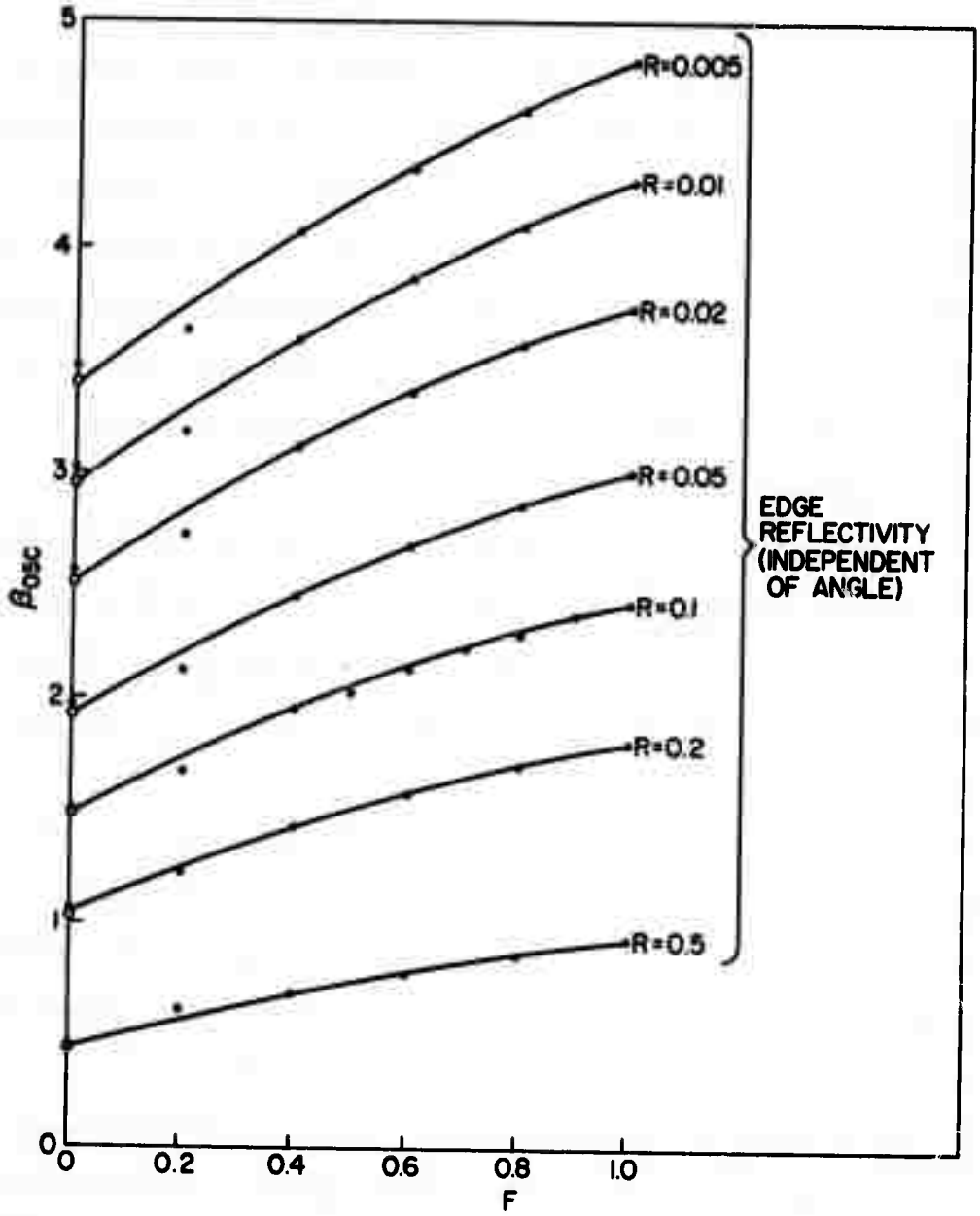

Fig. 18 - The moderate improvement in oscillation threshold achieved by various amounts of edge roughening. F is proportional to the amount by which the reflected rays are smeared out in angle about the specular direction.

diffraction will spread the reflected energy, but we have seen that such spreading causes only small threshold improvements. Thus a well-index-matched material must be applied extremely well to a flawless surface if a high parasitic oscillation threshold is to be achieved.

IV. EFFECTS ON PUMPING

Our discussion so far has been confined to an instantaneous snapshot of the fluorescence amplification and parasitic oscillation processes. Lasers are usually pumped by relatively slow pump pulses, and we are interested in knowing what decrease in efficiency is caused by the loss processes we have calculated during such a pulse. We will first find the effect of fluorescence amplification, and then the effect of parasitic oscillation.

A. Fluorescence Amplification

In the low-gain case, when fluorescence amplification is negligible, the stored energy decays with the fluorescent lifetime τ. The gain has the same behavior, and so we may write a differential equation for the across-disc gain log β in the form

$$\dot{\beta} = p(t) - \beta/\tau$$

where p(t) is the pump pulse (in appropriate units). At higher gain, fluorescence amplification increases the loss by a factor M, and so we have

$$\dot{\beta} = p(t) - \beta M(\beta)/\tau.$$

If we normalize to $\tau = 1$, and assume a half-sine approximation to the pump pulse, we get

$$\dot{\beta} = \frac{\pi\beta_o}{2T} \sin\left(\frac{\pi t}{T}\right) - \beta M(\beta) \qquad 0 < t < T$$

where β_o is the area of the pump pulse and T is the base width of the pump pulse (in units of the fluorescent lifetime). In the range $0 \leq M \leq 5$, we may make a good approximation to M for any of the geometries and lineshapes studied by using the form

$$M \cong \exp\left(F\,\beta + G\,\beta^2 + H\,\beta^3\right).$$

Note that F may be found from the low-gain value of A, since $A \cong F\,\beta$ when $\beta \ll 1$. We may then find G and H by fitting a straight line to $(\ln M/\beta - F)/\beta = G + H\beta$.

Once M is approximated, we may integrate the differential equation for β until it reaches its peak value. A plot of such maximum values is shown in Fig. 19 as a function of the pumping β_o, for various values of the pump pulse width. We see that fluorescence amplification is more serious for slow, large-area pump pulses while faster or smaller pulses suffer less loss. In the design of a flashlamp-pumped laser, the effects of current density on the pumping efficiency of flashlamps, and the effects of energy input on flashlamp life, should be integrated with this decay information in order to choose the optimum operating point.

Spatially uniform gain has been assumed in all our calculations of fluorescence amplification. However, the removal of energy due to

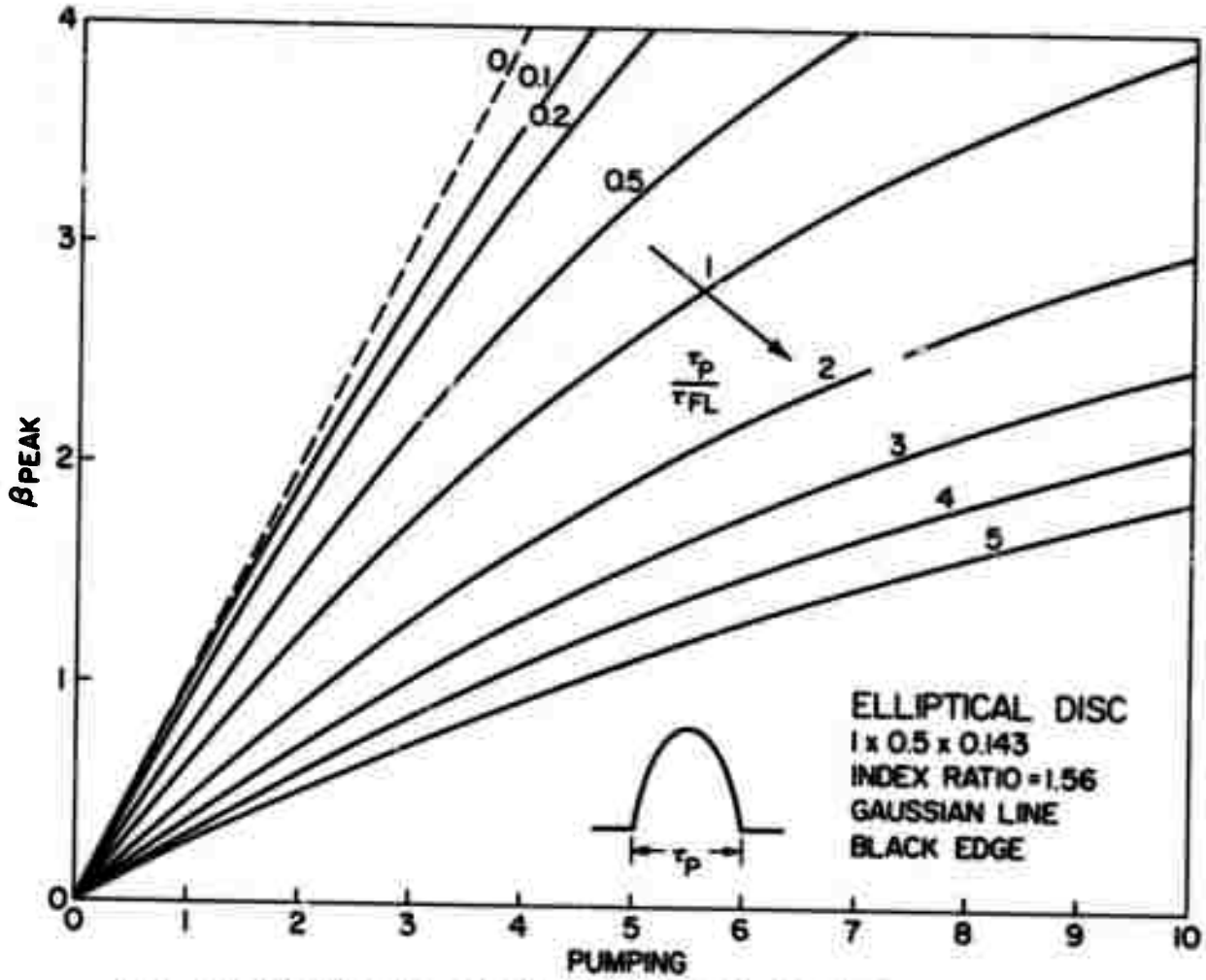

Fig. 19 - The maximum gain log β produced by half-sine pump pulses of various durations as a function of the pulse area. Since the inversion is proportional to β, this shows the achievable inversion for various ratios of pump width to fluorescent lifetime as a function of effective pump energy.

fluorescence amplification will be spatially non-uniform in general. Thus the gain will become non-uniform during a pumping pulse even if the pumping is uniform. The analysis of this problem is beyond the scope of this paper, but it is clear that proper tailoring of the spatial distribution of the pump energy can reduce or eliminate the difficulty.

B. Parasitic Oscillation

Parasitic oscillation causes a rapid limitation of stored energy, rather than the slow limitation we have seen above for fluorescence amplification. This is because a mode below its oscillation threshold contributes little to the loss rate, but once the mode is over threshold the loss rate is equal to the energy input rate. Thus the gain is sharply limited at the oscillation threshold. Figure 20 shows again the curve of gain versus pump area for a pump pulse of base width equal to the fluorescent lifetime, and also shows the type of gain saturation expected from the onset of oscillation. The oscillation threshold is shown for various ratios of the refractive index of the disc edge coating to the refractive index of the disc; this ratio determines the reflectivity at the edge. We have again assumed a disc-to-environment index ratio of 1.56. This diagram illustrates that unless very good index matching (or other reflection suppression) is used, parasitic oscillation will limit available energy storage well before fluorescence amplification losses become appreciable.

V. CONCLUSIONS

The effects of fluorescence amplification and parasitic oscillation on laser energy storage and pumping efficiency have been analyzed. Fluorescence

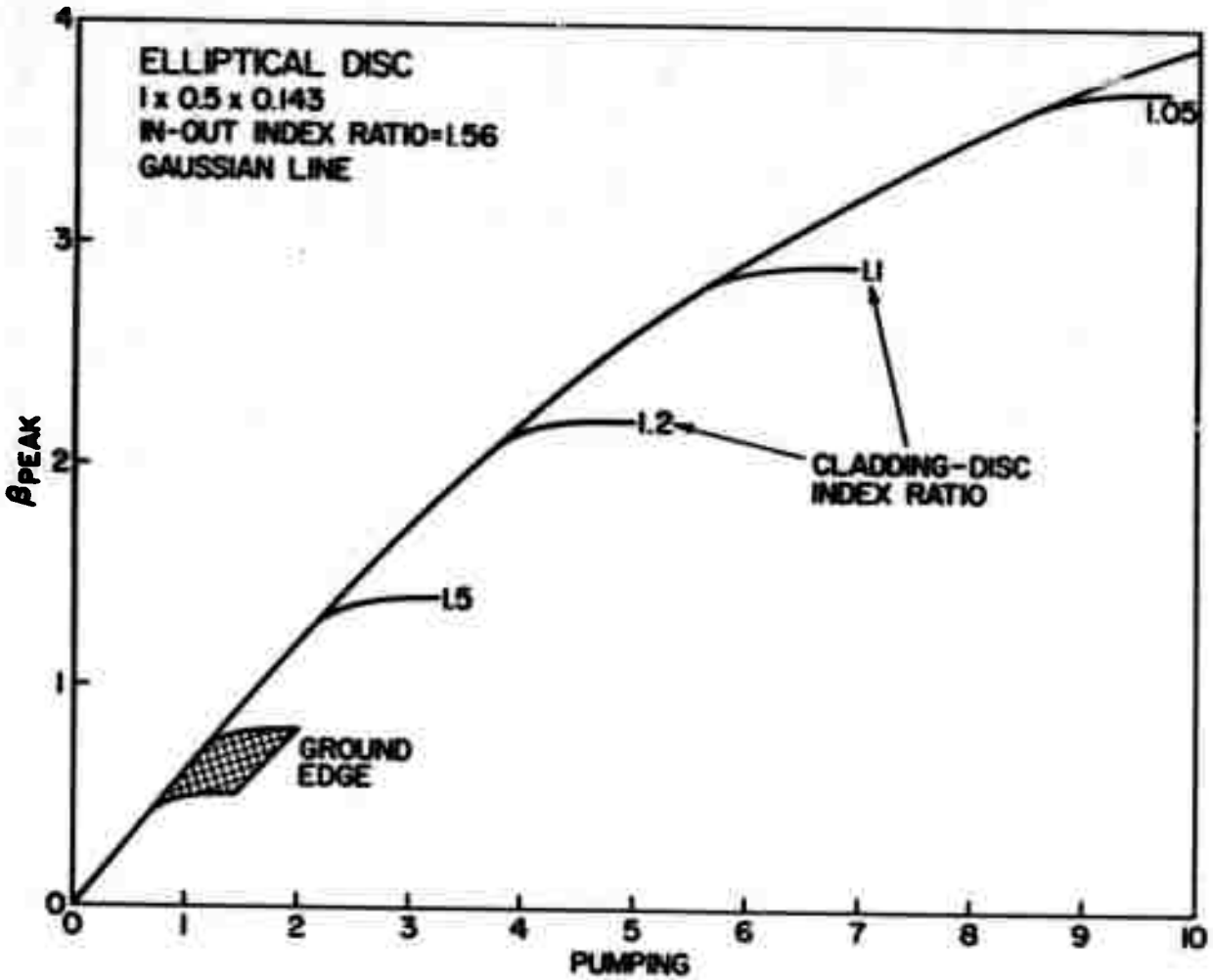

Fig. 20 - Parasitic oscillation limits shown on one of the pumping effectiveness curves of Fig. 19. The limitation gets more severe as the edge cladding index mismatch increases. Also shown are experimental limits for fine-ground, acid-etched disc edges.

amplification sets no definite upper limit on stored energy, but instead makes pumping more and more difficult as the energy density rises. Parasitic oscillation, on the other hand, sets an abrupt upper limit to stored energy at the oscillation threshold.

Fluorescence amplification is minimized by index-matching the material in contact with the faces of a laser disc to the refractive index of the disc. Increasing the disc thickness causes only a slow increase in the amount of fluorescence amplification, so thicker discs are of value if pump uniformity and thermal distortion limits are not exceeded.

Parasitic oscillation will occur at very low gain levels if the edge cladding material has a lower refractive index than the disc material. If this error is avoided, the level at which oscillation occurs will be maximized if the cladding index is as close as possible to the disc index. In addition, index-matching the faces raises the oscillation threshold. Roughening of the edges does not cause a great increase of the oscillation threshold, and may increase the average reflectivity of the edge, thus doing more harm than good.

What limitations do fluorescence amplification and parasitic oscillation place on glass laser amplifier disc size? Figure 20 shows that parasitic oscillation is the worst problem. Unless stringent precautions are taken, oscillation will set in at an across-disc gain of exp(3) or less, assuming the disc is in air to avoid self-focusing problems. With .5 J cm^{-3} stored, the line-peak gain will be on the order of .1 cm^{-1}. This implies a 30 cm disc at most. This value will vary with stored energy and the amount of gain per

unit stored energy, but values much smaller than those quoted increase the amount of energy lost to the fixed loss coefficient in the glass. Thus operation with discs of dimension larger than about 30 cm will be very difficult, and operation in the 30 cm region will require great care in edge treatment to suppress parasitic oscillations.

REFERENCES

1. W.R. Sooy, R.S. Congleton, B.E. Dobratz, and W. King, in Quantum Electronics - Proceedings of the Third International Conference, Vol. 2, Columbia University Press, New York, 1964, p. 1103.

2. L. Tonks, J. Appl. Phys. 35, 1134 (1964).

3. Yu. A. Anan'ev, A.A. Mak, and B.M. Sedov, Sov. Phys.-JETP 21, 4 (1965).

4. B.A. Ermakov, A.V. Lukin, and A.A. Mak, Opt. Spectrosc. 18, 201 (1965).

5. J.A. Fleck, Jr., J. Appl. Phys. 36, 1301 (1965).

6. Yu. A. Anan'ev, I.F. Balashov, and A.A. Mak, Sov. Phys.-Dokl. 11, 124 (1966).

7. E. Sibert and F. Tittel, J. Appl. Phys. 40, 4434 (1969).

8. A.A. Mak, B.G. Malinin, V.A. Novikov, D.S. Prilezhaev, A.I. Stepanov, and V.I. Ustyugov, Sov. Phys. - Tech. Phys. 14, 1418 (1970).

9. G.I. Peters and L. Allen, J. Phys. A: Gen. Phys. 4, 238 (1971).

10. L. Allen and G.I. Peters, Phys. Letters 31A, 95 (1970).

11. C.G.B. Garrett, W. Kaiser, and W.L. Bond, Phys. Rev. 124, 1807 (1961).

Appendix G

NRL Memorandum Report 2510

Faraday Rotation of EY-1 Glass

JOHN F. HOLZRICHTER

Laser Physics Branch
Optical Sciences Division

September 1972

NAVAL RESEARCH LABORATORY
Washington, D.C.

Approved for public release; distribution unlimited.

TABLE OF CONTENTS

Abstract..... ii

INTRODUCTION..... 1

DESIGN CONCEPTS..... 1

EY-1 GLASS MEASUREMENTS..... 1

Verdet-Constant vs Field Strength..... 2

Verdet Constant vs Wavelength..... 2

Verdet Constant vs Temperature..... 3

EXTINCTION RATIO VS CHANGE IN VERDET CONSTANT..... 4

ABSORPTION..... 6

REFERENCES..... 7

ACKNOWLEDGEMENTS 7

ABSTRACT

EY-1 is a terbium-silicate glass recently developed by Owens-Illinois. It offers great potential as a Faraday rotator-isolator in high power laser systems because of its high Verdet constant, $V = -4.06 \pm 0.1 \times 10^{-2}$ min/Oe-cm at 1.064 μ. This allows one to use shorter lengths of glass and lower magnetic fields than with other rotator glasses. We have measured V in this glass at 1.06 μ with fields up to 60 kOe and, in addition, the change in V with temperature and wavelength:

$$\left(\frac{\partial V}{\partial T}\right)_{1.064\mu} = -2.2 \pm 0.4 \times 10^{-4} \text{ min/Oe-cm-°C}$$

$$\left(\frac{\partial V}{\partial \lambda}\right)_{12°C} = 1.1 \pm 0.2 \times 10^{-5} \text{ min/Oe-cm-cm}^{-1}.$$

The requirements that these numbers impose on the field, temperature and wavelength stability and uniformity are discussed.

PROBLEM STATUS

This is an interim report on a continuing problem.

AUTHORIZATION

NRL Problem K03-08.502

ARPA Order 2062

I. INTRODUCTION

Faraday rotators are used in laser plasma experiments to isolate the laser from light back-reflected from the target. These back-reflections are especially serious in large multistage laser systems because low reflected light intensities can be amplified to destructive levels by propagating backwards through the amplifying chain. The use of Faraday rotators and polarizing optical elements offers one method of preventing this destructive feedback. This paper considers some design concepts concerning Faraday rotators for laser systems and presents measurements made on Owens-Illinois EY-1 Faraday rotator glass.

II. DESIGN CONCEPTS

The design of a Faraday rotator system for a high power laser ($>10^{12}$ W) is governed by the diameter of the laser beam and the length of the Faraday rotator material. The length is determined by the self-focusing length of the material at the desired laser power density. The Verdet constant and the length determine the necessary magnetic field strength.

Glasses are presently used as the Faraday rotator material in high power laser systems. Recently Owens-Illinois has developed for commercial sale a terbium-silicate base glass, EY-1, that has a Verdet constant of about -4×10^{-2} min/Oe-cm. It is a paramagnetic glass. A similar glass composition was first formulated for Faraday rotator purposes by Robinson and Graf.[1] For comparison[2,3], at 1.06 μ, Schott SF-6 lead-silicate glass has a Verdet constant of $+ 1.9 \times 10^{-2}$ min/Oe-cm and a common soda lime silicate glass has a Verdet constant of $+ 0.65 \times 10^{-2}$ min/Oe-cm. These last two glasses are both diamagnetic. The high Verdet constant of EY-1 allows a shorter length of material to be used for a given field. This reduces the energy in the magnetic field and increases the self-focusing damage threshold.[4] The base glass is similar to the Owens-Illinois laser glass ED-2 and consequently it should exhibit desirable surface and bulk damage characteristics.

III. EY-1 GLASS MEASUREMENTS

We have measured the following properties of EY-1 glass:

(1) Verdet constant V up to 60 kG at 1.06 μ and 19°C.

(2) $\left(\frac{\partial V}{\partial T}\right)_\lambda$ change in V with temperature at constant wavelength at 30 kG

(3) $\left(\frac{\partial V}{\partial \lambda}\right)_T$ change in V with wavelength at constant temperature at 30 kG.

These numbers determine the field strength of the system and the temperature and wavelength stability required to maintain a given extinction ratio with crossed polarizers.

The experimental arrangement is shown in Fig. 1. The Verdet constant was measured by noting the change in rotation with magnetic field $\theta = V\ell H$[5]. θ is traditionally measured in minutes, ℓ in cm, H in Oe, and V, consequently, in min/Oe-cm. The magnetic field was provided by the NRL magnet facility and was constant to ±1% over the sample volume (1.0 cm dia x 3.9 cm long). The rotation was detected by measuring the null in transmitted light through Glan-Thompson prisms with a photomultiplier detector. The extinction ratio was 100:1, and the angular error was ± 20 min. The temperature was monitored with an iron-constantan thermocouple that was thermally attached to the glass surface with silicone grease. The reference junction was held at a constant temperature in ice water, and the overall temperature was held to ±1°C during the constant temperature experiments.

A Chromatix Model 1000C Nd:YAℓG laser was used as the light source. The wavelength was varied by adjusting the wavelength selector prism on the laser to the different Nd^{3+} laser transitions, and the laser was operated at about 10 pps in a pulsed mode. No attempt was made to synchronously detect the pulses or to use boxcar integration techniques because the accuracy of the experiments was sufficient for Faraday rotator design purposes.

III-1. Verdet-Constant vs Field Strength

Figure 2 shows the rotation as function of field strength. The Verdet constant at 1.064 μ and 19°C is $V = -4.06 \pm 0.1 \times 10^{-2}$ min/Oe-cm. This is lower than the value quoted in Ref. (1) because of the lower Tb content[6].

III-2. Verdet Constant vs Wavelength

Figure 3 shows the variation in the Verdet constant with wavelength. The field was held constant at 30 kOe ± 1% and the temperature was held at 12°C to ± 0.2°C. The laser was tuned over the available frequencies from 0.946 μ to 1.079 μ, and the change in rotation was determined. The change in Verdet constant is:

$$\left.\frac{\partial V}{\partial \lambda}\right|_{T = 12°C} = 1.1 \pm 0.2 \times 10^{-5} \text{ min/Oe-cm-cm}^{-1}.$$

The rotation increases with frequency and the variation per cm^{-1} is about 10^{-3} x Verdet constant at 1.06 μ.

III-3. Verdet Constant vs Temperature

Figure 4 shows the variation in the Verdet constant with temperature[6,7]. This measurement is the least accurate of those made. The sample was heated with hot air and allowed to cool to the equilibrium magnet temperature. During the cooling period the temperature was found to be reasonably uniform in the sample by changing the direction of hot air flow and remeasuring $\frac{\partial V}{\partial T}$. Also the rate of cooling to the plexiglass holder was slower than the calculated rate of thermal equilibrium in the glass itself (~ 5 sec), which indicates that a reasonably flat temperature profile existed across the sample. The measurements at the highest temperature are less accurate as they were taken under the most non-uniform heat distributions in the sample. The value is:

$$\left(\frac{\partial V}{\partial T}\right)_{\lambda = 1.064} = -2.2 \pm 0.4 \times 10^{-4} \text{ min/Oe-cm-°C.}$$

This value per degree Kelvin is about 10^{-2} x Verdet constant at 1.06 μ.

The Faraday rotation by a paramagnetic material as a function of field and temperature is given by[5,7]:

$$\begin{aligned} \theta &= A\ell \tanh(\mu_e H/kT) + BH \\ &\cong c\,\ell H/T \text{ for } \frac{\mu_e H}{kT} \ll 1 \end{aligned} \qquad (1)$$

where $\frac{c}{T}$ = Verdet constant at the specified wavelength λ, μ_e is magnetic moment in Bohr Magnetons, H is field in Oe, k is Boltzman's constant, ℓ is the sample length, and A is a constant. B is a temperature independent term which is usually found to be negligible[7]. It will not be considered further here. Thus

$$\frac{d\left(\frac{\theta}{\ell H}\right)}{dT} = \frac{dV}{dT} = -\frac{c}{T^2} = -\frac{V}{T} \qquad (2)$$

which in our case for T = 12°C, yields:

$$\frac{dV}{dT} = -1.4 \times 10^{-4} \text{ min/Oe-cm-°C.}$$

This is less than the measured value, and outside of the experimental error limits. A systematic error may be due to the fact the center of the glass rod is slightly higher in temperature than the edge where the temperature was monitored. This is caused by the cylindrically symmetric temperature profile of a cooling thin cylinder. This however would not reduce the value by more than 20 - 30%. We use the experimental value which is higher than the theoretical value. The measured value allows one to calculate the required temperature uniformity conditions in a Faraday rotator system.

IV. EXTINCTION RATIO VS CHANGE IN VERDET CONSTANT[3,8,9]

For transmission of unpolarized light through crossed polarizers, which we assume is the normal operating condition of the Faraday rotator, the following equation is obtained[3] (see Fig. 5):

$$I_T = \tfrac{1}{2} I_o \sin^2(\theta - \pi/4) \qquad (3)$$

in which $\theta = \theta(y)$ where y can be field, temperature, or wavelength, and θ is defined such that $I_T = 0$ at $\theta = \pi/4$. The rotation of the direction of polarization by the glass is nominally set to be 45°, but variation in the rotation with temperature and wavelength may occur. To determine the effect of these variations we note that:

for $\theta = \pi/4 + \Delta\theta$

$$\sin^2(\theta - \pi/4) \simeq \Delta\theta^2$$

$$\Delta\theta = \frac{\partial\theta}{\partial y}\Delta y \quad (\Delta\theta \text{ measured in radians}) \qquad (4)$$

then $I_T \simeq \tfrac{1}{2} I_o \left(\frac{\partial\theta}{\partial y}\Delta y\right)^2$

$$\frac{I_T}{I_o} = \tfrac{1}{2}\left(\frac{\partial\theta}{\theta y}\Delta y\right)^2 = \text{Extinction Ratio} = E. \qquad (5)$$

Using the relation $\theta = \ell HV$ where

$$\frac{\partial\theta}{\partial y} = \ell H \frac{\partial V}{\partial y}$$

then

$$\frac{I_T}{I_o} = \tfrac{1}{2}\left(\frac{\theta}{V}\frac{\partial V}{\partial y}\Delta y\right)^2 \qquad (6)$$

(1) Transmission vs change in temperature ($y = T$ °K) using equation (6) and the measured values for V and $\frac{\partial V}{\partial T}$, ($\theta = 45°$):

$$\frac{\theta}{V} = \frac{2700}{.04} = 6.74 \times 10^{4} \text{ Oe-cm}$$

$$\frac{\partial V}{\partial T} = -2.2 \times 10^{-4} \text{ min/Oe-cm-°C} = -6.5 \times 10^{-8} \text{ rad/Oe-cm-°C}$$

$$\frac{I_T}{I_o} = 0.96 \times 10^{-5} (\Delta T)^2, \ \Delta T \text{ in °C.}$$

To maintain an extinction ratio of $< 10^{-4}$, one must hold the temperature to ± 1.5°C.

(2) Transmission vs change in wavelength ($y = \lambda$ cm^{-1}) using equation (6) and the measured values for V and $\frac{\partial V}{\partial \lambda}$:

$$\frac{\theta}{V} = 6.74 \times 10^{4} \text{ Oe-cm}$$

$$\frac{\partial V}{\partial \lambda} = 1.1 \pm 0.2 \times 10^{-5} \text{ min/Oe-cm-cm}^{-1}$$

$$= 3.3 \times 10^{-9} \text{ rad/Oe-cm-cm}^{-1}$$

$$\frac{I_T}{I_o} = 2.45 \times 10^{-8} (\Delta\lambda)^2, \quad \Delta\lambda \text{ in cm}^{-1}.$$

In Nd^{3+} glass, where $\Delta\lambda \simeq 100$ cm^{-1}, $\frac{I_T}{I_o} \simeq 2 \times 10^{-4}$. This extinction ratio is tolerable in a large Nd glass system.

(3) Transmission vs change in magnetic field ($y = H$ in Oe). From equation (5):

$$E = \frac{I_T}{I_o} = \frac{1}{2}\left(\frac{\partial\theta}{\partial H}\Delta H\right)^2$$

using

$$\frac{\partial\theta}{\partial H} = \ell V, \qquad \text{then}$$

$$E = \tfrac{1}{2}\, \ell^2 V^2\, \Delta H^2$$

or

$$\Delta H = \frac{\sqrt{2E}}{\ell V} \; .$$

Using

$$H = \frac{\theta}{\ell V}$$

$$\frac{\Delta H}{H} = \frac{\sqrt{2E}}{\theta} \; .$$

For an extinction ratio E of 10^{-4}, and $\theta = 45° = .79$ rad.

$$\frac{\Delta H}{H} = 1.8 \times 10^{-2} = 1.8\% \; .$$

The magnetic field inhomogeneity must be less than 1.8%.

V. ABSORPTION

Faraday rotator glasses typically have higher intrinsic absorption coefficients than normal optical glass. This is due to the strong optical transitions in the UV and blue spectral regions which provide the field dependent indices of refraction. A figure of merit that has been used for Faraday rotator materials[2] is V/α. Where V is the Verdet constant in min/Oe-cm and α is the intrinsic absorption coefficient in cm^{-1}. At 1.06 μ, α for EY-1 is less than 0.005 cm^{-1},[6] for Schott SF-6 it is ≈ 0.001 cm^{-1}.[3] The Schott glass is probably superior to the EY-1 glass using this figure of merit. However, the selection criteria for Faraday rotator glass that is to be used in high energy laser systems is maximum damage resistance and highest Verdet constant. Residual intrinsic absorption and temperature and wavelength stability are secondary considerations. EY-1 appears to be a very suitable material for high power optical rotators.

REFERENCES

1. C.C. Robinson and R.E. Graf, "Faraday Rotators in Pr, Tb, and Dy-Alumia-Silicate Glasses", Appl. Opt. 3, 1190 (1964).

2. C.C. Robinson, "The Faraday Rotation of Diamagnetic Glasses from 0.334 μ to 1.9 μ", Appl. Opt. 3, 1163 (1964).

3. C.F. Padula and C.G. Young, "Optical Isolators for High-Power 1.06 μ Glass Laser Systems", IEEE J. of Q.E. QE-3, 493 (1967).

4. P.L.Kelley, "Self Focusing of Optical Beams", Phys. Rev. Letters 15, 1005 (1965).

5. N.F. Borelli, "Faraday Rotation in Glasses", J. Chem. Phys. 41, 3289 (1966).

6. Mr. Haynes Lee, Owens-Illinois, Private Communications. An exact measurement of the intrinsic absorption coefficient has not been made, but it is comparable to O-I ED-2 laser glass for which $\alpha \simeq .002/cm$.

7. M. Daybell, W.C. Overton, Jr., and H.L. Laguer "The Faraday Effect at Low Temperatures in Terbium Alumina Silicate Glass", Appl. Phys. Letters 11, 79 (1967).

8. L.G. DeShazer and E.A. Maunders, "Optical Isolator for Near Infrared", Rev. Sci. Instrum. 38, 248, (1967).

9. K. Eidmann, P. Sachsenmaier, H. Salzmann and R. Sigel, "Optical Isolators for High Power Giant Pulse Lasers" J. of Physics E 5, 56 (1972).

ACKNOWLEDGEMENTS

I would like to thank Mr. R. Burns and Mr. E. Turbyfill, and the NRL magnetic facility staff for their assistance. I am indebted to Mr. John Myers for a test sample of EY-1 glass, and to Dr. John Emmett and Mr. John McMahon for their suggestions and assistance.

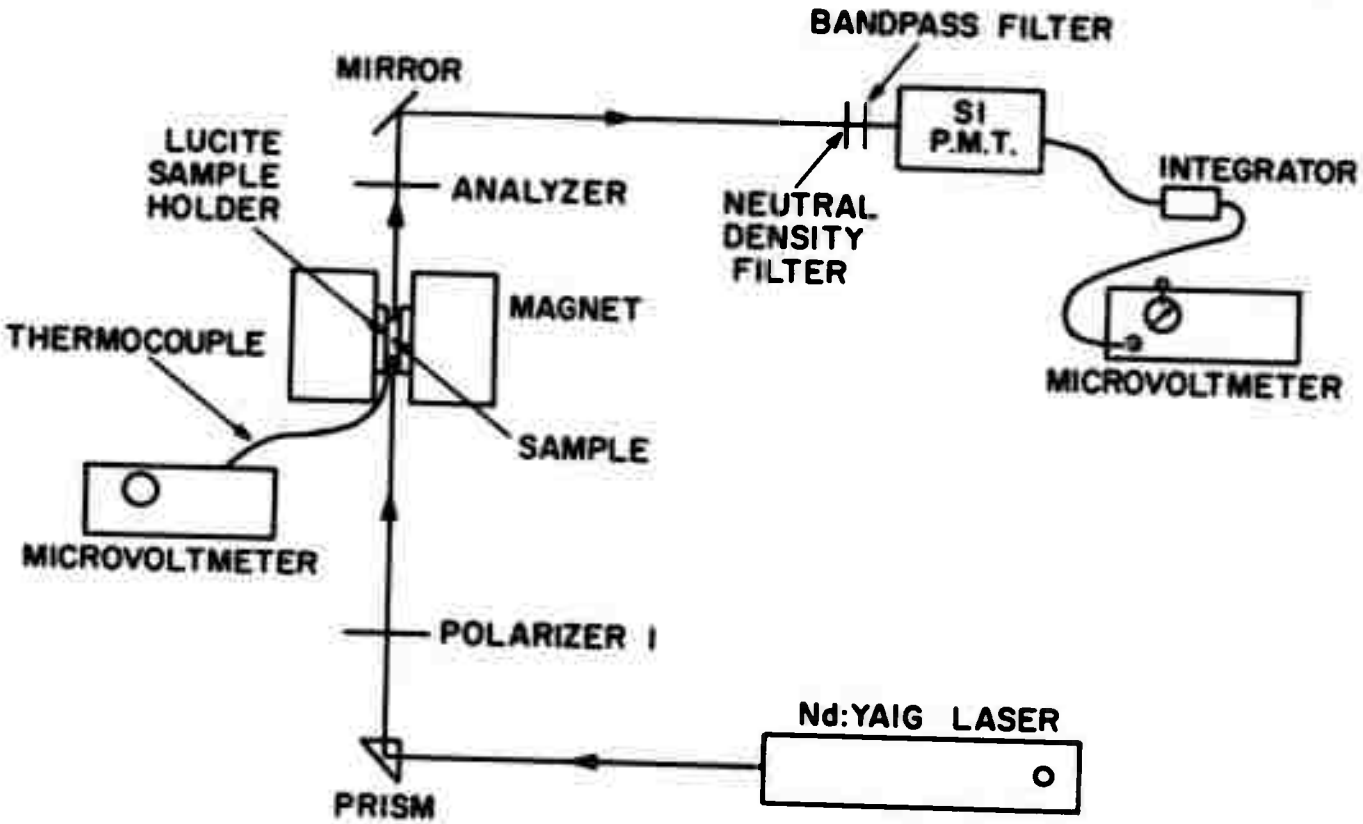

Fig. 1 - Experimental arrangement

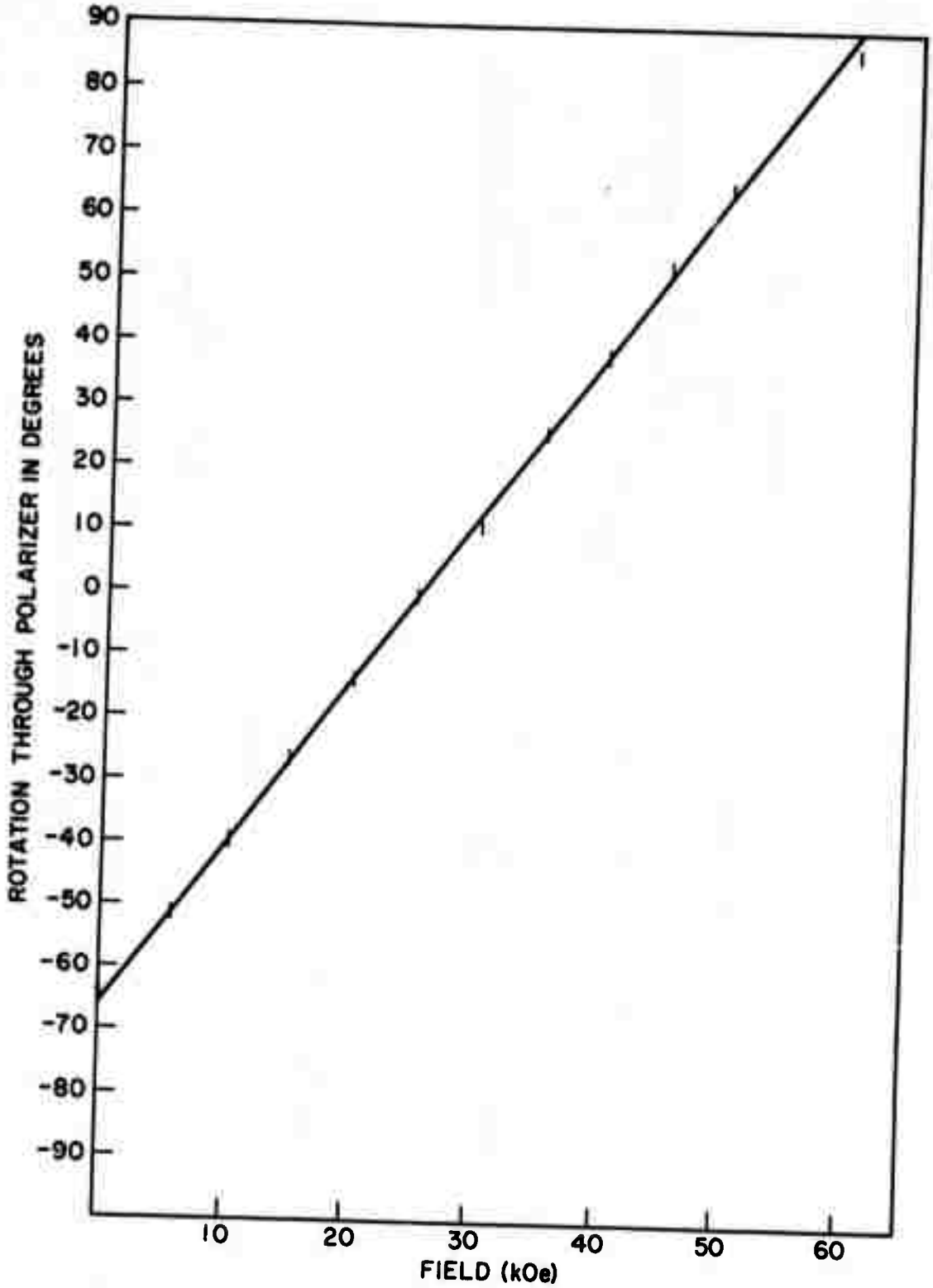

Fig. 2 - Rotation vs field at 19° C. Vertical bars show uncertainty in the data points.

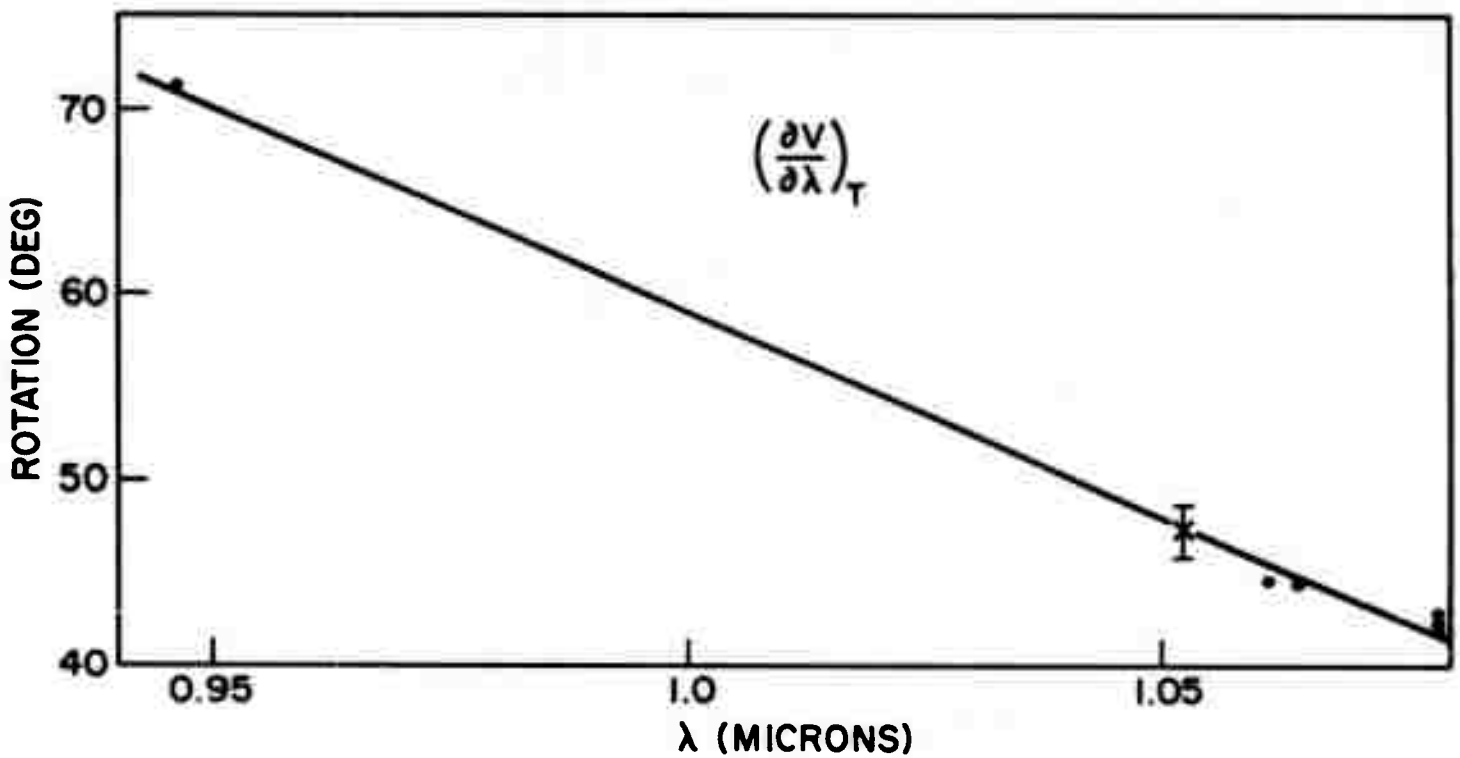

Fig. 3 – Rotation vs wavelength at constant temperature and field H = 30 k0e and T = 12°C

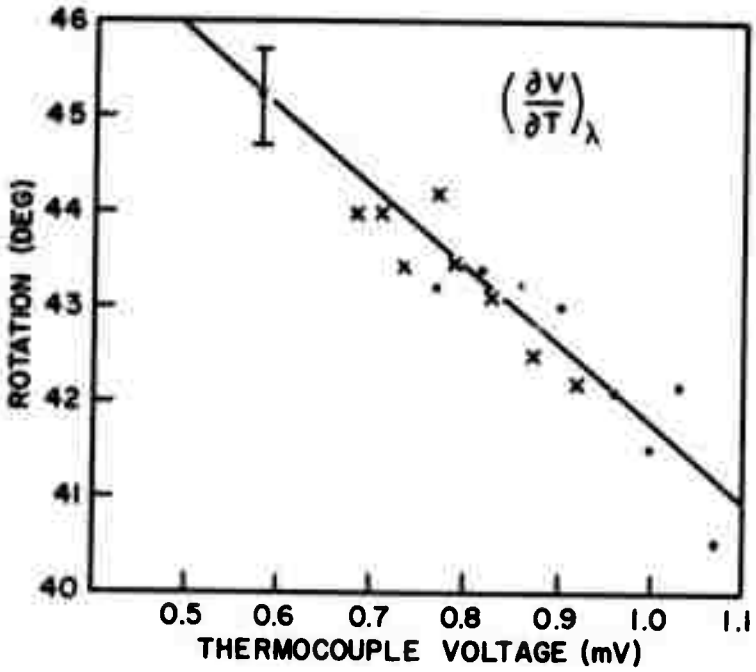

Fig. 4 - Rotation vs temperature at constant wavelength and field. H = 30 kOe and λ = 1.064 μ. Points and crosses are different data sets. The thermocouple response is 18.9° C/mVolt.

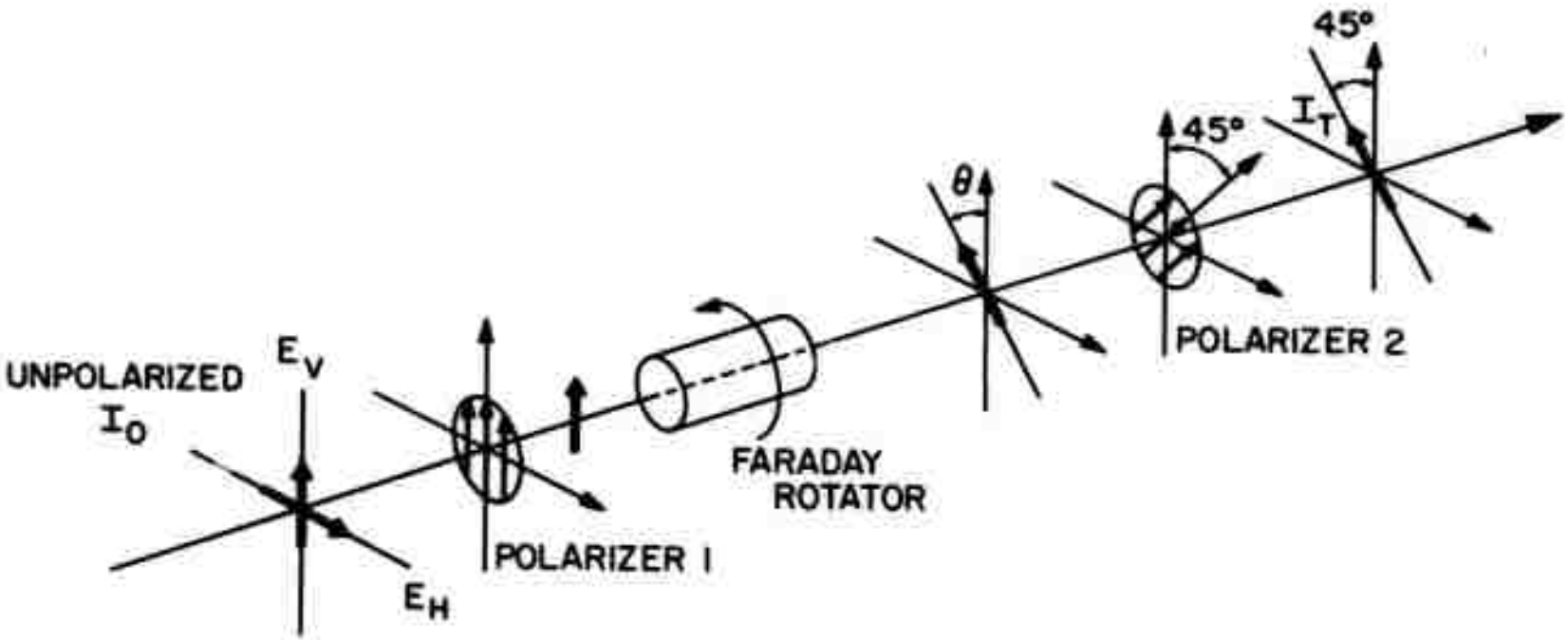

Fig. 5 - Schematic of Faraday rotator isolator system. Unpolarized light, I_o, is incident from the left. The transmitted light intensity, I_T, is equal to the extinction ratio, E, times I_o.

APPENDIX H

MODE LOCKING OF CaLaSoap:Nd*†

J.P. Letellier

Laser Physics Branch
Optical Sciences Division

Naval Research Laboratory
Washington, D.C. 20390

ABSTRACT

Nonlinear effects have generally precluded the generation of time-bandwidth limited pulses shorter than 15-20 psec. In this letter the generation of 5 psec time bandwidth limited pulses from a crystalline neodymium host with properties intermediate between Nd:YAG and Nd:glass is reported.

Mode locking has been obtained in a number of neodymium hosts, but reliable time-bandwidth limited operation has been obtained only in neodymium:YAG[1,2]. In neodymium glass, very early weak pulses may exhibit time bandwidth limited behavior and picosecond duration, but self-focusing and the consequent self-phase modulation destroy the time-bandwidth limited character of the more energetic pulses in the pulse train (as has been shown by the elegant work of Carmen et al[3]).

In order to generate time-bandwidth limited pulses shorter than the 15-20 psec reported from Nd:YAG, a host material with a smaller n_2 value than Nd:glass and a broader bandwidth than Nd:YAG is required. This letter reports the demonstration of apparent time-bandwidth limited operation with one such material, neodymium doped calcium lanthanum silicate oxyapatite (CaLaSoap:Nd). The properties of this material have been reported by its developers; those relevant to this investigation are that the fluorescence linewidth is $\simeq 53\ cm^{-1}$ and the induced emission cross section is $\simeq 1.6 \times 10^{-19}\ cm^2$.[4]

A laser rod 5.4 cm long and 6.4 mm diameter of CaLaSoap doped with 2 wt% neodymium was flashlamp pumped and mode locked in a 110 cm long cavity formed by one 100% reflectivity 5 meter radius mirror and one flat 75% reflectivity mirror. The rod had flat AR coated ends, but had to be cocked at two degrees to the optical axis to prevent the formation of satellite pulse trains. Eastman 9740 dye in 1,2-Dichoroethane was used in a flowing dye cell $\simeq$ 0.13 mm thick.

---

* This work supported by the Advanced Research Projects Agency under ARPA Order 2062.

† To be submitted to Applied Physics Letters for publication.

Figure 1 shows an oscillogram of the pulse train taken from a Tektronix 519 oscilloscope at 50 nanoseconds/cm. The total energy was ~25 mJ in a TEM_{00} spatial mode. The pulse train duration was only roughly optimized to be as short as possible using a 75% mirror. A 55% mirror would have been a more optimum choice in principle[5], but was not available at the time. It should be noted that scatter from the AR coatings apparently caused some interpulse noise to develop late in the pulse train.

The spectrum of the entire pulse train was recorded on a Baird Atomic 2-meter spectrometer having a dispersion figure of $\simeq$ 3.2 A/mm at 1.06 μm. Figure 2 shows a densitometer scan of a representative spectrogram. The center frequency was determined to be 1.06113 μm and the width at half intensity was determined to be 1.1 $cm^{-1} \pm 0.2\ cm^{-1}$. No evidence of gross spectral broadening corresponding to self-phase modulation was observed, hence the interpulse noise appeared to correspond to scattered light from the rod ends with the same spectral content as the main pulse rather than to pulse breakup due to self focusing.

The pulse duration was examined using two photon fluorescence in a 10 cm long cell of Rhodamine 6B. A half width of $\simeq$ 5 psec was obtained by this method with a contrast ratio of $\simeq$ 2:1. The experimental set up was similar to that of Clobes and Brienza[1] in which a similar contrast ratio was obtained photographically while a thin cell and photomultiplier set up gave a 2.9:1 ± .2 contrast ratio.

One final experiment was done in which the spectra was found to substantially overlap the fluorescence line of the second strongest Nd:YAG transition ($^4F_{3/2} \rightarrow {}^4I_{11/2}$) at 1.06111 μm to an extent sufficient to permit amplification of this pulse in Nd:YAG amplifiers.

ACKNOWLEDGMENTS

The author is indebted to the Westinghouse Research Laboratories, Pittsburgh for the use of a CaLaSoap laser rod, and to J.M. McMahon for helpful technical discussions.

REFERENCES

1. A.R. Clobes and M.J. Brienza, Appl. Phys. Letters 14, 287 (1969).

2. J.L. Emmett, et al, VII International Quantum Electronics Conference, C.8.

3. R.L. Carman, J. Fleck, and L. James, IEEE JQE-8, 586 (1972).

4. K.B. Steinbruegge, et al, Applied Optics 11, 999 (1972). (The value of 1.6 x 10^{-19} cm^2 compares well with the 1.7 x 10^{-19} cm^2 obtained here by comparing the slope efficiencies of YAG and CaLaSoap in the same cavity.)

5. M. Menat, J. Appl. Phys. 36, 73 (1965).

PUBLICATIONS AND PRESENTATIONS FOR FY-72

John L. Emmett "Generation of Kilojoule Subnanosecond Laser Pulses", talk given at Gordon Research Conference on Laser Interaction with Matter, Beaver Dam, Wisconsin, August 23-27, 1971.

H.S. Pilloff, S.K. Searles, N. Djeu, "CW CO Laser from the CS_2-O_2 Flame", Applied Physics Letters, 19, 9, 1 July 1971.

John L. Emmett, J.P. Letellier, J.M. McMahon, "The NRL Disc Laser System", presented at the Conference of the Quantum Electronics Section of the European-Physical Society, Hull, England, September 6, 1971.

T. Kan, J.S. Stregack, W.S. Watt, "Electric-Discharge Gasdynamic Laser (EDGDL)", Applied Physics Letters, Vol. 20, p. 137, February 1972.

J. C. Kershenstein and W. Graham, "Comparison of CW and Pulsed Operation of Carbon Monoxide Laser (CO, N_2, Xe Mix)", presented at the Twenty-Fourth Annual Gaseous Electronics Conference and Third Arc Symposium, October 1971, Gainesville, Florida.

W. T. Whitney, "Operating Parameters of Sealed-off CO_2 and CO_2-He Lasers", presented at the Twenty-Fourth Annual Gaseous Electronics Conference and Third Arc Symposium, October 1971, Gainesville, Florida.

T. Kan, J. Stregack, W. Watt, "A CW Electric Discharge Gas Dynamic CO Laser", presented at the 1971 IEEE International Electron Devices Meeting, Washington, D.C., October 1971.

N. Djeu, "On the Vibrational Rotational Population Distribution of CO Produced in Low Pressure CS_2/O_2 Flames", presented at the 3rd International Colloquium on Gas-Dynamics of Explosions and Reactive Systems, Marseille, France, September 1971.

T. Kan, J.A. Stregack, W.S. Watt, "Characteristics of an Electric Discharge Gas Dynamic CO Laser", presented at the American Physical Society for the APS Winter Meeting, 31 January - 3 February 1972, San Francisco, California.

N. Djeu and S.K. Searles "Determination of Absolute Populations of CO (v, J) in a CS_2-O_2 Flame by a New Technique", presented at the ACS Spring Meeting, April 1972, Boston, Massachusetts.

N. Djeu and S.K. Searles, "Relative Einstein A Coefficients for $\Delta v = 1$ Transitions in CO", presented at the VII International Quantum Electronics Conference held in Montreal, Canada, May 1972.

T. Kan, J.A. Stregack, W.S. Watt, "Operating Parameters of an Electric Discharge Gas Dynamic CO Lasers", presented at the VII International

Quantum Electronics Conference held in Montreal, Canada, May 1972.

John F. Holzrichter, John McMahon, "Generation of Subnanosecond 10 μ Pulses", presented at the VII International Quantum Electronics Conference held in Montreal, Canada, May 1972.

David I. Rosen, Richard N. Sileo and Terrill A. Cool, "A Spectroscopic Study of cw Chemical Lasers", presented at the 3rd Conference on Chemical and Molecular Lasers, May 1972, St. Louis, Missouri.

J.R. Airey, "Proposal for a New Chemically Pumped CO_2 Laser", presented at the 3rd Conference on Chemical and Molecular Lasers, May 1972, St. Louis, Missouri.

Tehmau Kan, Wayne Whitney, Manuel Pablo, "A Fast Flow Carbon Monoxide Laser", presented at the 3rd Conference on Chemical and Molecular Lasers, May 1972, St. Louis, Missouri.

W.S. Watt, J.A. Stregack, "The Effect of Electronegative Additives on the Characteristics of a Transverse-Discharge CO Laser", presented at the 3rd Conference on Chemical and Molecular Lasers, May 1972, St. Louis, Missouri.

S.K. Searles and N. Djeu, "Flame Laser Studies", presented at the 3rd Conference on Chemical and Molecular Lasers, May 1972, St. Louis, Missouri.

Terrill A. Cool, "Transfer Chemical Lasers: A Review of Recent Research", presented at the 3rd Conference on Chemical and Molecular Lasers, May 1972, St. Louis, Missouri.

John L. Emmett, John M. McMahon, J.P. Letellier, John Trenholme, "Generation of High Energy Subnanosecond Pulses by Solid State Lasers", presented at the VII International Quantum Electronics Conference, Montreal, Quebec, Canada, May 1972.

N. Djeu, "Energy Exchange Processes in a Low Temperature N_2-CO Transfer Laser", Chemical Physics Letters, Vol. 15, No. 3, August 15, 1972.

N. Djeu and S.K. Searles, "A New Method of Measuring Temperature, Inversion Ratio and Pressure Broadened Linewidth in a cw Molecular Laser", submitted to the IEEE Journal of Quantum Electronics.

N. Djeu, S.K. Searles, "Review of Flame Lasers", presented at the Fourth Northeast Regional Meeting of the American Chemical Society, Hartford, Connecticut, October 1972.

N. Djeu, S.K. Searles, "A Method for Measuring Relative Transition Probabilities of Cascading Molecular Bands: Application to CO

Fundamental Bands", presented at the Fourth Northeast Regional Meeting of the American Chemical Society, Hartford, Connecticut, October 1972.

S.K. Searles, N. Djeu, "Gain Measurements on CO P-Branch Transitions in a C_2H_2-O_2 Flame", submitted to the JQE.

N. Djeu and S.K. Searles, "A Method for Measuring Relative Transition Probabilities of Cascading Molecular Bands: Application to CO Fundamental Bands", submitted to the Journal of Chemical Physics.